Novel Mechanisms of Antiviral Innate Immune Regulation by the Hepatitis C Virus NS3-NS4A Protease

by

Christine Vazquez

Department of Molecular Genetics and Microbiology
Duke University

Date:_____

Approved:

_____
Stacy Horner, Supervisor

_____
Andrew Alspaugh

_____
Jörn Coers

_____
Micah Luftig

_____
Mari Shinohara

Dissertation submitted in partial fulfillment of
the requirements for the degree of Doctor of Philosophy
in the Department of Molecular Genetics and Microbiology
in the Graduate School
of Duke University

2019

ABSTRACT

Novel Mechanisms of Antiviral Innate Immune Regulation by the Hepatitis C Virus NS3-NS4A Protease

by

Christine Vazquez

Department of Molecular Genetics and Microbiology
Duke University

Date:_____

Approved:

_____
Stacy Horner, Supervisor

_____
Andrew Alspaugh

_____
Jörn Coers

_____
Micah Luftig

_____
Mari Shinohara

An abstract of a dissertation submitted in partial fulfillment of the requirements for the degree of Doctor of Philosophy in the Department of Chemistry in the Graduate School of Duke University

2019

Abstract

Hepatitis C virus (HCV) evasion of the host immune system is largely mediated by the actions of the HCV NS3-NS4A protease complex, which consists of the serine protease and RNA helicase NS3 and its membrane targeting co-factor NS4A. NS3-NS4A has multiple functions in the HCV life cycle, with roles in both HCV replication and regulation of innate immune signaling. To regulate innate immune signaling, NS3-NS4A inactivates multiple signaling proteins, including MAVS, an adaptor protein in the RIG-I antiviral signaling pathway, and Riplet, an E3 ubiquitin ligase that activates RIG-I. Inactivation of these host proteins results in an inhibition of downstream signaling through the transcription factor IRF3 and inhibition of the subsequent induction of IFN-β. What directs the multiple functions of NS3-NS4A throughout the HCV life cycle is largely undetermined. Here, we identify a tyrosine residue within the transmembrane domain of NS4A that uncouples the various function of NS3-NS4A.

First, to uncouple the roles of NS3-NS4A in replication and immune evasion, I focused on the NS4A transmembrane domain and generated an NS4A mutant (Y16F) in a full-length HCV infectious clone, a subgenomic replicon, and an over-expression construct. I then assessed viral replication of HCV wild-type (WT) and Y16F viruses by measuring replication of a subgenomic HCV replicon in two related liver hepatoma cell lines: Huh7, which have functional RIG-I signaling, and Huh-7.5 cells, which lack functional RIG-I signaling. The HCV Y16F virus replicated to similar levels as WT HCV in Huh-7.5 cells. However, in Huh7 cells, replication of HCV Y16F was decreased compared to the HCV WT. I used CRISPR-Cas9 gene editing to delete proteins in the RIG-I pathway, including RIG-I, MAVS, and IRF3, in Huh7 cells, infected these cells with

HCV WT or Y16F viruses, and then measured virus replication. I found that Y16F viral replication was not restored to the levels of WT in Huh7-RIG-I KO cells or the Huh7-MAVS KO cells, but it was restored to the levels of WT in the Huh7-IRF3 KO cells. I also found that the HCV NS3-NS4A Y16F mutation reduced the ability of over-expressed NS3-NS4A to block IRF3 activation, as measured through nuclear translocation via immunofluorescence microscopy. Further the NS3-NS4A Y16F mutation also had a reduced ability to block the induction of interferon-stimulated genes during both HCV replication and infection. This reveals that HCV NS4A Y16 can regulate a RIG-I-independent, yet IRF3-dependent, signaling pathway that limits viral replication.

Second, to further characterize this RIG-I-independent, IRF3-dependent signaling pathway, I examined the interactions of HCV NS3-NS4A with two of its known host substrates, MAVS and Riplet. To test whether the Y16F mutation prevented NS3-NS4A cleavage of MAVS, I performed a MAVS cleavage assay during both overexpression of NS3-NS4A and MAVS and also during infection with HCV WT and Y16F viruses. NS3-NS4A Y16F was able to cleave MAVS just like WT during both conditions. Next, I found that over-expression of NS3-NS4A WT changed Riplet intracellular localization and that NS4A interacted with Riplet. However, the NS4A Y16F mutation prevented NS4A-Riplet interactions in both of these contexts. Interestingly, I found that Huh-7.5 cells express lower levels of Riplet protein and mRNA compared to Huh7 cells. When full-length Riplet was added exogenously to Huh-7.5 cells, HCV Y16F virus replication was reduced compared to WT. However, when a Riplet construct missing the RING domain, which is essential for Riplet signaling, was added exogenously to Huh-7.5, both WT and Y16F viruses now replicated similarly. Taken

together, these data identify NS3-NS4A Y16 as important for regulating a previously uncharacterized Riplet-mediated signaling pathway that limits HCV infection.

Dedication

To my parents – Victor and Naida Vazquez – for showing me the value of hard work, for believing in me when I didn't believe in myself, for fostering my love of reading and science, and for teaching me the importance of education.

Contents

List of Tables

List of Figures

Acknowledgements

Graduate school has been one of the most challenging times of my life, but also one of the most rewarding times, with moments of personal, emotional, intellectual, and professional growth. I will forever remember the moments and memories from the past 6+ years at Duke. These years have been blessed by numerous people, and I could not have succeeded without the support and encouragement of so many.

First, I would like to thank my advisor Stacy Horner. I was one of her first graduate students, and she taught me many of the HCV techniques I have used throughout graduate school. I remember a snowstorm was about to fall but I really wanted to get a month-long experiment started (those purple plates), and she helped me that day and then drove me to my apartment before the snow fell (the experiment worked!). She has fostered my interest in virology and innate immunity. Stacy encouraged my desire to arrive at an answer independently but then was also there for support when I clearly needed it. Stacy – thank you for being a great conference partner and it's been exciting watching the Horner lab evolve from our first year to now.

Thank you to all my committee members – Dr. Andrew Alspaugh, Dr. Jörn Coers, Dr. Micah Luftig, and Dr. Mari Shinohara – for all of your support and valuable advice during every committee meeting which helped keep me on task.

I have spent most of my graduate school time with my labmates (Mike, Matt, Dia, Daltry, Moonhee, Graham, Michelle, Allison, Kevin, Mouna, Chin Yee) more than any other group of people so it is safe to say that many have become my closest friends. Nandan, thank you for the coffee walks and for re-affirming that I do not like ABBA. Mike, thank you for late night coffee sessions and positive words of encouragement when I needed it. Matt, thank you for being a great baymate and one-way road announcer (and

no, you cannot turn my desk into your mega-desk). Daltry, thank you for sharing your love of reading and recommending amazing memoirs for me to read, and Dia, thank you for your listening ear. I am grateful for all of your support, friendship, kindness, and encouragement throughout the years. In addition, I would also like to thank Annette Kennett for the daily lunches and conversation. I've been blessed with the knowledge of Trombone Shorty because of you.

Duke, especially MGM, has been a very supportive place, and there are many programs and people at Duke that have helped me throughout graduate school. The Duke BioCoRe, program, in particular Dr. Sherilynn Black, introduced me to my first group of friends at Duke, which helped my adjustment into grad school.

I am so grateful to have been surrounded by such an amazing group of women, whom I hope will forever be in my life. Chynna, Cait, Steph, Molly, and Allison - thank you for the baseball games, mall shopping adventures, rom-com movie watching, venting sessions, and nights out at Mateo.

Last, but most certainly not least, I would like to thank my parents, Victor and Naida Vazquez. They gave me everything when we had nothing and the faith to believe I could do anything. They supported me through everything and taught me that where you come from doesn't determine where you can go.

1. Introduction

Sections of this chapter were adapted with permission from manuscripts entitled (1) "Hepatitis C Virus: Strategies to Evade Antiviral Responses" [1] published in Future Virology by authors Nandan S. Gokhale, Christine Vazquez, and Stacy M. Horner and (2) "MAVS Coordination of Antiviral Innate Immunity" [2] published in Journal of Virology by authors Christine Vazquez and Stacy M. Horner.

1.1 RIG-I like receptors

Precise coordination of innate immune detection pathways provides the first line of host defense and primes adaptive immune responses against RNA virus infection. Upon viral infection, pathogen associated molecular patterns (PAMPs) are detected by pattern recognition receptors (PRRs) in a parallel, non-redundant manner to produce a type I and III interferon (IFN) response that then activates the expression of interferon-stimulated genes (ISGs) and pro-inflammatory cytokines. Multiple PRRs can sense and respond to RNA virus infection. These include the retinoic acid-inducible gene I (RIG-I)-like receptors (RLRs), the Toll-like receptors (TLRs), the NOD-like receptors (NLRs), and the double-stranded RNA (dsRNA)-activated protein kinase R (PKR). Cytosolic PRRs important for the detection of viral nucleic acids include those belonging to the RIG-I family, such as RIG-I, melanoma-differentiation antigen-5 (MDA5), and laboratory of genetics and physiology (LGP2).

While the TLRs, NLRs, and PKR are important sensors and regulators of virus infection, the focus of my dissertation is on the cytosolic PRR family of RLRs, particularly RIG-I. The RLRs belong to a family of aspartate-glutamate-X-aspartate/histidine (DExD/H)-box family of receptors, and have diverse roles in ATP binding and hydrolysis,

as RNA helicases, and as sensors of viral PAMPs to initiate downstream IFN signaling [3]. Structural features of the RLRs facilitate these diverse functions. RIG-I and MDA5 share high sequence similarity and both contain N-terminal caspase activation and recruitment domains (CARDs), internal DExD/H and helicase (Hel1, Hel2, Hel2i) domains, a linker region and a C-terminal domain (CTD) [3]. For RIG-I and LGP2, the CTD also encodes a repressor domain (RD) [4]. The CARDs are important for downstream IFN signaling as crucial interactors of adaptor signaling molecules; the DExD/H and helicase domains function in ATP hydrolysis and RNA unwinding; and the RD functions to keep RIG-I or LGP2 in an autoinhibitory state and as the viral RNA recognition/binding domain [3]. The structure of LGP2 varies from that of RIG-I or MDA5 in that LGP2 lacks the N-terminal CARDs, and thus has no known role as an enzymatic signaling molecule. The role of LGP2 in sensing virus infection is not as concrete as those ascribed to RIG-I and MDA5. LGP2 may both positively and negatively regulate RIG-I function, and this function may depend on cell type or on virus infections examined. For instance, IFN-β production was reduced in mice lacking LGP2 and infected with encephalomyocarditis virus (EMCV), vesicular stomatitis virus (VSV), or reovirus, yet remained unchanged during influenza A virus (IAV) infection [5]. During hepatitis C virus (HCV) and Sendai virus (SV) infection, the LGP2 RD interacts with RIG-I to prevent RIG-I signaling [4]. While the exact function of LGP2 is incompletely understood, the consensus among the current literature supports a role for LGP2 in sensing both single-stranded RNA (ssRNA) and dsRNA, and it is likely that the functions of LGP2 are more nuanced than currently appreciated [6].

The RLRs recognize and bind to viral PAMPs. These include the 5’ tri- or di-phosphate moieties present on viral genomes, which thus enable these sensors to

recognize self from non-self RNA, as cellular RNA lacks these features [7, 8]. Though RIG-I and MDA5 are highly similar in both sequence and structure, they play non-redundant roles in viral RNA sensing. RIG-I senses the 5'-ppp and blunt-end stretches of polyU/UC regions, such as those present in the HCV genome [7-9]. MDA5 senses longer dsRNA or higher order RNA structures, which can be viral replication intermediates, particularly those present in the internal RNA regions [10-12]. Further, MDA5 recognition of dsRNA occurs in a length-dependent manner, with head-to-tail filament oligomer assembly [13]. Upon recognition of these viral PAMPs, the RLRs then initiate downstream events leading to IFN induction.

Virus sensing enables conformational changes to the RLRs that propagate downstream signaling activation. Upon viral PAMP binding, RIG-I and MDA5 undergo drastic conformational changes that initiate their activation. In the absence of a viral ligand, RIG-I is in an auto-inhibited signaling state, with the helicase and RD in an open and flexible conformation [14, 15]. In this state, the RIG-I CARD domains are sequestered by the helicase domain, masking the ability of the helicase domain to bind RNA and holding the protein in this auto-repressed state [15, 16]. RIG-I signaling activation begins when the RD senses and captures the 5′ triphosphate in PAMP RNA, inducing a coordinated conformational change within the helicase-RD that forms a compact, closed structure around the dsRNA, likely stabilized by ATP binding and hydrolysis [16]. This ordered activation and compaction of the helicase-RD of RIG-I results in exposure of the two RIG-I CARDs and the ATP-dependent formation of RIG-I filaments for interaction with downstream signaling adaptor proteins. Ubiquitination events by the E3 ubiquitin ligases tripartite motif containing 25 (TRIM25) and Riplet result in a conformational change in RIG-I [17, 18]. Riplet ubiquitination at the RIG-I RD

releases RIG-I from its autorepressed state, thereby allowing TRIM25 to ubiquitinate RIG-I at the second CARD and initiate downstream IFN signaling [17].

While the structural domains of RIG-I and MDA5 are similar, unlike RIG-I, MDA5 does not contain a repressor domain that maintains autoinhibition. Instead, dimerization and oligomerization following viral RNA binding initiate MDA5 activation. In the absence of viral ligands, MDA5 is kept in a monomeric state with a flexible linker extending between the CARD and helicase domains and between the helicase domains and CTD [19]. Upon viral RNA binding to MDA5, MDA5 forms a filament of repeating MDA5 dimers along viral RNA [13]. This, along with a dephosphorylation event at the MDA5 CARD by the phosphatase PP1, results in the interaction of MDA5 with MAVS for downstream antiviral immune signaling [20].

During virus infection, viral RNA can be sensed by one or more of these pathways. My work will focus on RIG-I activation as RIG-I is the best described sensor of HCV infection [21].

1.2 Activation of RIG-I-mediated antiviral immune signaling

Following viral RNA recognition by RIG-I, interactions with adaptor molecules initiate a downstream signaling cascade leading to the transcriptional induction of IFN and ISGs (Fig. 1). Following dsRNA-RIG-I binding, RIG-I is ubiquitinated by multiple E3 ligases, including TRIM25 and Riplet, resulting in its conformational activation and interaction with the molecular chaperone, 14-3-3ε [17, 18, 22]. While the relative importance of TRIM25 and Riplet for RIG-I activation is currently controversial, multiple studies have highlighted the contributions of TRIM25 and Riplet, leading to a prevailing model of RIG-I activation. First, Riplet ubiquitinates RIG-I at multiple lysine residues in

the RIG-I RD. This ubiquitination allows RIG-I to undergo a conformational change that exposes the CARDs [17] and allows TRIM25 to ubiquitinate RIG-I at Lys172 in the second CARD. Following TRIM25 ubiquitination, RIG-I:dsRNA, 14-3-3ε, and TRIM25 form a complex called a translocon that then translocates from the cytoplasm to membranous sites of signaling where MAVS, a classic tail-membrane anchored protein, resides [22]. RIG-I interacts with MAVS via CARD-CARD interactions, resulting in MAVS oligomerization on the outer mitochondrial membrane and formation of a MAVS signalosome [23, 24]. Following MAVS oligomerization, MAVS recruits and interacts with TRAF2, 3, 5, and 6 (reviewed in [23]). At this step, the RIG-I signaling pathway can birfucate into IRF3-mediated signaling or NF-κB-mediated signaling.

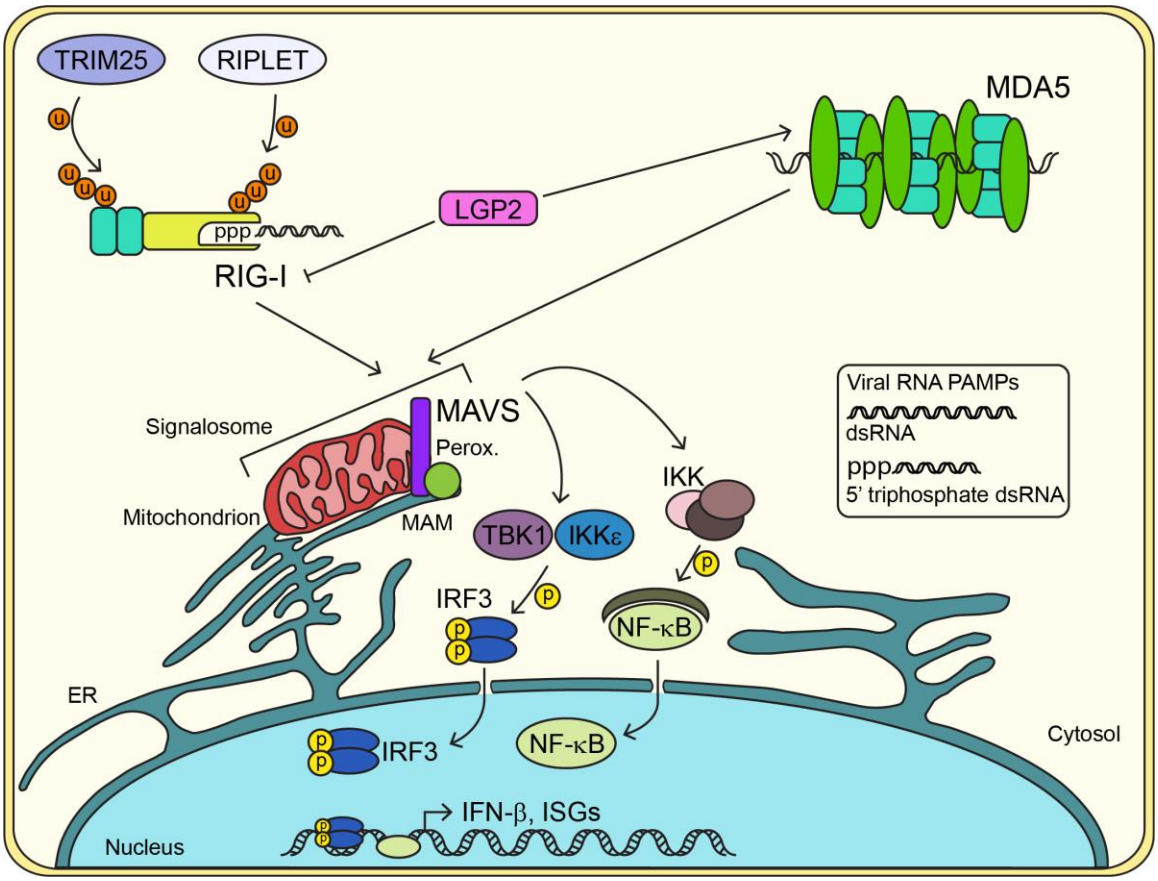

Figure 1: Intracellular innate immune response (adapted from [25]). Viral RNA PAMPS (dsRNA or 5' triphosphate dsRNA) are recognized by cytosolic receptors, such as RIG-I and MDA5. RIG-I is ubiquitinated (U) by the E3 ubiquitin ligases TRIM25 and Riplet. RIG-I binds to RNA via its C-terminal helicase domain and contains two caspase activation and recruitment domains. MDA5, upon viral RNA recognition, forms repeating dimers along the length of the viral RNA. LGP2, another cytosolic receptor, can negatively or positively regulate this IFN induction. RIG-I and MDA5 can then interact with MAVS, which is localized at the mitochondrion, the mitochondrial-associated endoplasmic reticulum membrane (MAM), and at peroxisomes (Perox.), and form a MAVS signalosome. This then leads to interaction with the kinases IKK, TBK1, and IKKε that then phosphorylate (P) the transcription factors IRF3 and NF-κB. This leads to their nuclear translocation and the transcriptional induction of IFN-β and IFN-stimulated genes (ISGs).

For IRF3-mediated signaling, the TRAF proteins ubiquitinate the kinases TANK-binding kinase (TBK1) and IκB kinase (IKKε) [26]. Following autophosphorylation of TBK1 and IKKε, TBK1 and IKKε phosphorylate IRF3 [27, 28]. IRF3 activation occurs via a multi-step process. First, IRF3 is phosphorylated at two phosphosites: phosphosite 1 encompasses the amino acid residues Ser385 and Ser486, and phosphosite 2 encompasses the amino acid residues Ser396, Ser398, Ser402, Thr404, and Ser405 [29, 30]. The residues in phosphosite 2 are phosphorylated first, releasing autoinhibition, and allowing phosphorylation at phosphosite 1. Phosphorylation at phosphosite 1 then promotes the second step of IRF3 activation, dimerization [29]. Following dimerization, IRF3 translocates from the cytoplasm to the nucleus, where it can facilitate the transcription of IFN-β and lead to the transcriptional induction of several hundreds of ISGs [31].

Similar to IRF3 activation, NF-κB activation requires nuclear translocation, but the upstream signaling events necessitate degradation of inhibitor proteins. In an uninfected cell, NF-κB is kept in an inhibited dimeric state (consisting of the proteins RelA and p50) by cytoplasmic inhibitors called inhibitors of NF-κB (IκB). Following virus infection, MAVS activation, and TRAF6 engagement, the IKK complex is recruited. This recruitment phosphorylates IkB [32]. Phosphorylated IkB is ubiquitinated by the ligase $SCF^{\beta TrCP}$ via K48 ubiquitin linkages, resulting in the proteasome-dependent degradation of IκB [33]. This degradation results in an active NF-κB dimeric state, followed by NF-κB nuclear translocation and transcriptional induction of IFN-β and other cytokines (reviewed in [34]). The IRF3 and NF-κB-mediated signaling pathways converge upon induction of IFN-β, to induce ISGs that limit virus replication.

1.3 The antiviral role of ISGs during HCV infection

Although HCV utilizes several strategies to interfere with the signaling pathways that activate IFN, ISG mRNA expression is paradoxically upregulated in the livers of infected patients [35, 36]. Of the hundreds of ISGs upregulated by IFNs, the results of several overexpression or RNA-interference screens have identified only a few key ISGs that play a role in restriction of HCV replication [37-40]. One of the most well-characterized ISGs against HCV includes the IFN-induced protein with tetratricopeptide repeats (IFIT) family, including IFIT1, IFIT2, and IFIT3. In a humanized liver chimeric mouse model and *in vivo* HCV infection assays, decreases in HCV RNA expression in liver tissue correlated with increase mRNA expression of *IFIT1, IFIT2, and IFIT3* [41]. IFIT1 and IFIT3 suppress HCV replication by inhibiting IRES-mediated translation. While the exact antiviral mechanism of IFIT2 during HCV infection remains to be defined, it is known that IFIT2 is induced during HCV infection of Huh7 cells and that IFIT2 is able to interact with the translation initiation factor eIF3 p48 subunit and with AU-rich RNA, likely indicating its role in inhibiting viral RNA translation [41, 42]. Among the ISGs with anti-HCV activity are members of the OAS/RNaseL pathway. OAS1 senses HCV dsRNA produced during viral replication, and this sensing stimulates the enzyme RNaseL to cleave cellular and viral mRNAs into fragments that may serve as PAMPs for RIG-I [43-45]. Interestingly, the HCV NS5A protein has been proposed to impair OAS1 function, thus counteracting the antiviral effect of this pathway [46]. At least two members of the IFN-inducible transmembrane protein family, IFITM1 and IFITM3, are antiviral toward HCV *in vitro* [38, 47, 48]. IFITM1 blocks HCV entry by binding to and preventing the interaction between the HCV coreceptors CD81 and occludin at tight junctions in hepatocytes [49]. IFITM3 has been proposed to function as an anti-HCV ISG by

impairing HCV IRES-mediated translation [50]. IFITM3 may also function in blocking HCV entry. In other viral infections, IFITM3 negatively regulates the interaction between the lipid and cholesterol homeostasis proteins VAP-A and OSBP to repress viral entry by preventing endosomal fusion [51]. As both VAP-A and OSBP are known proviral factors for HCV, inhibition of their function by IFITM3 could similarly repress HCV entry by sequestration of HCV virions within endosomes [52, 53] . Indeed, IFITM3 colocalizes with the Rab5a and Rab7 proteins, known markers of early endosomes and late endosomes, respectively, in hepatocytes [49]. Another ISG that regulates HCV replication is Viperin, which localizes to lipid droplets and prevents VAP-A and HCV NS5A interactions required for replication [54, 55]. Myxovirus resistance 1 (Mx1) is a dynamin-like GTPase protein that is evolutionarily conserved across all vertebrates. The Mx1 GTPase activity is necessary for inhibition of some DNA viruses [56]. While one study has indicated a pro-viral regulatory role of Mx1 on HCV replication, several other studies have identified a negative regulatory role, in the context of Mx1 overexpression followed by HCV infection [57]. However, the exact mechanism of Mx1 antagonism on HCV is unclear, but it may be possible that human Mx1 can inhibit positive-sense RNA viruses by binding to the viral capsid protein or inhibiting mRNA translation, as is observed for the fish homolog of Mx1 during RNA virus infection (reviewed in [56]). While some ISGs can be activated during HCV infection, HCV, and multiple RNA viruses, possess several mechanisms by which they can evade the IFN response program to establish persistent infection.

1.4 Multiple RNA viruses evade RIG-I-mediated signaling

Viral evasion mechanisms and host immune countermeasures beautifully depict the tug-of-war evolutionary battle between viruses and human hosts. Viruses have evolved mechanisms to evade nearly every step of the RIG-I signaling pathway, from preventing recognition of viral RNA to degradation of the RIG-I signaling proteins.

One mechanism of viral immune evasion involves hiding or preventing viral dsRNA binding from cytosolic PRRs. Some RNA viruses can hide their viral RNA in membrane compartments to avoid detection by RIG-I in the cytosol. For instance, tick-borne encephalitis virus, dengue virus (DENV), and HCV can hide their dsRNA in intracellular membrane vesicles [58-60]. Some viruses, such as IAV and Ebola virus, encode proteins, such as NS1 and VP35, respectively, that can bind dsRNA and block the ability of RIG-I to bind it (reviewed in [61]).

Additionally, viruses can bind to, cleave, and/or promote the degradation of the signaling proteins in the RIG-I innate immune response pathway. Poliovirus induces the degradation of MDA5 by activating the caspase and proteasome machinery [62]. HCV cleaves multiple proteins involved in antiviral signaling via the actions of its NS3-NS4A protease complex. NS3-NS4A cleaves the RIG-I adaptor protein MAVS at position C508, just upstream of the transmembrane domain [63-66]. This cleavage releases MAVS from membranes, where cytosolic MAVS cannot activate downstream IFN signaling. HCV NS3-NS4A also cleaves the TLR adaptor protein TRIF at position C372, resulting in TRIF proteolysis [67].

Posttranslational modifications (further described in Section 1.6) are key regulators of IFN induction. Consequently, viruses modulate the function of these modifications to subvert antiviral signaling. MDA5 is constitutively phosphorylated to

maintain its inactive state and is then de-phosphorylated by PP1α and PP1γ for activation [20]. The measles V protein binds to PP1α and PP1γ to prevent dephosphorylation of MDA5 [68]. As described above, RIG-I undergoes multiple posttranslational modifications that propagate IFN induction. Both HCV and IAV using their NS3-NS4A and NS1 proteins, respectively, can bind to and inactivate TRIM25 and Riplet, to prevent RIG-I activation and downstream signaling [17, 69]. The focus of my research, and thus this dissertation, will be on HCV NS3-NS4A inactivation of the RIG-I signaling pathway.

1.5 Hepatitis C virus

The work described in this dissertation focuses on the RNA virus, hepatitis C virus. HCV is a 9.6 kilobase-long, positive-sense, ssRNA virus belonging to the *Flaviviridae* family of viruses. This virus remains a global public health threat, with greater than 180 million individuals infected worldwide, and approximately 80% of those infected establish a chronic infection. Many HCV-infected individuals are asymptomatic and thus are unaware of their HCV status until secondary manifestations, such as liver cirrhosis and hepatocellular carcinoma, arise decades later. There are currently seven well-established HCV genotypes, with genotype 1 being the most common genotype in the United States. Individuals infected with genotype 3A are more likely to develop advanced liver disease and hepatocellular carcinoma compared to any other HCV genotype in the US [70]. The recent development of direct-acting antivirals for HCV has dramatically improved successful treatment of HCV infection [71]. Notably, although the current direct-acting antivirals treat HCV-induced disease, they do not always prevent re-

infection in cured individuals. Therefore, there is an urgent need for future studies into the development of a vaccine to reduce the global burden of HCV infection.

1.5.1 From discovery of HCV to cell culture

Upon entry into hepatocytes, the HCV mRNA genome is translated into a polyprotein that is co-and posttranslationally processed by both host and viral proteases into 3 structural proteins (Core, E1, and E2) and 7 non-structural proteins (p7, NS2, NS3, NS4A, NS4B, NS5A, NS5B) (Fig. 2). The structural proteins comprise the bulk of the HCV virion and aid in cellular entry by interacting with cellular entry factors, such as CD81, claudin, and occludin. The non-structural proteins function in replication and assembly of replication complexes on re-structured membranes called the membranous web. HCV was first discovered in 1975, but was not given the name hepatitis C virus until 1989 [72, 73]. In 1975, Feinstone *et al.* treated patients with transfusion-associated hepatitis whose symptoms differed from those observed with patients infected with hepatitis A and hepatitis B viruses and called this disease non-A, non-B hepatitis [73]. However, it was not until 1989 that cDNA containing the non-A, non-B hepatitis infectious material was isolated from infected chimpanzees [72]. This isolated infectious clone closely associated with genomes from non-A, non-B hepatitis infected patient samples, contained a positive-stranded RNA genome, contained a lipid envelope, and resembled viruses belonging to the *Flaviviridae* family. Thus, this new isolated virus was termed hepatitis C virus.

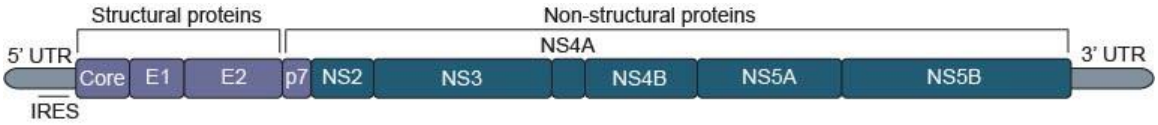

Figure 2: Schematic of the HCV proteins. HCV contains an internal ribosomal entry site (IRES) at the 5' untranslated region (UTR). It consists of the 10 proteins: Core, E1, E2, p7, NS2, NS3, NS4A, NS4B, NS5A, and NS5B, and is flanked at the 3' end by the 3' UTR.

HCV is a very host-restricted virus and to this day, chimpanzees remain the only non-human host able to become infected with HCV. As such, development of a cell culture system in which HCV was able to be propagated was the focus of much of the early HCV research. In 1999, Lohmann and colleagues developed a subgenomic replicon system to support HCV replication [74] (Fig. 3). Here, a bicistronic system was utilized, in which the HCV structural proteins are replaced with a neomycin resistance cassette, which is flanked at the 5' end by the HCV internal ribosomal entry site (IRES), and the 3' end by the EMCV IRES. The HCV IRES drives translation of the neomycin cassette while the EMCV IRES drives translation of the non-structural proteins of HCV. This RNA was then transfected into Huh7 cells, a liver hepatoma cell line, selected for G418 (neomycin), and resulting clones that survived selection were analyzed for viral RNA. This system provided the first opportunity for HCV replication studies in cell culture.

Figure 3: Schematic of an HCV replicon. The structural proteins and the NS2 protein of HCV are replaced by a neomycin (Neo)-resistance cassette. The internal ribosomal entry site (IRES) at the 5' untranslated region (UTR) drives the translation of neomycin, while an EMCV IRES drives the translation of the non-structural HCV proteins.

While the generation of the HCV replicon provided the framework for cell culture exploration of HCV replication, HCV replication was rather limited in the Huh7 cells. Further work, including from our lab, has defined cell culture adaptations that the virus undergoes to allow permissiveness in cells [75-79]. One determining factor for HCV permissiveness is the cell type in which the HCV replicates. In hosts, hepatocytes, peripheral blood mononuclear cells, and dendritic cells can propagate HCV both *in vitro* and *in vivo* [80]. In cell culture, two main cell lines are used for HCV replication. The first is the Huh7 cell line, which was established in 1982 from a biopsy from a hepatoma in a Japanese male patient with hepatocellular carcinoma [81]. The biopsy was homogenized and plated in growth medium. One colony that replicated from this original hepatoma culture was designated Huh7 and propagated [81]. The second cell line is the related Huh-7.5 cell line [82]. Huh-7.5 cells were generated by taking an Huh7 cell clone that replicated an HCV replicon and treating that cell line with IFN-α to remove the HCV, thereby creating an HCV "cured" cell clone. From this cured cell line, an HCV replicon was re-introduced and this cell line, named Huh-7.5, was found to support HCV replication at much higher levels than before. Further analysis of Huh-7.5 cells found that a reason for the increased permissiveness of HCV replication was due to a mutation in the first CARD of RIG-I at position T55, T55I [83]. This mutation prevents TRIM25 interaction with RIG-I, which ultimately prevents downstream IFN signaling mediated by RIG-I. Both cell lines were utilized in the studies described in Chapters 2 and 3.

The most commonly used HCV isolate in the laboratory is the Japanese Fulminant Hepatitis-1 (JFH-1) genotype 2A strain. This strain was originally isolated in 2001 from a 32-year old patient presenting with fulminant hepatitis and positive for HCV RNA [84]. Patient serum was collected, and the entire HCV genome was recovered and

sequenced. This sequence was then compared to six other strains isolated from patients chronically infected with HCV and found that the JFH-1 strain clustered around genotype 2A, but there were mutations between JFH-1 and the other strains in the 5' UTR region, Core, NS3, and NS5A, likely suggesting that additional mutations occur during progression to chronic disease [84]. The studies outlined in Chapters 2 and 3 of this dissertation utilize this JFH-1 genotype 2A strain.

1.5.2 HCV evasion of RIG-I-mediated signaling

HCV is one of the most efficient viruses at blocking downstream antiviral signaling. HCV encodes a serine protease complex, NS3-NS4A, that targets and inactivates multiple proteins in the RIG-I signaling pathway [17, 64-67, 85]. These include the E3 ligase Riplet, which is necessary for RIG-I ubiquitination and subsequent activation, and the innate immune adaptor protein, MAVS. Prior to my work outlined in this dissertation, it was found that overexpression of NS3-NS4A resulted in loss of Riplet protein expression, which was attributed to cleavage at amino acid position C21 [17]. Cleavage of MAVS as amino acid position C508, near the transmembrane domain, removes MAVS from intracellular membranes [86]. Both cleavage events prevent downstream signaling to IFN-β. HCV can circumvent TLR-mediated signaling by cleaving the adaptor protein TRIF at position C372, resulting in TRIF degradation [67]. The cleavage functions of the NS3-NS4A protease complex is one of the contributing factors in establishing a persistent infection in approximately 80% of those infected [87]

1.5.3 The NS3-NS4SA protease complex

NS3 contains the enzymatic activity of the protease complex and NS4 is a co-factor that enhances protease activity, stabilized NS3, and localizes the complex to

membranes. NS3 is composed of a serine protease and RNA helicase domain. The protease domain sits at the N-terminal region of the protein and contains a trypsin/chymotrypsin-like fold [88]. A catalytic triad (His57, Asp81, Ser139) maintains the protease activity [88]. The zinc binding pocket is located opposite of the catalytic triad and consists of the residues Cys97, Cys99, Cys145, His149. These residues coordinate zinc binding, which increases the thermal and conformational stability of NS3 [89]. In the absence of NS4A, the first 28 amino acids of the protease domain of NS3 are in a flexible loop that extends away from the core of the protein, and the remainder of the protease domain forms six beta barrels [90]. In this conformation, the catalytic triad is obstructed from potential substrates by the helicase domain, and the overall structure of NS3 is loosely arranged (Fig. 4). However, upon NS4A binding, the NS3 protease domain undergoes major conformational changes. NS4A binding to NS3 changes the flexible loop into an alpha-helix and another beta strand. Interactions with NS4A stabilizes the NS3 catalytic triad, positioning the His57 closer to the Ser139 for nucleophilic attack on the accessible serine hydroxyl group [91]. Therefore, NS4A functions to keep NS3 in a more tightly associated conformation. In the absence of NS4A, the N-terminal NS3 residues are flexible and extend away from the protein. NS4A binding to NS3 at the NS3-interaction domain also optimizes the geometry of the catalytic triad, which enhances protease activity [92].

Figure 4: NMR structure of NS3. Teal indicates the catalytic triad. Magenta indicates the NS3 helix α_0. Green indicates the NS3 loop. PDB entry 1CU1 [93].

1.5.3.1 Localization and Function

The localization of the NS3-NS4 protease complex largely depends on three factors: (1) the NS3 amphipathic helix alpha zero, (2) NS3 loop residues 38-40, and (3)) the NS4A transmembrane domain [93]. The NS3 amphipathic helix alpha zero comprises amino acid residues 12-23 of NS3 and forms a hydrophobic patch. These hydrophobic residues are highly conserved in NS3 among the different HCV genotypes. NMR analysis revealed that a construct of NS3 containing only these hydrophobic residues unfolded in water but folded into an alpha-helix in membrane mimetics, indicating that this portion of NS3 is also lipophilic and associates with membranes [93]. The NS3 loop also localizes the complex to membranes as it may contact the membrane

surface [93]. Last, NS4A directs the localization of the protease complex to intracellular membranes. NS3, without NS4A, localizes diffusely throughout the cytoplasm [94]. However, this NS3 is not stable, and addition of NS4A to NS3 drastically stabilizes the protein complex, increasing its intracellular half-life and preventing NS3 degradation [94, 95]. Further, studies that analyzed amino acid substitutions in the NS3 interaction domain of NS4A have shown reduced protease activity, suggesting that the NS3-NS4A protease complex must be formed for efficient protease activity [92, 96, 97]. What does NS3 helicase activity do?

NS3-NS4A localizes to the endoplasmic reticulum, where it is functions in virus replication [98]. NS3-NS4A also localizes to the mitochondria where it blocks MAVS-signaling by cleaving MAVS [63, 65, 99] . MAVS is also cleaved by NS3-NS4A at mitochondrial-ER contact sites, called the mitochondrial associated ER membrane (MAM) [100]. The MAM plays roles in inflammasome signaling, phospholipid transport to the mitochondria, and calcium signaling, and physically tethers the ER to the mitochondria (reviewed in [101]). Lastly, NS3-NS4A also localizes to peroxisomes, which are small membrane-enclosed organelles important for metabolism [102, 103]. Here, NS3-NS4A can cleave peroxisomal-localized MAVS [103, 104]. It was previously shown that cleavage of MAVS at the mitochondria/MAM results in blocking of downstream type I IFN induction, whereas cleavage of peroxisomal-localized MAVS results in blocking of downstream type III IFN induction [63, 65]. However, it has more recently been demonstrated that cleavage of peroxisomal-MAVS does not block more type III IFN compared to that blocked by cleavage of mitochondrial/MAM-localized MAVS [104]. More studies are needed to examine why NS3-NS4A cleaves MAVS localized on different membranes, and the implications of that cleavage on IFN induction.

The previously described localization profiles of NS3-NS4A also highlight the idea that depending on where NS3-NS4A localizes, its function is different (i.e. ER for replication and MAM for innate immune evasion). What directs this localization and functional change has largely been unexplored, and this is the central question leading to my dissertation research.

1.5.4 NS3-NS4A substrates

Cleavage of host and viral substrates is one of the hallmark functions of the NS3-NS4A protease complex. Cleavage of the HCV polyprotein by NS3-NS4A (and NS2 at the NS2-NS3 junction) is necessary for the viral cycle. NS3-NS4A cleaves at four junctions with the polyprotein: NS3-NS4A, NS4A-NS4B, NS4B-NS5A, and NS5A-NS5B. Cleavage at the NS3-NS4A junction occurs co-translationally and *in cis*. Cleavage at the other three junctions (NS4A-NS4B, NS4B-NS5A, NS5A-NS5B) occurs *in trans*. These cleavage events release the individual HCV proteins for their various roles in the HCV life cycle (reviewed in [105]).

While the exact mechanisms determining which substrates are cleaved by NS3-NS4A and how NS3-NS4A localizes to those substrates are not known, early studies on NS3-NS4A have identified a consensus cleavage sequence. The consensus sequence recognized by NS3-NS4A is a decapeptide sequence: NH2-P6-P5-P4-P3-P2-P1^P1'-P2'-P3'-P4'-OH, with NS3-NS4A cleaving the sissile bond located between P1 and P1' (indicated by ^) [106, 107]. HCV NS3 mutagenesis studies have determined that its substrate specificity is largely guided by placement of specific residues at the P6, P1, and P1' positions of the decapeptide sequence: 'D/E-X-X-X-X-C/T' | 'S/A-X-X-X' (where '|' indicates the point of cleavage and X indicates any amino acid) [108]. However, a cysteine at P1 seems to be the major determining factor of substrate specificity. While

multiple proteins contain this sequence, many are not cleaved by NS3-NS4A, suggesting that other factors, such as tertiary structure, may preclude NS3-NS4A substrate binding [63, 67]. As illustrated in Table 1, the known substrates of NS3/4A do not share the same sequence, suggesting that while the consensus sequence holds true for some substrates, other substrates can be targeted by NS3-NS4A. Indeed, Brass *et al.* has shown that in addition to the decapeptide sequence, other factors function as determinants of NS3 substrate selectivity. These factors include (1) NS3 amphipathic helix, (2) NS4A transmembrane domain, and (3) NS3 loop 38-40 [93]. These additional structural features may coordinate the positioning of the NS3 active site (as described above).

Table 1: NS3-NS4A cleavage substrates

Substrate	Amino acid at position									
	P6	P5	P4	P3	P2	P1	P1’	P2’	P3’	P4’
3-4A	D	L	E	V	V	T	S	T	W	V
4A-4B	D	E	M	E	E	C	S	Q	H	L
4B-5A	E	C	T	T	P	C	S	G	S	W
5A-5B	E	D	V	V	C	C	S	M	S	Y
MAVS	E	R	E	V	P	C	H	R	P	S
TRIF	$P_{(8)}$	S	S	T	P	C	S	A	H	L
Riplet	E	D	D	L	G	C	I	I	C	Q
DDB1	G	Q	L	V	T	C	S	G	A	F
Importin β1	D	G	V	V	A	C	A	A	G	L

TC-PTP(a)	K	E	S	V	K	Q	A	Q	Y	W
TC-PTP (b)	P	A	V	I	H	C	S	A	G	I
GPx8	A	Y	P	L	K	C	S	G	P	R

The first identified and most well-characterized host substrate of NS3-NS4A is MAVS, a central innate immune adaptor protein in the RIG-I signaling pathway. NS3-NS4A cleavage of MAVS at position C508 just upstream of the transmembrane domain has been detected biochemically, in cell culture, and in the infected human liver, highlighting the importance of this cleavage for HCV infection [63-66]. NS3-NS4A cleavage of MAVS blocks innate immune signaling during infection as it releases MAVS from intracellular membranes and the resulting cytoplasmic MAVS is unable to transduce RIG-I/MDA5 signals. NS3/4A cleavage of MAVS was originally thought to take place on mitochondria, however, immunoblot analysis of biochemically-purified subcellular fractions during HCV replication has now revealed that the MAM-localized MAVS is cleaved by NS3-NS4A, while surprisingly, the mitochondrial-MAVS remains uncleaved during HCV replication [100]. Additionally, NS3-NS4A cleaves MAVS localized on peroxisomes, [103, 104]. Future studies are needed to elucidate the mechanisms underlying the differential targeting of mitochondrial vs. MAM-localized MAVS.

Riplet, the E3 ubiquitin ligase that regulates the RIG-I signaling pathway upstream of MAVS, is also inactivated by NS3-NS4A [17]. One study has shown that Riplet contains canonical NS3-NS4A serine protease cleavage sites, is targeted at position C21, and mutation of these sites prevents cleavage by NS3-NS4A both in over-expression studies and also during HCV infection. Importantly, NS3-NS4A cleavage of

Riplet restricts Riplet-mediated ubiquitination of the RD of RIG-I, preventing the interaction of TRIM25 with RIG-I and subsequent downstream signaling [17]. However, in our studies, we were unable to detect Riplet cleavage (See Section 3.3 for further discussion). Nonetheless, Riplet is indeed important for blocking downstream signaling that induces IFN as we and others have shown that depletion of Riplet results in increased HCV replication, demonstrating that Riplet is required for the antiviral response to HCV [17]. Understanding why NS3-NS4A targets Riplet, when it already targets MAVS, which is downstream of Riplet in the RIG-I signaling cascade, and the mechanisms that regulate this differential targeting are only beginning to be explored. However, as my thesis research will illustrate, this seemingly redundant substrate targeting may be necessary to evade a secondary, noncanonical, RIG-I independent signaling pathway.

In addition to targeting proteins involved in the RIG-I/MAVS signaling branch of innate immunity, NS3-NS4A also cleaves and inactivates TRIF, the TLR3-signaling adaptor protein, at position C372 both *in vitro* and during infection [67]. Cleavage of TRIF blocks downstream TLR3-dependent signaling, prior to TLR3 bifurcation into the IRF3 and NF-κB branches of signaling, suggesting that this cleavage broadly limits IFN induction. TRIF has also been implicated as an adaptor protein for TLR3-independent signaling [109], and therefore NS3-NS4A cleavage of TRIF may prevent this non-canonical TLR3-independent innate immune signaling during HCV infection.

Additional NS3-NS4A substrates have been identified, yet their mechanism(s) of inactivation needs further characterization. These include damage-specific DNA binding protein 1 (DDB1), glutathione peroxidase 8 (GPx8), and T cell protein tyrosine phosphatase (TC-PTP) [110-112]. DDB1, a member of the Cul4-ubiquitin ligase

complex, is cleaved by NS3-NS4A at position C378 both *in vitro* and infection [110]. NS3-NS4A cleavage of DDB1 may be important for viral replication, and that either the cleavage of DDB1 or inactivation of the Cul4 ligase complex is necessary for HCV replication, as the DDB1 cleavage products did not impact viral replication.

The glutathione peroxidase GPx8 is cleaved by NS3-NS4A at position C11 both *in vitro* and in HCV infected liver biopsies. GPx8 contains an N-terminal cytosolic tip and a predicted transmembrane α-helix [111]. Importantly, GPx8 contains an alanine residue at position P6, and all other NS3-NS4A substrates contain an acidic residue, yet GPx8 is able to be cleaved by NS3-NS4A. This provides further support for the idea that strict membrane positioning of NS3-NS4A into membranes, in addition to the decapeptide cleavage sequence, dictates NS3-NS4A cleavage specificity. NS3-NS4A cleavage of GPx8 results in the removal of the cytosolic tip. While there is no known function of this cytosolic tip and whether or not a localization change occurs after GPx8 is unknown. It may be likely that removal of the cytosol-exposed portion of GPx8 may impact GPx8 protein-protein interactions. While the catalytic activity of GPx8 is important for HCV particle production, why NS3-NS4A cleaves GPx8 remains to be explored.

The last known NS3-NS4A substrate is TC-PTP, a protein involved in the epithelial growth factor receptor/Akt pathway [112]. NS3-NS4A cleaves TC-PTP at two distinct sites, C123 and C216 [112]. Interestingly, cleavage of TC-PTP is pro-viral, as cleavage results in down-regulation of TC-PTP, which increases Akt and promotes viral replication. TC-PTP is unique NS3-NS4A substrate in that it is the only known substrate that is cleaved at two sites with cleavage shown to be directly pro-viral. Future studies are needed to uncover why cleavage occurs at multiple sites, whether cleavage at both sites is pro-viral, and whether this cleavage event occurs in HCV-infected livers.

1.6 E3 ligases and RIG-I-mediated signaling

Posttranslational modifications, most notably phosphorylation and ubiquitination, regulate the antiviral innate immune response. These modifications regulate protein function by activating target proteins, by inducing localization changes in target proteins, and by altering protein-protein interactions of target proteins, or even by inducing degradation of target proteins. This section will highlight the roles of ubiquitin in antiviral signaling.

Ubiquitination is a multi-step enzymatic cascade requiring an E1 (activating enzymes), E2 (ubiquitin-conjugating enzymes), and E3 (ligating enzymes). Ubiquitin is a small molecule of 76 amino acids that gets added to the lysines of target proteins, either by covalent linkages or by unanchored linkages [113]. There are 7 lysine residues in ubiquitin (K6, K11, K27, K29, K33, K48, and K63) that can undergo such linkages, and each linkage provides a different fate for the targeted protein. For instance, ubiquitin linkages at position lysine-48 of the ubiquitin molecule (K48), cause proteasomal degradation of the substrate, while linkages on position lysine-63 of ubiquitin (K63) promote protein activation through mechanisms such as conformational changes or protein localization changes. The other types of ubiquitin linkages are less characterized, but are becoming more appreciated. There are approximately 5 E1 enzymes described in the literature, 100 E2 proteins, and approximately 600 E3 ligases. The E3 ligases catalyze the transfer of ubiquitin from the E2 to target substrates. There are 3 classes of E3 ligases: really interesting new gene (RING), homologous to the E6AP C-terminus (HECT), and RING-between-RING (RBR) (Reviewed in [114]). These classes differ mostly in the motif that binds to the E2 and in the mechanism of ubiquitin transfer from the E2 to the substrate. RING domain containing proteins encode a RING motif usually

at the N-terminus, and a PRY-SPRY motif at the C-terminus. The RING motif is $CX_2CX_{(9–39)}CX_{(1–3)}HX_{(2–3)}C/HX_2CX_{(4–48)}CX_2C$ with C representing cysteine residues, H representing histidine residues, and X representing any amino acid [115, 116]. RING proteins catalyze the direct transfer of ubiquitin from the E2 to the substrate, and play essential roles in antiviral immunity by ubiquitinating several innate immune proteins, including MAVS and RIG-I.

During RNA virus infection, MAVS is polyubiquitinated (K48) on lysine residues 7 and 10 at the amino terminus, resulting in its proteasome-mediated degradation of MAVS [117]. This ubiquitination of MAVS appears to be catalyzed by TRIM25, which also mediates the K63-linked ubiquitination of RIG-I. TRIM25 is also part of the RIG-I translocon and would thus be expected to be in proximity of MAVS to facilitate MAVS ubiquitination [22]. Other direct posttranslational modifications of MAVS that regulate antiviral signaling include phosphorylation and ubiquitination at several sites in the protein. Negative regulators of MAVS include several E3 ubiquitin ligases that catalyze the K48 ubiquitination of MAVS leading to degradation by the proteasome, as well as kinases such as polo-like kinase 1 (PLK1) that phosphorylate MAVS to prevent signaling factor recruitment [23].

RIG-I undergoes multiple ubiquitination events. As described previously, RIG-I is ubiquitinated by multiple E3 ligases, namely TRIM25 and Riplet. Early studies identified TRIM25 as being the primary E3 ligase for RIG-I activation, as ubiquitination of RIG-I by TRIM25 at K172 in the second CARD, allows RIG-I to form a translocon complex to interact with MAVS [18, 22]. However, recently, ubiquitination of RIG-I by the E3 ligase Riplet is becoming more appreciated as an important event in the activation of RIG-I. Riplet ubiquitinates RIG-I at multiple lysine residues in the RD to release RIG-I

autoinhibition Further, at the N-terminal end of RIG-I, multiple E3 ubiquitin ligases can ubiquitinate RIG-I, even at the same amino acid site, suggesting dynamic regulation of RIG-I activation and that compensatory ubiquitination events on RIG-I most likely occur. For instance, if K172 is unable to become ubiquitinated, other K residues in RIG-I can become ubiquitinated. RIG-I is also ubiquitinated by the ligases MEX3C and TRIM4, with TRIM4 also ubiquitinating RIG-I at K172, the same site of TRIM25-mediated ubiquitination (reviewed in [118]). The factors that trigger these ubiquitination events remains to be explored.

1.7 Summary of the work presented in this dissertation

My thesis work has focused on how a tyrosine residue (tyrosine-16) within the NS4A transmembrane domain regulates NS3-NS4A function in innate immune evasion. I have identified that mutation of tyrosine-16 to phenylalanine impacts NS3-NS4A targeting of Riplet, an E3 ligase, and subsequent IFN induction. In Chapter 2, I will discuss my work on identifying a non-canonical antiviral signaling that is regulated by NS4A tyrosine-16. In Chapter 3, I will discuss the role of NS4A tyrosine-16 in targeting Riplet and the implications of this targeting on virus replication. Taken together, this work has elucidated additional mechanisms of NS3-NS4A regulation of immune signaling, identified the existence of another signaling pathway that can limit HCV replication, and has highlighted that NS4A alone is sufficient for modulating interferon signaling.

2. NS4A Y16 evades a non-canonical antiviral signaling pathway

This chapter is adapted with permission from a manuscript entitled "Hepatitis C virus infection is inhibited by a non-canonical antiviral signaling pathway targeted by NS3-NS4A" published in Journal of Virology [119]. The authors are Christine Vazquez, Chin Yee Tan, and Stacy M. Horner.

2.1 Introduction

Several factors contribute to the ability of HCV to establish a chronic infection, including its ability to evade detection and dysregulate the host antiviral innate immune response through the actions of the HCV NS3-NS4A protease complex [87]. The NS3-NS4A protease is a protein complex formed between NS3, which contains protease and helicase domains, and NS4A. NS4A is a 54 amino acid protein that contains an N-terminal transmembrane domain, an NS3 interacting domain, and a C-terminal acidic domain [93]. The NS4A transmembrane domain anchors NS3 to membranes [94] and mediates NS4A dimerization [120]. NS3-NS4A has diverse functions in the HCV life cycle, with roles in HCV RNA replication, viral assembly, and innate immune evasion (reviewed in [105])[121]. The mechanisms that regulate these diverse functions of NS3-NS4A are not completely understood. However, it is known that NS4A directs the protease complex to distinct intracellular membranes to perform some of these functions: the ER for viral replication; and mitochondria and mitochondrial-ER contact sites (often referred to as mitochondrial-associated ER membranes (MAM)) for immune evasion [63, 65, 98, 100, 122].

Antiviral innate immune signaling against HCV can be initiated by the RNA sensor proteins RIG-I and MDA5 [4, 83, 123]. RIG-I is directly activated by multiple

ubiquitination events by E3 ubiquitin ligases, namely TRIM25 and Riplet, which binds to and adds K63-linked ubiquitin chains to RIG-I, but not MDA5 [17, 18, 124, 125]. Once activated, RIG-I and MDA5 signal to the adaptor protein MAVS to drive a signal transduction cascade that induces the phosphorylation of IRF3 and then the transcriptional induction of interferon (IFN)-β. HCV infected can also be sensed by TLR3, which signals via TRIF and IRF3 to induce antiviral innate immunity [126]. During HCV infection, NS3-NS4A cleaves and/or inactivates MAVS [63-66], TRIF [67] and Riplet [17] to block IRF3 activation [127].

Here, we aimed to uncouple the roles of NS3-NS4A in replication and immune evasion. We focused on the NS4A transmembrane domain and found a residue, Y16, which regulates a non-canonical, RIG-I-signaling-independent pathway.

2.2 Results

2.2.1 A Y16F substitution in NS4A disrupts replication of an HCV subgenomic replicon in Huh7 cells, but not in Huh-7.5 cells.

The transmembrane domain of NS4A contains two aromatic amino acids: a tryptophan at position 3 (W3) and a tyrosine at position 16 (Y16) (Fig. 5A). These two aromatic amino acids, which are conserved in all sequenced HCV strains in the Los Alamos HCV sequence database ([128] and Fig. 5A), are located at each end of the NS4A transmembrane domain at the lipid bilayer interface [93, 120]. Interestingly, aromatic residues at the termini of transmembrane domains are often important for positioning membrane proteins within lipid bilayers [129-131]. Therefore, we hypothesized that these residues may play a role in the proper localization and/or function of the NS3-NS4A protease complex during HCV infection. While both the W3

and the Y16 residues in NS4A are conserved across the eight known HCV genotypes, we chose to focus specifically on the Y16 residue (Fig. 5A)**,** with the goal of uncoupling the function of Y16 in HCV replication from targeting of innate immune substrates, such as MAVS and Riplet. As a prior study found that a Y16A substitution inhibited HCV replication [120], we made the more conservative phenylalanine mutation (Y16F) to maintain aromaticity at this position. Here, we analyzed the role of this amino acid in regulating HCV replication and innate immune regulation by NS3-NS4A.

To determine if the Y16F substitution in NS4A altered HCV replication, we first engineered this amino acid change into an HCV replicon encoding a G418 marker (HCV genotype 1B subgenomic replicon; HP replicon [83]). Following *in vitro* transcription, wild-type (WT) or Y16F HCV replicon RNA was electroporated into either liver hepatoma Huh-7.5 cells, which do not have functional RIG-I signaling due to the T55I mutation [83], or Huh7 cells, which have functional RIG-I signaling. In the Huh-7.5 cells, the number of G418-resistant colonies in the WT versus the Y16F HCV replicon-transduced cells was equivalent, indicating that WT and Y16F replicated similarly. However, in Huh7 cells, the Y16F HCV replicon had a reduced transduction efficiency (~3-fold) compared to the WT HCV replicon (Fig. 5B)**.** As control, we also measured the interaction of NS4A WT or Y16F with NS3 by co-immunoprecipitation and found that the Y16F substitution did not alter the interaction of NS4A with NS3, nor the ability of the NS3-NS4A protease to process the NS3-NS4A polyprotein junction (Fig. 5C). Together, these data reveal that the Y16F mutation results in reduced HCV replication in Huh7 cells, but not Huh-7.5 cells, suggesting that NS4A Y16F may regulate RIG-I-mediated innate immune signaling to promote HCV immune evasion and replication.

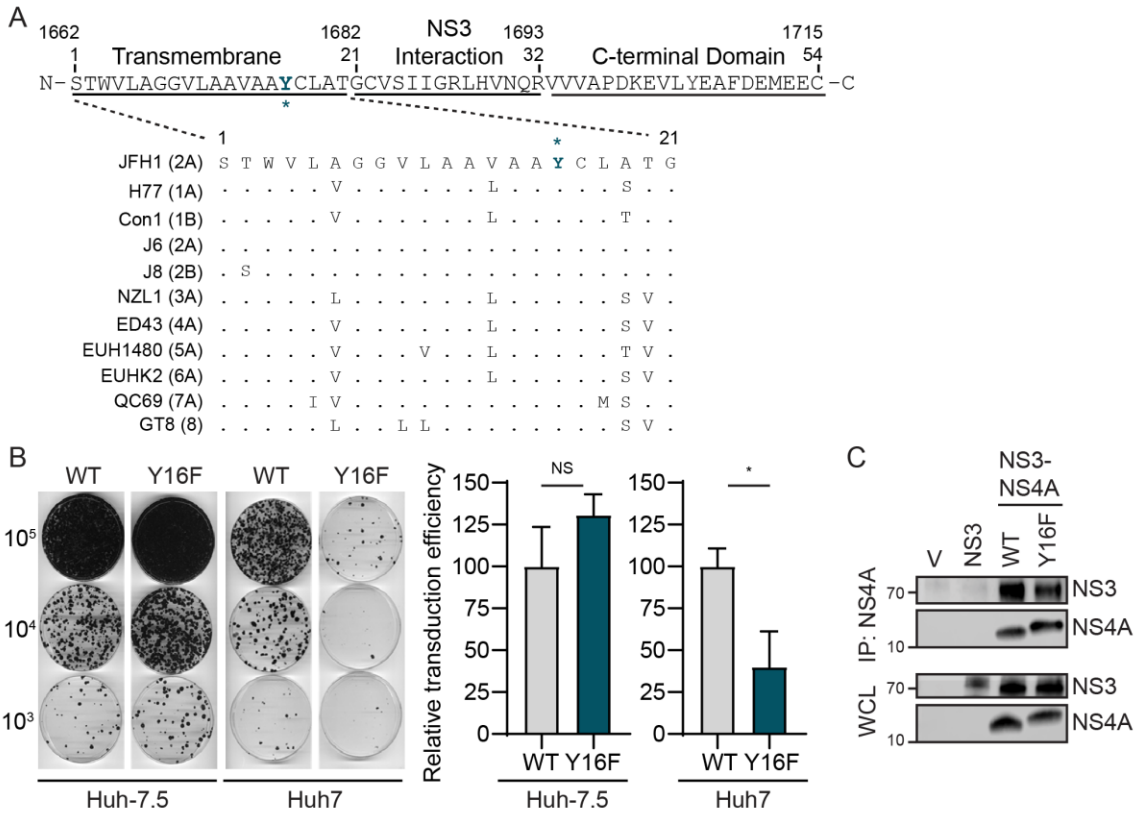

Figure 5: A Y16F substitution in NS4A disrupts replication of an HCV subgenomic replicon in Huh7 cells, but not in Huh-7.5 cells. **(A)** Amino acid sequence of NS4A, with the Y16 residue starred and indicated in teal. Numbers correspond with the amino acid position within NS4A (aa 1-54) or the full-length HCV polyprotein (aa 1662-1715). Strain names are listed as found in the Los Alamos HCV sequence database. Conserved amino acids are indicated with a dot, while differences are listed. **(B)** Representative images of Huh-7.5 or Huh7 cells electroporated with *in vitro* transcribed HCV subgenomic replicon RNA (HP, genotype 1B; WT or Y16F). Cells were plated in serial dilutions (2 x 10^5, 2 x 10^4, 2 x 10^3) and then stained with crystal violet after three weeks of G418 selection. Graphs show the relative transduction efficiency, which denote the % of colonies in Y16F transduced cells relative to WT. Bars indicate mean ± SEM (n = 3-4 biological replicates), with data analyzed by Student's *t*-test; *p < 0.05, NS = not significant. **(C)** Immunoblot analysis of anti-NS4A immunoprecipitated extracts or whole cell lysate (WCL) from 293T cells transfected with the indicated HCV proteins (genotype 1B) or vector (V). Panels are representative of three independent experiments.

2.2.2 RIG-I deletion does not restore HCV NS4A Y16F viral replication.

To determine if the Y16F substitution in NS4A specifically altered HCV replication in Huh7 cells during infection, we engineered the NS4A Y16F substitution into the full-length HCV infectious clone (JFH1, genotype 2A [75]). We generated low-passage viral stocks and confirmed that the Y16F mutation was maintained in the resulting virus by PCR amplification of the NS4A region and Sanger sequencing. We then infected Huh-7.5 or Huh7 cells with the HCV WT or Y16F virus, harvested protein lysates over a time course of infection, and measured HCV NS5A protein expression by immunoblot. We found that HCV NS5A protein levels were equivalent in Huh-7.5 cells infected with WT or Y16F HCV (Fig. 6A). However, in Huh7 cells, the level of NS5A protein from the Y16F virus was reduced as compared to WT HCV (Fig. 6B). To determine if this reduction in Y16F virus replication was due to an inability to block the innate immune response, we examined induction of *IFNB1* mRNA by RT-qPCR during infection with both WT and Y16F viruses and found that Y16F virus was unable to block induction of *IFNB1* mRNA as well as WT virus (Fig. 6C)**.** In addition to RIG-I, there are likely other genetic differences between Huh7 and Huh-7.5 cells. Thus, to determine if RIG-I was the factor accounting for the differential replication observed between WT and Y16F HCV in Huh7 cells versus Huh-7.5 cells, we generated Huh7-RIG-I KO cells using CRISPR/Cas9 genome editing. These Huh7-RIG-I KO cells contain a 252 nucleotide deletion that removes the start codon, preventing RIG-I protein expression (Fig. 6D). To confirm a loss of RIG-I signaling, we infected Huh7-RIG-I KO cells with Sendai virus (SV), a virus known to activate RIG-I signaling [83, 132], and observed no SV-mediated induction of RIG-I protein or signaling to the IFN-β promoter, which was restored upon over-expression of RIG-I [4, 83] (Fig. 6E).

We next infected these Huh7-RIG-I KO cells with either WT or Y16F HCV and measured HCV NS5A expression from lysates harvested over a time course of infection by immunoblotting. Surprisingly, we found that NS5A protein level from Y16F HCV was not restored to the level of WT in the Huh7-RIG-I KO cells (Fig. 6F). We then compared the production of infectious virus from the WT and Y16F viruses in each of these cell lines. In these assays, the supernatants of infected cells were used to infect naïve Huh-7.5 cells to determine the viral titer, which ultimately measures a second round of infection. We found that the while the Y16F virus harvested from Huh-7.5 cells resulted in a somewhat lower level of infectious virus as compared to WT (~40% lower), its level of infectious virus harvested from Huh7 or two independent clones of Huh7-RIG-I KO cells was significantly lower as compared to WT (now ~75% lower) (Figs. 6G, 6H, 6I). Taken together, these data suggest that NS4A Y16 regulates a RIG-I-independent signaling pathway that is non-functional in Huh-7.5 cells.

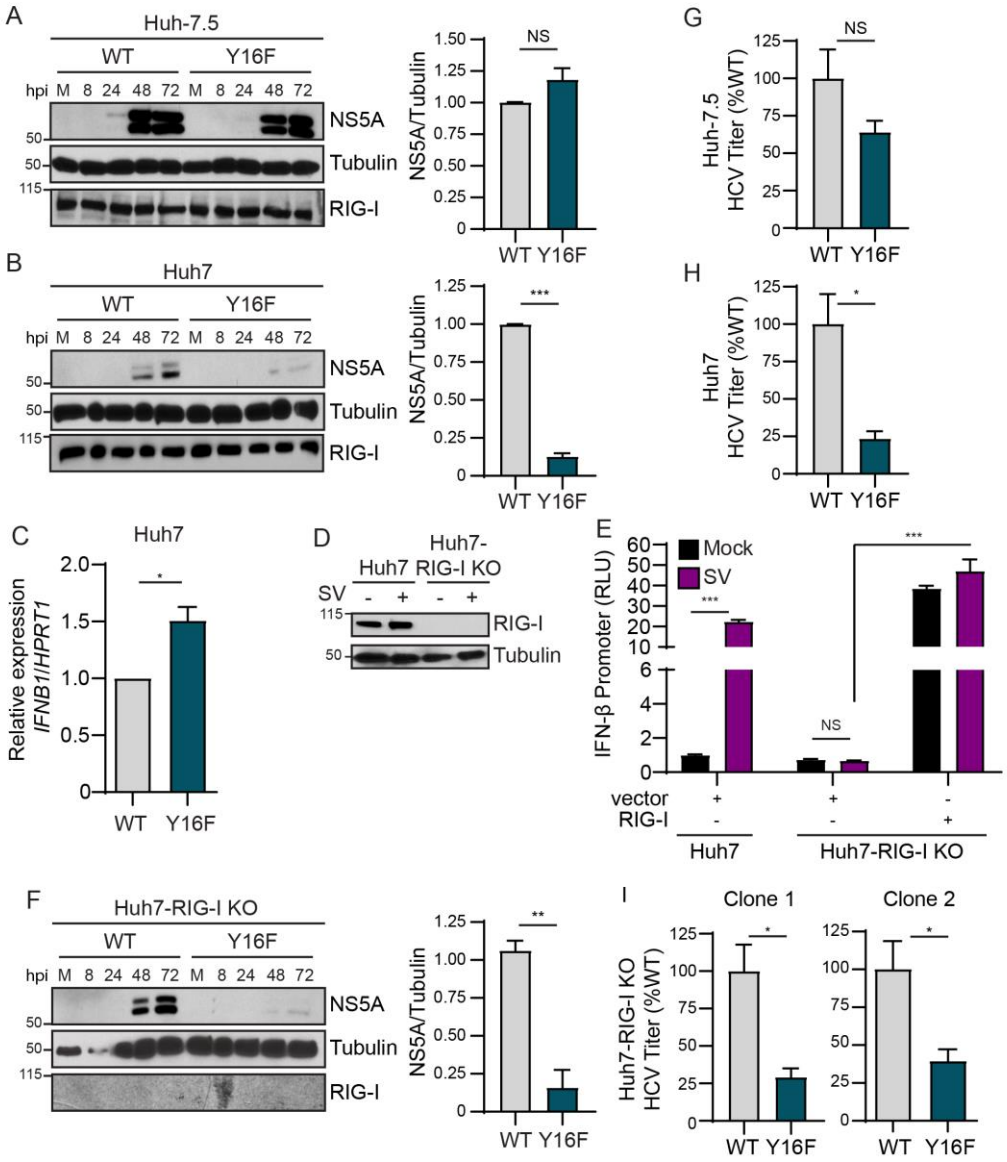

Figure 6: RIG-I deletion in Huh7 cells does not restore HCV NS4A Y16F replication. Huh-7.5 cells **(A)** or Huh7 cells **(B)** were infected with HCV, WT or NS4A Y16F (JFH1, MOI 0.3). Immunoblot analysis was performed on lysates extracted at the indicated hours post infection (hpi) or mock (M). Graphs directly to the right of each blot (here, and in (F)) show quantification of NS5A protein relative to Tubulin at 72 hpi (mean ± SEM; n = 3 biological replicates). **(C)** *IFNB1* expression relative to *HPRT1* from Huh7 cells infected with HCV, WT or NS4A Y16F (JFH1, MOI 1) at 72 hpi as analyzed by RT-qPCR, with data displayed as mean ± SEM (n = 3 biological replicates) **(D)** Immunoblot of extracts of Huh7 and Huh7-RIG-I KO cells that were mock- or Sendai virus (SV)-infected (20 h). **(E)** IFN-β promoter reporter luciferase expression of Huh7 and Huh7-

RIG-I KO cells expressing either vector or full-length RIG-I that were either mock- or SV-infected (20 h). Values show the mean ± SD (n = 3 technical replicates) in relative luciferase units (RLU). **(F)** Huh7-RIG-I KO cells were infected with HCV, WT or NS4A Y16F (JFH1, MOI 0.3). Immunoblot analysis was performed on lysates extracted at the indicated times or mock (M). The graph directly to the right of this blot show quantification of NS5A protein relative to Tubulin at 72 hpi (mean ± SEM; n = 3 biological replicates). **(G-I)** Focus forming assay of supernatants harvested from Huh-7.5 (G), Huh7 **(H)**, and Huh7-RIG-I KO (clone 1 and clone 2) **(I)** cells at 72 hpi (MOI 0.3). Data are presented as the percent HCV titer from Y16F relative to the WT (set at 100%) and show the mean ± SEM (n = 2 or 3 biological replicates). Data were analyzed by Student's *t*-test; *p < 0.05, **p < 0.01, ***p < 0.005, NS = not significant.

2.2.3 HCV NS3-NS4A Y16F retains the ability to cleave MAVS.

As NS4A Y16 is located at the membrane lipid bilayer interface [93, 120], and NS4A membrane interactions regulate the molecular mechanisms by which the NS3-NS4A protease targets substrates [120], we hypothesized that the Y16F substitution in NS4A may regulate NS3-NS4A cleavage of MAVS. To test this, we co-expressed NS3-NS4A with Flag-tagged MAVS and found that both NS3-NS4A WT and Y16F cleaved MAVS, while NS3-NS4A containing a mutation that inactivates the protease active site (S139A; SA) did not (Fig. 7A). We also found that MAVS cleavage was similar following HCV WT and Y16F infection in both Huh-7.5 and Huh7 cells (Fig. 7B). Further, in Huh7 cells that were either deleted of MAVS via CRISPR/Cas9 (Fig. 7B) or depleted of MAVS via shRNA (Fig. 7C), we found that Y16F viral replication was not restored to WT levels in either Huh7-MAVS KO cells, as measured by NS5A expression, or Huh7-shMAVS cells, as measured by relative HCV copy number. Together, this reveals that MAVS does not differentially regulate HCV WT or Y16F replication and that the NS4A Y16F substitution does not alter MAVS cleavage by NS3-NS4A.

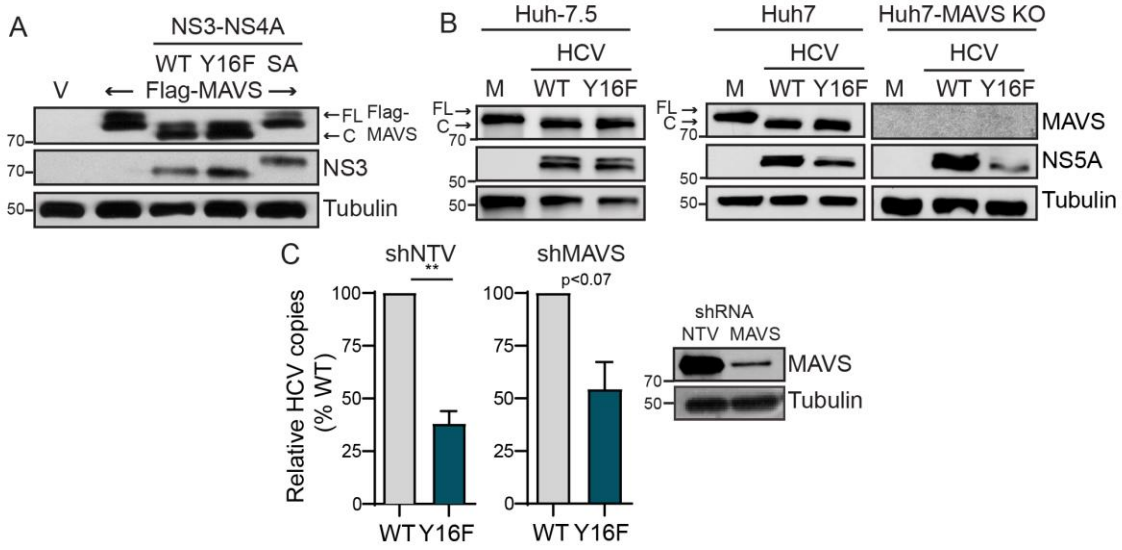

Figure 7: HCV NS3-NS4A Y16F retains the ability to cleave MAVS. (A) Immunoblot analysis of lysates harvested from Huh7 cells expressing NS3-NS4A (WT, Y16F, or SA (NS3 active site mutant S139A)) and vector (V) or Flag-MAVS. Arrows indicate the full-length (FL) and cleaved (C) forms of MAVS. **(B)** Immunoblot analysis of lysates harvested at 72 hpi from Huh-7.5, Huh7, or Huh7-MAVS KO cells that were either mock-infected (M) or infected with HCV, WT or NS4A Y16F (JFH1, MOI 0.3). Arrows indicate the full-length (FL) and cleaved (C) forms of MAVS. **(C)** Intracellular HCV RNA levels in Huh7 cells expressing non-targeting shRNA (shNTV) or MAVS shRNA (shMAVS) infected with HCV, WT or NS4A Y16F (JFH1, MOI 0.3) and harvested at 72 hpi, as measured by RT-qPCR. Data are presented as relative HCV copies from Y16F relative to WT (set at 100%) and show the mean ± SEM (n = 2 biological replicates). Immunoblots to the right of the graph shows MAVS protein expression in the shNTV and shMAVS cell lines. Data were analyzed by Student's *t*-test; **p < 0.01 or as indicated.

2.2.4 IRF3 deletion in Huh7 cells restores HCV Y16F replication to the levels of HCV WT.

We next wanted to determine if the signaling pathway that inhibits HCV Y16F replication requires the IFN-β transcription factor IRF3 (reviewed in [133]). We first generated Huh7-IRF3 KO cells using CRISPR/Cas9 genome editing and determined IRF3 expression and function in these cells by sequencing the IRF3 genetic locus, analyzing IRF3 expression by immunoblot, and confirming that loss of IRF3 prevented

SV-mediated antiviral signaling to the IFN-β promoter and that this signaling was restored by IRF3 over-expression (Figs. 8A-8B)**.** To determine if IRF3 regulates HCV Y16F replication, we infected Huh7 or Huh7-IRF3 KO cells (two independent clones) with either HCV WT or Y16F, measured HCV NS5A expression by immunoblot, and measured release of infectious virus by focus forming assay. While the levels of NS5A expression and infectious Y16F virus were reduced relative to the WT in parental Huh7 cells, as before, these levels were restored to that of WT virus in two independent clones of Huh7-IRF3 KO cells (Figs. 8C-8D)**.** Together, these data reveal that NS4A Y16 regulates an IRF3-dependent signaling pathway that can inhibit HCV replication.

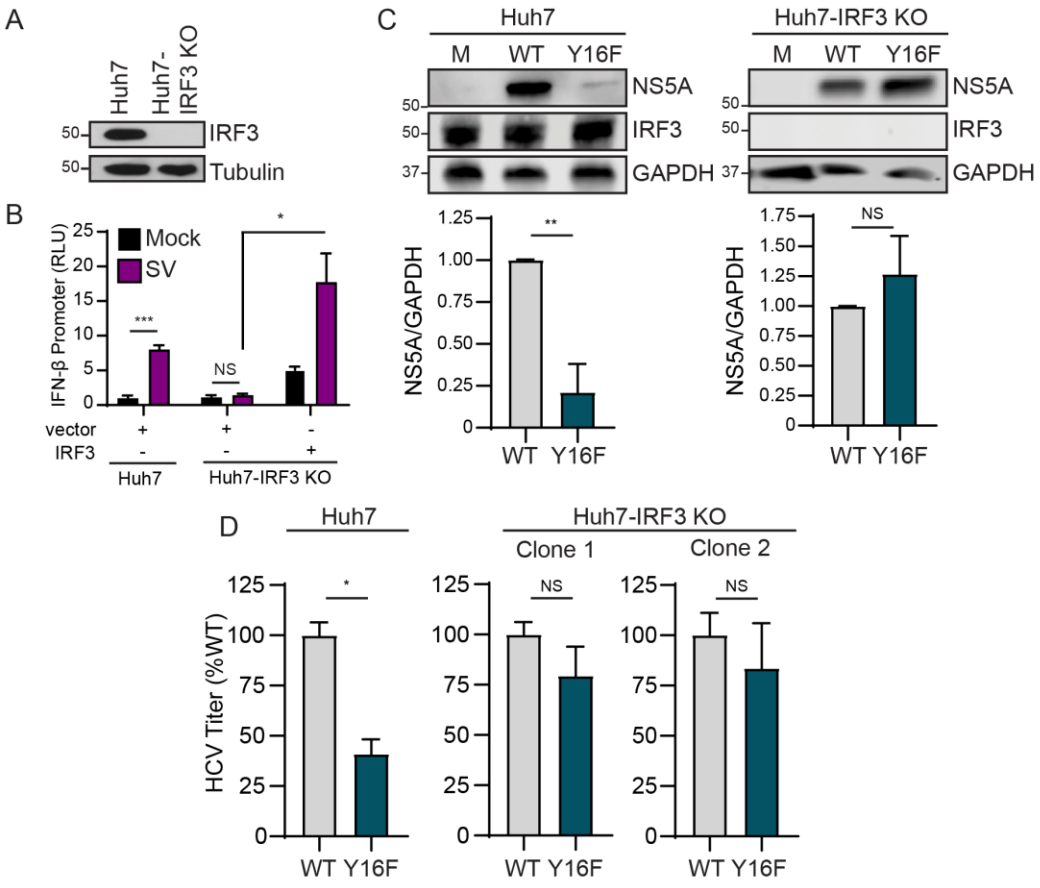

Figure 8: IRF3 deletion in Huh7 cells restores HCV Y16F replication to the level of HCV WT. (A) Immunoblot of extracts of Huh7 and Huh7-IRF3 KO cells. **(B)** IFN-β promoter reporter luciferase expression of Huh7 and Huh7-IRF3 KO cells expressing either vector or IRF3 that were either mock- or SV-infected (20 h). Values show the mean ± SD (n = 3 technical replicates) in relative luciferase units (RLU). **(C)** Immunoblot analysis of lysates harvested at 72 hpi from Huh7 and Huh7-IRF3 KO cells infected with HCV, WT or NS4A Y16F (JFH1, MOI 0.3). Graphs below each blot show quantification of NS5A protein relative to GAPDH (mean ± SEM; n = 3 biological replicates). **(D)** Focus forming assay of supernatants harvested at 72 hpi from Huh7 or Huh7-IRF3 KO cells (clone 1 and clone 2) infected with HCV, WT or NS4A Y16F (MOI 0.3). Data are presented as the percent of HCV titer from Y16F relative to WT (set at 100%) and show the mean ± SEM (n = 2 biological replicates). Data were analyzed by Student's *t*-test; *p < 0.05, **p < 0.01, ***p < 0.005, NS = not significant.

2.2.5 HCV NS3-NS4A Y16F does not block IRF3 activation.

As our data suggested that HCV Y16F replication was inhibited by IRF3-mediated signaling, we hypothesized that NS3-NS4A Y16F would be unable to block IRF3 activation. During viral infection, IRF3 is activated by a multi-step process, including phosphorylation by the kinases TBK1 and IKKε, resulting in dimerization, and finally translocation from the cytosol to the nucleus, where it activates transcription of IFN-β [134]. Importantly, it is well-known that over-expression of the WT NS3-NS4A protease can block this nuclear translocation of IRF3 in response to virus infection [65, 85]. Therefore, we measured the ability of WT or Y16F NS3-NS4A to block the nuclear translocation of endogenous IRF3 in response to SV. IRF3 translocated to the nucleus in 8% of the SV-infected cells, as measured by immunofluorescence assay (Figs. 9A-9B). While the NS3-NS4A WT blocked nearly all of this nuclear translocation, NS3-NS4A Y16F only partially blocked this nuclear translocation, as compared to the SV-infected cells in the absence of HCV protein (Figs. 9A-9B), revealing that NS3-NS4A Y16F has a reduced ability to inhibit IRF3 activation.

To test if NS3-NS4A Y16F similarly did not block IRF3 activation in the context of HCV replication, we utilized the HCV replicon system, which activates RIG-I signaling but prevents the transduction of IRF3 signaling by NS3-NS4A cleavage of MAVS, to prevent HCV or SV-induced innate immune signaling [85]. We infected control cells and cells stably expressing either WT or Y16F subgenomic replicons with SV and then measured induction of IFN-β and several ISGs by RT-qPCR. While the WT HCV replicon prevented SV-mediated induction of all ISGs tested, the HCV Y16F replicon did not block induction of *IFNB1*, *IFNL1*, *IFITM1*, and *RSAD2*, and only partially blocked induction of several other ISGs (Fig. 9C). Taken together, these data reveal that the

Y16F substitution prevents NS3-NS4A from fully blocking IRF3 activation and signaling in response to viral infection.

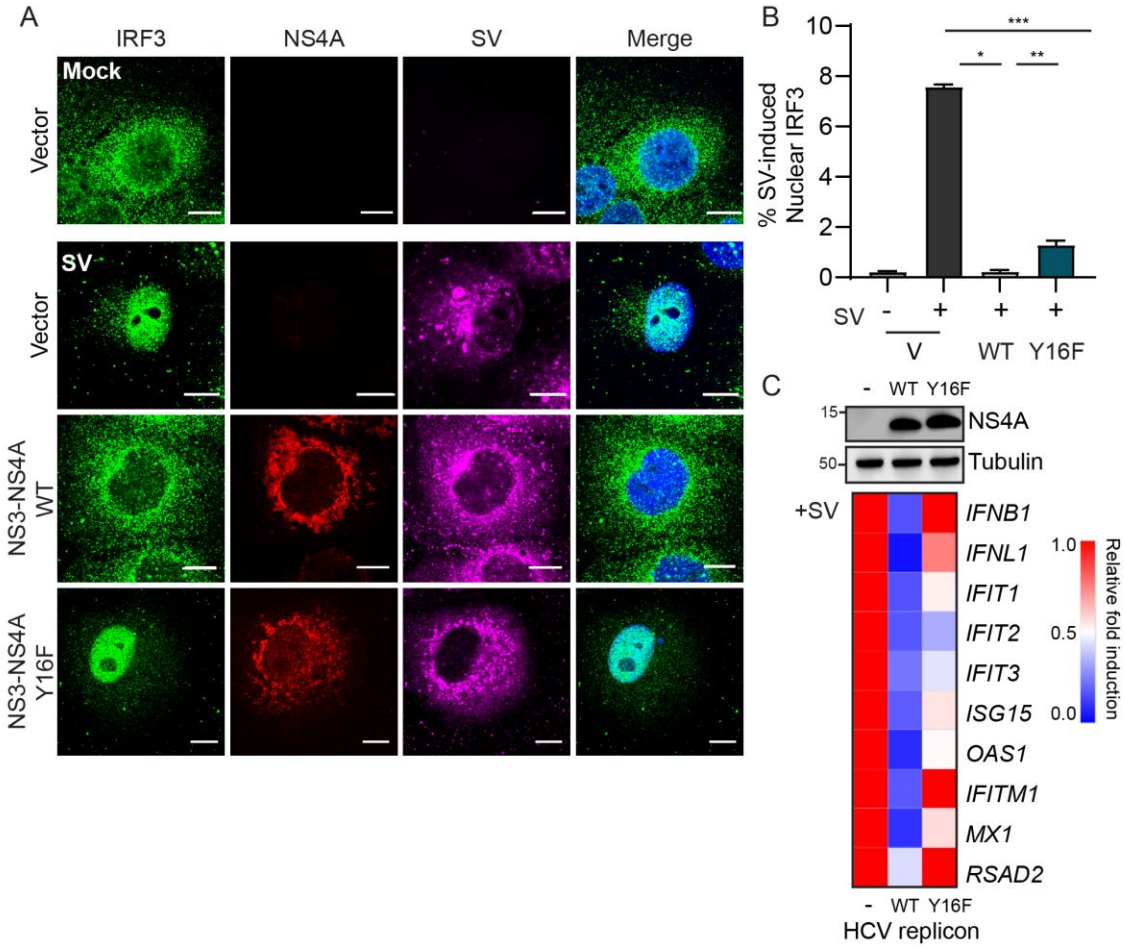

Figure 9: HCV NS3-NS4A Y16F does not block IRF3 activation. **(A)** Confocal micrographs of Huh7 cells expressing either NS3-NS4A WT or Y16F (genotype 1B), or vector, that were either mock- or SV-infected (20 h) and immunostained with anti-IRF3 (green), anti-NS4A (red), or anti-SV (magenta). Nuclei were stained with Hoescht (blue). Scale bar: 10 μm. **(B)** Quantification of the percent of cells positive for SV (and either WT or Y16F NS3-NS4A, as indicated) that had nuclear IRF3. Data are displayed as mean ± SEM (n = two biological replicates of >500 cells counted in each condition and replicate). Data were analyzed by one-way ANOVA; **p < 0.01, ***p < 0.005. **(C)** Immunoblot analysis of lysates from Huh7 (-), Huh7-HP WT replicon, or Huh7-HP Y16F replicon cells, and a heatmap (below) that shows the mean relative fold induction (SV-infected/mock-infected, relative to *HPRT1*) of specific genes as measured by RT-qPCR

analysis of RNA from mock- or SV-infected (20 h) Huh7, Huh7-HP WT replicon, or Huh7-HP Y16F replicon cells from three biological replicates.

2.2.6 TBK1 inhibition restores HCV Y16F viral replication.

Since IRF3 deletion was able to restore Y16F viral replication to the level of HCV WT, we wanted to determine whether the signaling pathway regulated by Y16 would require TBK1 or IKKε, the kinases that phosphorylate and activate IRF3. To this end, we utilized the TBK1/IKKε inhibitor, BX795 [135]. First, we verified that the treatment of BX795 blocks phosphorylation of TBK1 (p-TBK1) induced by SV by immunoblot (Fig. 10A)**.** We then treated Huh7 cells with either DMSO or BX795, mock-infected or infected with HCV WT or Y16F, and then measured NS5A protein expression from lysates harvested at 72 hours post infection. While the level of NS5A expression of the Y16F virus in the DMSO-treated cells was reduced compared to the WT virus, as seen before in the parental Huh7 cells, the levels were similar in the BX795-treated cells (Fig. 10B), indicating that Y16 regulates a TBK1-dependent signaling pathway that can inhibit HCV infection.

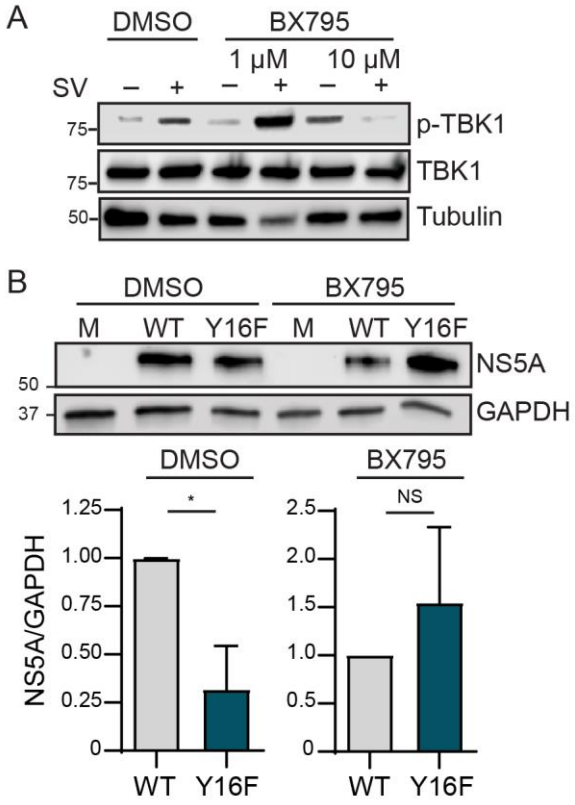

Figure 10: TBK1/IKKε inhibition restores Y16F virus replication. **(A)** Immunoblot analysis of lysates harvested from DMSO-treated or BX795 (1 μM or 10 μM)-treated Huh7 cells that were either mock-infected (M) or infected with SV (20 h). **(B)** Immunoblot analysis of lysates harvested at 72 hpi from Huh7 cells either pre-treated for one hour with DMSO or with BX795 (10 μM), infected with HCV, WT or NS4A Y16F (JFH1, MOI 0.3). Graphs below each blot show quantification of NS5A protein relative to GAPDH (mean ± SEM; n = 3 biological replicates). Data were analyzed by Student's *t*-test; *p < 0.05, NS = not significant.

2.3 Discussion

Our results identify a new antiviral signaling program regulated by HCV NS3-NS4A. We found that mutation of NS4A Tyr-16 to phenylalanine, in both the context of an HCV subgenomic RNA replicon and in the context of fully infectious HCV, results in reduced viral replication in Huh7 cells, but not in Huh-7.5 cells. We show that both NS3-

NS4A WT and Y16F cleave MAVS. We found that HCV containing an NS4A Y16F substitution in two HCV genotypes, either the JFH1 genotype 2A virus or the HP genotype 1B subgenomic replicon, has lower levels of replication than WT in Huh7 cells (Fig. 5B, Fig. 6A and 6B), but that both the WT and Y16F viruses have similar levels of replication in Huh-7.5 cells or in Huh7-IRF3 KO cells (Fig. 6B, Figs. 8C-8D). Although we did find that in experiments that assessed viral titer, the Y16F virus from Huh-7.5 cells had a reduced viral titer as compared to the WT. This reduction (~50%) was not as much as that of virus harvested from the Huh7 parental or Huh7-RIG-I KO, (~80%). Similar to our findings, Kohlway and colleagues found that the replication of a genotype 2A subgenomic replicon (pYSGR-JFH1/GLuc) containing this Y16F substitution was not altered in Huh-7.5 cells (7), while Brass and colleagues did find reduced replication of a Y16F genotype 1B subgenomic replicon (pCon1/SG-Neo(I)/AflII) in Huh-7.5 cells (5). While it is unclear what mediates the difference in our HCV replication results from those of Brass and colleagues, it is possible that this could be due to differences in the replication fitness of the replicons used or that Huh-7.5 cells from different labs do not have the same expression levels of Riplet (discussed in Chapter 3).

Our results suggest that HCV activates a signaling cascade to IRF3 that is independent of both RIG-I and MAVS. The following pieces of evidence presented within this manuscript support the existence of this pathway: (1) NS3-NS4A WT and Y16F both cleave MAVS (Fig. 7), (2) NS3-NS4A WT, but not Y16F, blocks SV-mediated IRF3 activation and induction of ISGs (Fig. 6; Fig. 9**)**; (3) WT and Y16F viruses only grow equivalently to each other in cells that lack both RIG-I or lack IRF3 (Fig. 5-6; Fig. 8). While the identification of this RIG-I-MAVS independent signaling cascade that induces IRF3 activation and IFN-β was surprising to us, others have shown that infection of RIG-I

KO mouse embryonic fibroblasts with vesicular stomatitis virus, known to be sensed by only RIG-I [136], does result in a small induction of IFN-β mRNA, even though other stimuli do not induce IFN-β in these cells [125]. Thus, it is possible that in our human Huh7-RIG-I KO cells, ISGs are induced during HCV infection to limit Y16F viral replication.

Taken together, this work has revealed a residue within the NS4A transmembrane domain, Y16, that uncouples replication from immune activation. For immune activation, NS4A Y16 regulates a signaling pathway that is RIG-I and MAVS-independent, but IRF3-dependent. The full identity of this signaling pathway remains to be explored.

2.4 Materials and Methods

2.4.1 Cell culture.

Huh7 and Huh-7.5 [83] cells (gift of Dr. Michael Gale Jr., University of Washington), as well as 293T cells (ATCC; CRL-3216), were grown at 37^{o}C with 5% CO_2 in Dulbecco's modification of eagle's medium (DMEM; Mediatech) supplemented with 10% fetal bovine serum (FBS; HyClone), and 25 mM 4-(2-hydroxyethyl)-1-piperazineethanesulfonic acid (HEPES; Thermo Fisher), referred to as complete DMEM (cDMEM). Huh7 and Huh-7.5 cells were verified using the Promega GenePrint STR kit (DNA Analysis Facility, Duke University), and all cells were tested and found to be *Mycoplasma*-free using the LookOut PCR Detection Kit (Sigma).

2.4.2 Plasmids and transfections.

These plasmids were used in this study: pEF-NS3, pEF-NS3-NS4A (genotype 1B), pEF-NS3-NS4A S1165A [137]; pHCV-HP WT (containing the following 7 amino acid

changes: NS3 (P1115L, K1609E), NS4B (Q1737R), NS5A (P2007A, L2198S, S2236P), and NS5B (V2971A)) and pHCV-HP ΔNS5B [138]; pEF-Tak-Flag MAVS [65]; pCR-BluntII-TOPO (Addgene #41824) [139], phCas9 (Addgene #41815) [139]; pCMV-Renilla and pGL4.74 [hRluc/TK] (Promega); pIFN-β-Luc [140]; pEF-Tak-Flag and pEF-Tak Flag RIG-I [141]; pEGFP-C1-IRF3 [142]; psJFHI-M9 WT [75]; pX330 (Addgene #42230) [143]; pcDNA-Blast [144]; pPAX2 and pMD2.G (Addgene #35002 [145]; Addgene #12259); and pCMV-Flag-IRF3 WT [146]. psJFHI-M9 Y16F, pEF-NS3-NS4A Y16F, pHCV-HP-Y16F, were generated by QuikChange site-directed mutagenesis (Stratagene) of psJFHI-M9, pEF-NS3-NS4A, and pHCV-HP. To generate the RIG-I CRISPR guide RNA plasmids (pCR-BluntII-Topo-sgRIGI-I and pCR-BluntII-Topo-sgRIGI-2), sgRNA oligonucleotides were annealed and inserted into *AflII*-digested pCR-BluntII-Topo by Gibson Assembly (New England Biolabs). To generate the IRF3 and MAVS CRISPR guide RNA plasmids, sgRNA oligonucleotides were annealed and inserted into *BbsI*-digested pX330 (pX330-sgIRF3; pX330-sgMAVS). All oligonucleotide sequences are listed in Table 1. The sequences of all plasmids were verified by DNA sequencing and are available upon request. DNA transfections were done using FuGENE6 (Promega) according to manufacturer's instructions.

2.4.3 Generation of knock out (KO) cell lines.

Huh7-RIG-I KO cells were generated by CRISPR/Cas9, using two guides targeting the intron before exon 1 (sgRNA 1) and within exon 1 (sgRNA 2) that were designed with the CRISPR design tool (http://crispr.mit.edu). pCR-BluntII-Topo-sgRIGI-I and pCR-BluntII-Topo-sgRIGI-2, along with phCas9, which expresses Cas9 and neomycin (G148) resistance, were transfected into Huh7 cells. Huh7-IRF3 KO cells were

generated by CRISPR/Cas9 using a single guide that targets exon 2 [147]. Huh7-MAVS KO cells were generated by CRISPR/Cas9 using a single guide that targets exon 5 [148]. pX330-sgMAVS and pX330-sgIRF3, along with pcDNA-Blast (which encodes blasticidin resistance), were transfected into Huh7 cells. In both cases, cells were re-plated the day after transfection at limiting dilutions into 15 cm dishes and then incubated with cDMEM containing either 0.4 mg/ml geneticin (G418; Life Technologies) for 5 days or 0.2 µg/ml blasticidin for 3 days. Individual cell clones were then selected and expanded. Isolated clones were screened for either RIG-I, MAVS, or IRF3 protein expression by immunoblot. Genomic DNA was isolated from candidate RIG-I or IRF3 KO cell clones using the QuickExtract DNA extraction solution (Epicentre). Genomic DNA isolated from the RIG-I, MAVS, or IRF3 KO cell clones was then amplified by PCR using primers spanning exon 1 for RIG-I, exon 5 for MAVS, or exon 2 for IRF3 (see Table 2). The resulting amplicons were cloned into pCR4-TOPO TA (Invitrogen) and Sanger sequenced. For RIG-I, all five of the sequenced genomic DNA clones had the start codon and exon 1 removed (four clones: 252 bp deletion and 1 clone: 250 bp deletion). For MAVS, all six of the sequenced genomic DNA clones contained a 128 bp insertion at the beginning of exon 5 that causes a frame shift resulting in a premature stop codon within exon 5. For IRF3, all five of the clones sequenced had a 4 bp deletion at the beginning of exon 2 that causes a frame shift resulting in a premature stop codon within exon 2.

2.4.4 Generation of shRNA cell lines.

Huh7 cells were either mock-infected or infected with Sigma MISSION TRC shRNA lentiviral particles (clone number TRC N0000148945) or non-targeting control (MISSION non-targeting shRNA, Sigma) at an MOI 2 in cDMEM containing 8 µg/ml

hexadimethrine bromide (Sigma). The following day, media was replenished with cDMEM. 48 hours post lentiviral infection, cDMEM containing 2μg/ml puromycin was added to the cells until mock cells died (3 days). Puromycin-resistant cells were harvested as pools, and cells were verified as transduced by immunoblot for MAVS.

2.4.5 HCV replicons.

RNA was *in vitro* transcribed (MEGAscript T7 transcription kit; Thermo Fisher) from *Sca*I-digested HP-HCV replicon plasmid DNA, either WT, Y16F, or ΔNS5B. The *in vitro* transcribed RNA was treated with DNase (Thermo Fisher), purified by phenol-chloroform extraction, and integrity verified on a denaturing gel. For electroporation, 1 μg of HCV replicon RNA was mixed with 4 x 10^6 Huh7 or Huh-7.5 cells in cold 1X phosphate buffered saline (PBS) in a 4 mm cuvette and then electroporated at 960 μF and 250 V with a Gene Pulser Xcell system (Bio-Rad). Electroporated cells were plated into 10 cm plates at 2 x 10^5, 2 x 10^4, 2 x 10^3 cells per dish, along with 2 x 10^5 cells that had been electroporated with ΔNS5B RNA. Four hours post electroporation, cells were washed three times with 1X PBS and then once with cDMEM. At twenty-four hours post electroporation, media was changed to cDMEM supplemented with 0.4 mg/ml G418. Following three weeks of G418 selection, cells were fixed and stained with crystal violet in 20% methanol. Colonies from triplicate plates were counted to determine the relative transduction efficiency, expressed as the percentage of Y16F colonies that were stably transduced relative to WT. Huh7-HP WT and Huh7-HP Y16F replicon cell lines were generated by isolating and expanding single clones. The presence of the HCV replicon was determined by sequencing the NS4A-containing region following cDNA synthesis on

extracted RNA (RNeasy RNA extraction kit, Qiagen) and PCR amplification of the NS4A region. Oligonucleotides used for PCR and sequencing are listed in Table 2.

2.4.6 HCV stock generation and infections.

HCV JFH1-M9 WT and Y16F virus stocks were generated as described previously [75]. The sequence of the virus at NS4A was confirmed after each passage by sequencing nested PCR products from generated cDNA using the oligonucleotides indicated in Table 1, as previously described [121]. For HCV infections, cells were incubated in a low volume of serum-free DMEM containing virus at a multiplicity of infection (MOI) of 0.3 for 2-3 hours, after which cDMEM was replenished. To quantify virus, cellular supernatants were analyzed by focus forming assay.

2.4.7 Focus forming assay.

To measure HCV titer, supernatants from infected cells were serially diluted and then used to infect naïve Huh-7.5 cells in triplicate wells of a 48-well plate for 3 hours. At 48 hours post infection, cells were washed with PBS and fixed with 4% methanol-free paraformaldehyde (Sigma) for 30 minutes, and then washed again with PBS. Cells were then permeabilized (0.2% Triton-X-100 (Sigma) in PBS), blocked (10% FBS in PBS), and immunostained with a mouse anti-HCV NS5A antibody (1:500). Infected cells were visualized following incubation with horseradish peroxidase (HRP)-conjugated secondary mouse antibody (1:500; Jackson ImmunoResearch) and VIP Peroxidase Substrate Kit (Vector Laboratories). Foci were counted at 10X magnification, and viral titer was calculated using the following formula: (dilution factor x number of foci x 1000)/volume of infection (in µl), resulting in units of focus forming units / ml (FFU/ml).

2.4.8 Immunoblotting.

Cells were lysed in a modified RIPA buffer (10 mM Tris pH 7.5, 150 mM NaCl, 0.5% sodium deoxycholate, 1% Triton X-100) supplemented with protease inhibitor cocktail (Sigma) and phosphatase inhibitor cocktail (Millipore), and post-nuclear supernatants were harvested by centrifugation. Protein concentration was determined by Bradford assay, and 10 µg quantified protein was resolved by SDS/PAGE, transferred to either PVDF (for NS4A) or nitrocellulose membranes using either the Trans-Blot Turbo System (BioRad) or a wet system (BioRad), and blocked with either 3% bovine serum albumin (Sigma) in PBS with 0.1% Tween (PBS-T) or 10% FBS in PBS-T. Membranes were probed with specific antibodies against proteins of interest, washed 3X with PBS-T, and incubated with species-specific HRP-conjugated antibodies (Jackson ImmunoResearch, 1:5000), washed again 3X with PBS-T, and treated with Clarity enhanced chemiluminescence substrate (BioRad). Membranes were then imaged on X-ray film or by using a LICOR Odyssey FC. Immunoblots imaged using the LICOR Odyssey FC were quantified with ImageStudio software, and raw values of the protein of interest were normalized to those of controls (either Tubulin or GAPDH, as indicated). For immunoblots developed on film, Fiji was used [149]. ImageStudio and Fiji give similar quantification results when compared directly.

2.4.9 Immunoprecipitation.

Quantified protein (between 80-160 µg) was incubated with protein-specific antibodies (either R anti-HA (Sigma) or anti-NS4A) in PBS at 4^{o}C overnight with head over tail rotation. The lysate/antibody mixture was then incubated with either Protein A

(for Flag-Riplet experiments) or Protein G Dynabeads (Invitrogen) for 2 hours. Beads were washed 3X in either PBS or RIPA for immunoprecipitation and eluted in 2X Laemmli Buffer (BioRad) supplemented with 5% 2-mercaptoethanol at 50^{o}C for 5 minutes. Proteins were resolved by SDS/PAGE and subjected to immunoblotting as described above.

2.4.10 Immunofluorescence and confocal microscopy.

Huh7 cells in 4-well chamber slides were fixed in 4% formaldehyde, permeabilized with 0.2% Triton-X-100, and immunostained with the following antibodies: mouse anti-HCV NS4A (Genotype 1B, 1:100, Virogen), rabbit anti-HA (1:100, Sigma), rabbit anti-IRF3 (1:100, Cell Signaling Technology) and rabbit anti-Sendai virus (SV) (1:1000, MBL International). Secondary antibody incubations were done with Alexa Fluor conjugated antibodies (Thermo Fisher) and with Hoescht (Thermo Fisher) for 1 hour. Following antibody incubations, slides were washed with 1X PBS, and mounted with ProLong Gold Antifade mounting medium (Invitrogen). Samples were imaged on a Zeiss 780 Upright Confocal using a 63X/1.25 oil objective and the 405, 488, 561, and 633 laser lines with pinholes set to 1 AU for each channel (Light Microscopy Core Facility, Duke University). Imaging analysis was done using Fiji software [149].

2.4.11 Antibodies.

Antibodies used for immunoblot and immunofluorescence analysis include: mouse anti-HCV NS4A (Genotype 1B, 1:1000, Virogen), mouse anti-HCV NS3 (Genotype 1B, 1:1000, Adipogen), mouse anti-HCV NS5A (Genotype 2A, 1:1000, clone 9e10, gift of Dr. Charles Rice, Rockefeller University), mouse anti-Tubulin (1:5000, Sigma), mouse anti-RIG-I (1:1000, Adipogen), anti-Flag-HRP (1:2500, Sigma), rabbit

anti-Flag (1:1000, Sigma), rabbit anti-MAVS (1:1000, Bethyl Laboratories), mouse anti-IRF3 (1:1000, gift from Dr. Michael Gale Jr., University of Washington [134]), rabbit anti-IRF3 (1:100, Cell Signaling Technology), rabbit anti-TBK1 (1:1000, Cell Signaling Technology), rabbit anti-phospho-TBK1 (1:1000, Cell Signaling Technology), mouse anti-V5 (1:1000, Sigma), mouse anti-HA (1:1000, Sigma), rabbit anti-GAPDH (1:1000, Cell Signaling Technology), Hoescht (1:500, Thermo Fisher), Alexa Fluor conjugated secondary antibodies (1:500, Life Technologies), rabbit anti-SV (1:1000, MBL International), mouse anti-Riplet (1:500, gift from Dr. Sun Hur, Harvard University,[125]).

2.4.12 IFN-β promoter luciferase assays

IFN-β promoter luciferase assays were performed by transfecting cells with pCMV-Renilla or pGL4.74 [hRluc/TK], pIFN-β-Luc, and expression plasmids as indicated. The following day, cells were infected with SV (Cantrell strain; Charles River labs). SV infections were performed in serum-free media at 200 hemagglutination units (HAU) for 1 h, after which complete media was replenished. At 20 hours post infection, cells were lysed, and a dual luciferase assay was performed (Promega). Values are displayed as relative luciferase units (RLU), which normalizes the Firefly luciferase (IFN-β-Luc) values to Renilla luciferase.

2.4.13 Reverse transcription-quantitative PCR (RT-qPCR).

RNA was extracted from cell lysates using the RNeasy RNA extraction kit, and cDNA synthesis was performed on extracted RNA using iScript (BioRad). The resulting cDNA was diluted (either 1:3 or 1:4) in ddH_2O. RT-qPCR analysis was performed using the Power SYBR Green PCR master mix (Thermo Fisher) on the QuantStudio 6 Flex RT-PCR system. The oligonucleotide sequences used for RT-qPCR are listed in Table

1. Heat map analysis was generated using Morpheus Software from the Broad (https://software.broadinstitute.org/morpheus). First the $2^{\Delta\Delta Ct}$ values (Comparative Ct Method) were calculated by setting the mock-infected Huh7 sample Ct value as the baseline for each biological replicate. Then, the mean of the SV-infected Huh7 triplicate samples is set to 1, and the relative fold induction for each gene between samples is shown. For HCV RT-qPCR, viral RNA was isolated from cells using the RNeasy kit (Qiagen). HCV copy number was measured in triplicate by using a TaqMan one-step assay (TaqMan Fast Virus 1-Step Mix, Qiagen) with an HCV-specific probe targeting the 5' untranslated region of HCV (assay identifier [ID] Pa03454801_s1), as previously described [52]. The copy number of HCV was calculated by comparison to a standard curve of a full-length *in vitro*-transcribed HCV RNA.

2.4.14 BX795 inhibitor treatment.

Huh7 cells were pre-treated with either DMSO or 10 μM BX795 (Invivogen) for 1 hour prior to HCV infection. After incubation with DMSO or BX795, media was removed and cells were infected at an MOI 0.3 with either HCV WT or Y16F viruses in serum-free DMEM as described above. Forty-eight hours post infection, cells were treated again with either DMSO or BX795 for 1 hour after which cDMEM was replenished. The following day (72 hours post infection), lysates were harvested for immunoblotting.

2.4.15 Statistical Analysis.

Student's unpaired *t* test or one-way ANOVA were implemented for statistical analysis of the data using GraphPad Prism software. Graphed values are

presented as mean ± SD or SEM (n = 3 or as indicated); *$p \leq 0.05$, **$p \leq 0.01$, and ***$p \leq 0.005$.

3. NS4A Y16 regulates Riplet-mediated signaling.

This chapter was adapted with permission from a manuscript entitled "Hepatitis C virus infection is inhibited by a non-canonical antiviral signaling pathway targeted by NS3-NS4A" published in the Journal of Virology [119]. The authors are Christine Vazquez, Chin Yee Tan, and Stacy M. Horner.

3.1 Introduction

Antiviral innate immune signaling is activated upon virus infection and serves to limit virus replication. However, many viruses can block this induction. One such virus is HCV. HCV can circumvent this immune induction through its NS3-NS4A protease complex. One mechanism of NS3-NS4A regulation of innate immune signaling is through cleavage of host proteins. Three known host proteins in the RIG-I signaling pathway that are cleaved by NS3-NS4A are MAVS, TRIF, and Riplet [17, 64-67]. My research has identified a residue within the NS4A transmembrane domain, Y16, that when mutated to phenylalanine (Y16F), regulates a signaling pathway that is RIG-I-independent, yet IRF3-dependent. However, the factor that NS4A Y16 regulates to evade this new pathway is unknown.

Here, we aimed to identify the upstream factor(s) that HCV NS4A Y16 could be regulating in the RIG-I-independent, IRF3-dependent signaling pathway discussed in Chapter 2.

3.2 Results

3.2.1 Riplet interaction with HCV NS4A is reduced by the Y16F mutation.

Our data described thus far reveal that NS4A Y16 regulates NS3-NS4A inhibition of TBK1/IKKε-IRF3-mediated antiviral signaling. This IRF3-mediated signaling, which limits HCV replication, is RIG-I-signaling-independent and MAVS-cleavage independent. Together, these data suggest: (1) that there is a factor that induces signaling to IRF3 that is targeted by NS4A Y16 (and not Y16F), and (2) that this factor is present in Huh7 cells but absent or non-functional in Huh-7.5 cells. NS3-NS4A cleaves and inactivates three known host proteins involved in the IRF3 signaling axis: MAVS, TRIF (the TLR3 signaling adaptor), and Riplet [17, 63-65, 67, 85]. Since we have demonstrated that NS3-NS4A Y16F cleaves MAVS (Fig. 7), and it is known that Huh7 cells do not have functional TLR3 signaling [150], we hypothesized that the E3 ubiquitin ligase Riplet may be differentially regulated by NS3-NS4A WT and Y16F. Interestingly, we found that Huh-7.5 cells express reduced levels of Riplet protein and Riplet (*RNF135)* mRNA as compared to Huh7 cells (Fig. 11A-11B). This low level of Riplet likely reduces its ability to drive functional signaling responses during infection. Therefore, we tested if Riplet ectopic expression in Huh-7.5 cells could limit HCV Y16F replication relative to HCV WT. We generated Huh-7.5 cells expressing V5-tagged Riplet (Figs. 11B-11C)**,** infected these cells with HCV WT or Y16F, and measured HCV NS5A expression. In Huh-7.5 + Riplet-V5 cells, but not Huh-7.5 cells, HCV Y16F replication was reduced compared to WT (Fig. 11C). Similarly, the amount of infectious virus generated in the Huh-7.5 + Riplet-V5 cells or Huh7 cells from the HCV Y16F virus was also much lower than WT (~90% lower in each) , but in the Huh-7.5 cells, the level of Y16F virus

was still only partially reduced compared to WT, similar to before (~50% lower) (Fig. 11C, Fig. 6). Further, to determine whether the reduction of Y16F virus replication was a result of an inability of Y16F to block induction of the IFN response, we analyzed mRNA expression of a subset of ISGs and found that in Y16F-infected cells, which have lower levels of virus, the expression of these ISGs is somewhat increased relative to WT-infected cells (Fig. 11D)**.** We note that the overall levels of HCV replication (both WT and Y16F) in the Huh-7.5 + Riplet-V5 cells were lower than those seen in the parental Huh-7.5 cells, likely due to the higher levels of Riplet expression in these cells (Fig. 11A-11B) and the known role of Riplet in inhibiting HCV replication

[17].

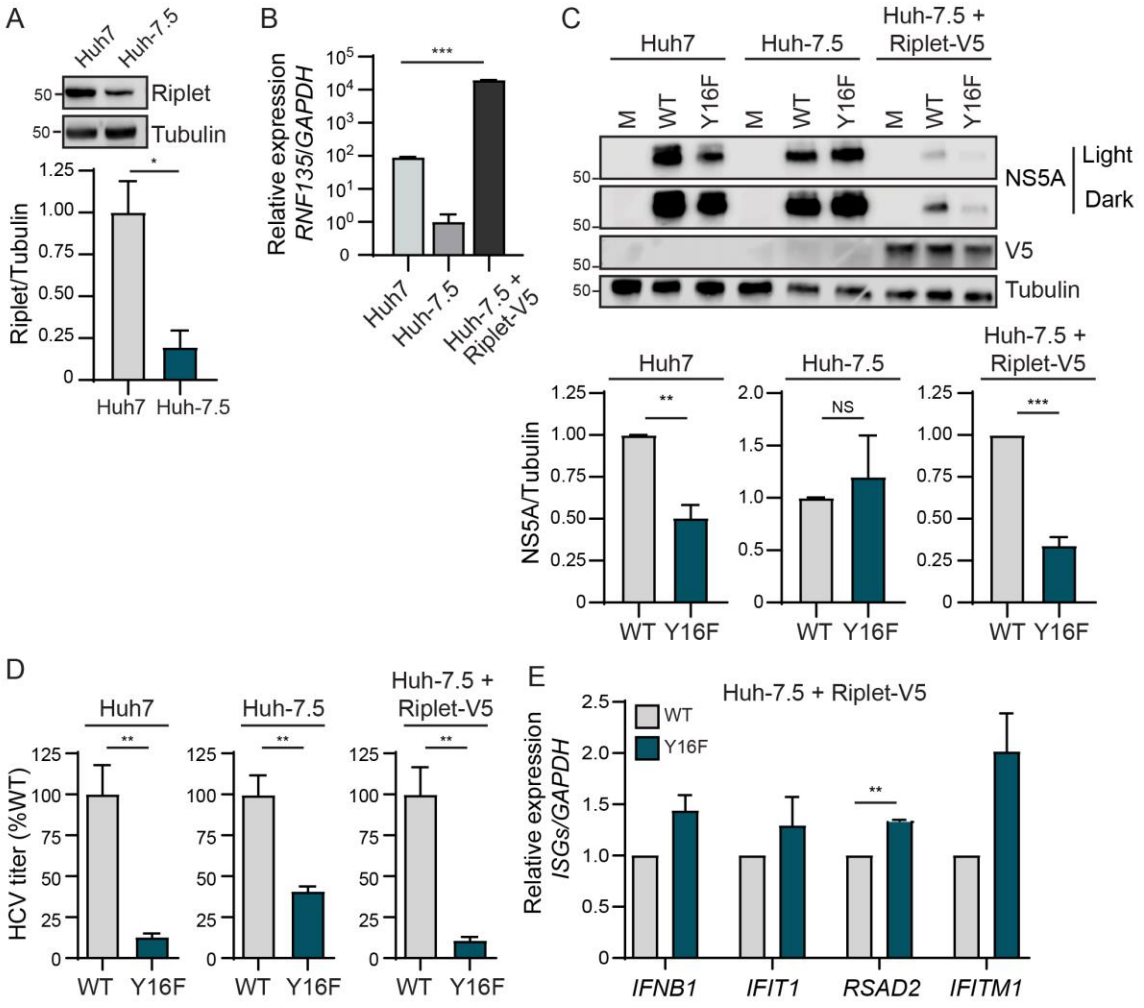

Figure 11: Over-expression of Riplet reduces HCV NS4A Y16F replication in Huh-7.5 cells. (A) Immunoblot analysis of lysates harvested from Huh7 and Huh-7.5 cells for endogenous Riplet protein expression. Graph below the blot shows the mean ± SEM (n = 3 biological replicates) of quantification of Riplet protein expression relative to Tubulin. **(B)** *RNF135* (Riplet) expression relative to *GAPDH* from Huh7, Huh-7.5, and Huh-7.5 + Riplet-V5 cells, as analyzed by RT-qPCR, with data displayed as mean ± SD (n = 2-3 technical replicates). Data were analyzed by one-way ANOVA analysis across the means of the three groups; ***p < 0.005. **(C)** Immunoblot analysis of lysates harvested from the indicated cell lines infected with HCV, WT or NS4A Y16F (JFH1, MOI 0.3), or mock-infected (M), at 72 hpi. Two different exposures (Light and Dark) are shown for NS5A. Graphs below each blot show mean ± SEM (n= 3 biological replicates) of

quantification of NS5A protein relative to Tubulin. **(D)** Focus forming assay of supernatants harvested at 72 hpi from the indicated cell lines infected with HCV, WT or NS4A Y16F (MOI 0.3). Data are presented as the percent HCV titer from Y16F relative to the WT (set at 100%) and show the mean ± SEM (n = 3 biological replicates). **(E)** RT-qPCR analysis of the indicated IFN-stimulated genes from RNA harvested from Huh-7.5 + Riplet-V5 cells infected with HCV, WT or NS4A Y16F (JFH1, MOI 1) at 48 hpi. Data are normalized to Huh-7.5 + Riplet-V5 mock-infected cells, are presented as the induction of indicated genes (relative to *HPRT1* with the WT level set at 1), and display the mean ± SEM (n = 2 biological replicates). Data were analyzed by Student's *t*-test; *p < 0.05, **p < 0.05, ***p < 0.005, NS = not significant.

To test the role of NS4A Y16 in targeting Riplet, we first examined the localization of over-expressed NS3-NS4A WT or Y16F with HA-tagged Riplet in Huh7 cells by immunofluorescence. Similar to others, we did not detect any major difference in the localization of NS4A WT or Y16F [93]. In cells expressing NS3-NS4A WT, we found that Riplet was localized in small, punctate aggregates throughout the cytoplasm, whereas in cells expressing NS3-NS4A Y16F, Riplet was diffusely localized throughout the cytoplasm, similar to that seen in vector-expressing cells and described previously [124] (Fig. 12A). We also found that in cells expressing NS3-NS4A WT, but not Y16F, Riplet and NS4A were in close proximity to each other (Fig. 12A, zoom)**,** suggesting that NS4A may interact with Riplet in a Y16-dependent manner. Indeed, we found that NS4A alone interacted with Flag-tagged Riplet and that the Y16F mutation reduced this interaction by approximately 70% (Fig. 12B). Taken together, these data suggest that the NS4A Y16 residue is necessary for the ability of NS3-NS4A to interact with Riplet and to block antiviral innate immune signaling during HCV infection

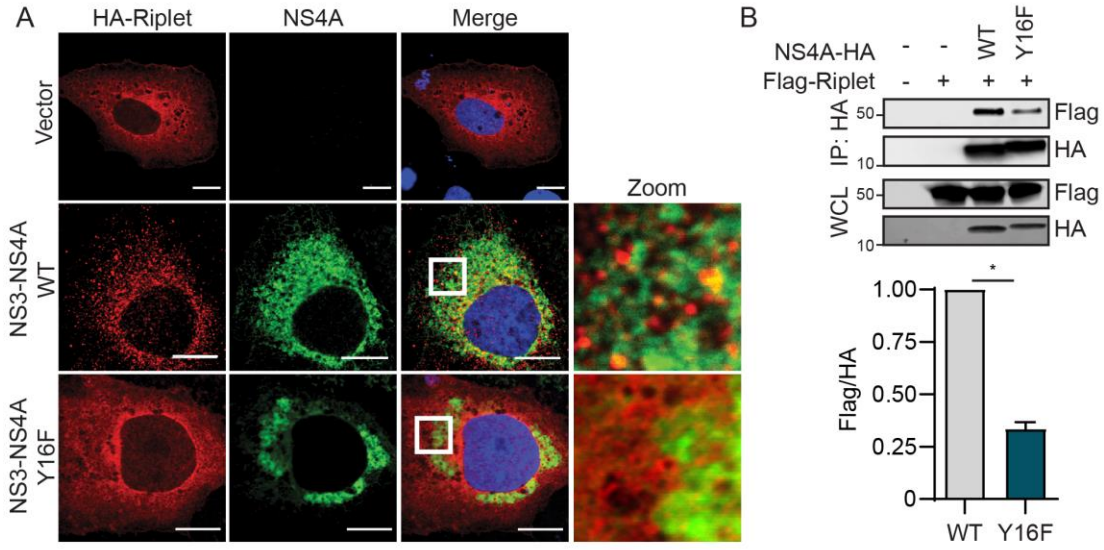

Figure 12: Riplet interaction with HCV NS4A is reduced by the Y16F mutation. (A) Confocal micrographs of Huh7 cells expressing HA-Riplet and either NS3-NS4A WT or Y16F (genotype 1B), or vector, that were immunostained with anti-NS4A (green) and anti-HA (red), with the nuclei stained with Hoescht (blue). Zoom panel is taken from the images in the white boxes. Images are representative of ~50 cells analyzed. Scale bar: 10 μm. **(B)** Immunoblot analysis of anti-HA (NS4A) immunoprecipitated extracts or whole cell lysate (WCL) from Huh7 cells transfected with plasmids expressing Flag-Riplet and NS4A-HA (genotype 1B) WT or Y16F, or vector (-). The graph directly below shows the mean ± SEM (n = 3 biological replicates) of the relative fold change of Flag-Riplet to NS4A-HA in the immunoprecipitated lanes. Data were analyzed by Student's *t*-test; *p < 0.05.

3.2.2 The RING domain of Riplet regulates HCV Y16F virus replication.

Riplet consists of three domains: an N-terminal RING domain, a predicted central coil-coil region, and a C-terminal PRY-SPRY motif [124, 125]. In general, RING domains of E3 ubiquitin ligases are required for interactions with E2 ubiquitin conjugating enzymes. As such, loss of the RING domain in an E3 ubiquitin ligase would prevent the ability of this ligase to conjugate K63-linked ubiquitin to its substrates. Thus, to determine whether the RING of Riplet is required to limit HCV replication, we generated

pools of Huh-7.5 cells over-expressing a Riplet lacking the RING domain (Flag-Riplet ΔRING) or full-length Riplet (Flag-Riplet FL) (Fig. 13A). We then either mock-infected or infected with HCV WT or Y16F viruses, and then measured NS5A protein expression in lysates harvested at 72 hours post infection. We found that, as previously observed (Fig. 11**),** Y16F viral replication is reduced nearly 50% compared to HCV WT in full-length Riplet-expressing cells. However, in the Riplet ΔRING-expressing cells, Y16F viral replication phenocopies that seen in Huh-7.5 cells, with nearly similar replication of both HCV WT and Y16F (Fig. 13B). Taken together, these data suggest that the RING domain of Riplet is important for its ability to restrict Y16 viral replication and block downstream antiviral signaling during HCV infection.

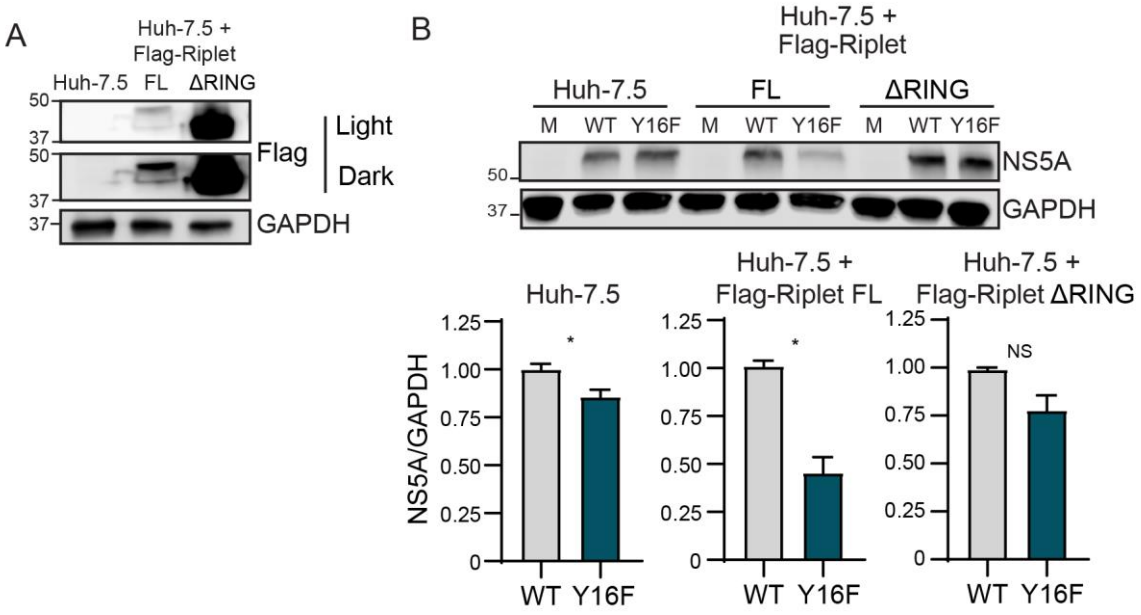

Figure 13: The RING domain of Riplet regulates HCV Y16F virus replication. (A) Immunoblot analysis of Huh-7.5 cells expressing Flag-Riplet full-length (FL) or Flag-Riplet ΔRING. Two different exposures (Light and Dark) are shown for Flag. **(B)** Immunoblot analysis of lysates harvested at 72 hpi from Huh-7.5, Huh-7.5 + Flag-Riplet FL, and Huh-7.5 + Flag-Riplet ΔRING cells infected with HCV, WT or NS4A Y16F (JFH1,

MOI 0.3). Graphs below the blot show quantification of NS5A protein relative to GAPDH (mean ± SEM; n = 3 biological replicates).

3.3 Discussion

The mechanisms by which the HCV protease targets and inactivates Riplet are not entirely clear. Riplet is an E3 ubiquitin ligase localized in the cytoplasm that activates RIG-I by both binding and adding K63-linked ubiquitin chains to it [125, 151]. While others have concluded that NS3-NS4A cleaves Riplet in the first amino acid of its RING domain resulting in its destabilization [17], we were not able to detect a Riplet cleavage product or a reduction in Riplet protein abundance by immunoblot analysis upon over-expression of NS3-NS4A in cells, although we cannot rule out this possibility. While it is possible that NS3-NS4A inactivation of Riplet via cleavage may result in its destabilization, analogous to how NS3-NS4A cleavage of TRIF accelerates its proteolysis [67], it is also possible that simply the binding of NS3-NS4A to Riplet can inactivate it. Indeed, we did find that the localization of Riplet changed from cytoplasmic to punctate, often near NS4A, following over-expression of NS3-NS4A WT, but not Y16F, which could either represent a differential localization as a result of binding to NS4A to prevent Riplet function or represent cleavage by the WT NS3-NS4A (Fig. 12A). Indeed, the dengue virus protease co-factor NS2 (analogous to HCV NS4A) inactivates cGAS simply by binding to it and inducing its autophagic degradation [152]. Additionally, the influenza A virus NS1 protein inactivates Riplet by binding to it [69]. While we have shown that NS4A Y16F interaction with Riplet is reduced compared to NS4A WT, NS3-NS4A inactivation of Riplet may also be a result of indirect mechanisms. Therefore, while it is clear that NS3-NS4A inactivates Riplet, further studies are needed to determine the exact mechanisms by which this occurs.

While HCV NS4A anchors the NS3-NS4A protease to intracellular membranes [94], we do not yet know the mechanisms by which the Y16F substitution in NS4A would specifically alter Riplet localization and to alleviate the block Riplet signaling. Similar to others, we did not find that the Y16F substitution altered the localization of NS4A within membranes [93]. Since NS4A can bind Riplet in the absence of NS3, it is possible that NS4A Y16 is simply required for Riplet binding, either directly or through other proteins. In fact, as the hydroxyl group of this tyrosine residue in NS4A is positioned such that it interacts with the phospholipid head groups of the membrane bilayer, while a phenylalanine at the position would be missing this hydroxyl group, Y16 may be poised to mediate protein-protein interactions directly with Riplet or with accessory binding proteins [93]. We also note that it is possible that phosphorylation of NS4A Y16 could regulate these protein-protein interactions. Thus, NS4A Y16 likely mediates interactions with Riplet to prevent Riplet from interacting with proteins that promote antiviral innate immune signaling.

Our results suggest that HCV activates a Riplet-dependent signaling cascade to IRF3 that is independent of both RIG-I and MAVS. While it is surprising to identify a RIG-I-independent signaling pathway, this may suggest that regulation of HCV replication may require a combination of factors, such as downstream signaling driven by T55 in the RIG-I CARD and Riplet, as well as other yet to be discovered factors. Overall, induction of this Riplet-IRF3 signaling pathway in the absence of RIG-I signaling is likely stimulus-dependent and cell type-dependent. We do not yet know the full identity of this Riplet-IRF3 signaling cascade regulated by NS3-NS4A Y16. We predict that Riplet is either directly adding K63-linked ubiquitin chains to signaling proteins in this pathway or that it interacts with these signaling proteins to activate them, as it does with RIG-I [124, 125].

The only known Riplet-interacting protein that is K63-ubiquitinated is RIG-I. The Riplet-signaling target is likely not MDA5, because it is not a Riplet substrate [124, 125] and the Y16F protease cleaves MAVS, the MDA5 downstream signaling adaptor. It could be the IRF3 kinases TBK1 and IKKε or some other unknown upstream factor [27, 153]. Future studies are needed to further identify the Riplet-interacting proteins that activate this non-canonical antiviral signaling pathway.

3.4 Materials and Methods

3.4.1 Cell culture.

Huh7 and Huh-7.5 [83] cells (gift of Dr. Michael Gale Jr., University of Washington) were grown at 37°C with 5% CO_2 in Dulbecco's modification of eagle's medium (DMEM; Mediatech) supplemented with 10% fetal bovine serum (FBS; HyClone), and 25 mM 4-(2-hydroxyethyl)-1-piperazineethanesulfonic acid (HEPES; Thermo Fisher), referred to as complete DMEM (cDMEM). Huh7 and Huh-7.5 cells were verified using the Promega GenePrint STR kit (DNA Analysis Facility, Duke University), and all cells were tested and found to be *Mycoplasma*-free using the LookOut PCR Detection Kit (Sigma).

3.4.2 Plasmids and transfections.

These plasmids were used in this study: pEF-NS3-NS4A (genotype 1B), pCCSB-Riplet-V5 (Dharmacon: NM_032322.4, cDNA clone MGC161700); pCAGGS-HA-Riplet [69] (Dr. Michaela Gack at the University of Chicago); and psJFHI-M9 Y16F, pEF-NS3-NS4A Y16F, pEF-NS4A-HA, and pHCV-HP-Y16F were generated by QuikChange site-directed mutagenesis (Stratagene) of psJFHI-M9, pEF-NS3-NS4A, pEF-NS4A-HA [121]

and pHCV-HP. pEF-Tak-Flag-Riplet was generated by InFusion (ClonTech) cloning of pCAGGS-HA-Riplet into pEF-Tak. To generate pEF-Tak-Flag-Riplet ΔRING Riplet, a mini gene containing the RING deletion (amino acids 21-67), was digested with NotI, treated with calf intestinal alkaline phosphatase (CIP, New England Biolabs), and ligated into NotI-digested pEF-Tak-Flag-Riplet with T4 DNA ligase (New England Biolabs). The sequences of all plasmids were verified by DNA sequencing and are available upon request. DNA transfections were done using FuGENE6 (Promega) according to manufacturer's instructions.

3.4.3 Generation of Huh-7.5 + Riplet-V5 cells.

To generate Riplet-V5 expressing lentivirus, 293T cells were transfected with pCCSB-Riplet-V5, psPAX2, and pMD2.G. Supernatant was harvested at 48 hours post transfection and filtered through a 0.45 μm filter. Huh-7.5 cells were then infected with the Riplet-V5 lentivirus (500 μl per well of a 6-well plate), and the next day virus was removed and replaced with cDMEM with 0.2 μg/ml blasticidin until mock-transduced cells died (3-4 days). Blasticidin-resistant cells were harvested as pools, and cells were verified as transduced by immunoblot for Riplet-V5 and RT-qPCR analysis for *RNF135* (Riplet).

3.4.4 Generation of Huh-7.5 + Flag-Riplet ΔRING and Flag-Riplet cells.

To generate Huh-7.5 cells expressing Flag-Riplet or Flag-Riplet ΔRING, we first linearized pcDNA-Blast and pEF-Tak-Flag-Riplet with BglII or AgeI, respectively. Huh-7.5 cells were then co-transfected with the linearized plasmids using Fugene 6, and 24 hours post transfection, media was replaced with cDMEM containing 0.2 μg/ml blasticidin. Once the mock-transduced cells died (5 days), blasticidin-resistant cells

were harvested as pools, and cells were verified by immunoblot for Flag to analyze Riplet expression.

3.4.5 HCV stock generation and infections.

HCV JFH1-M9 WT and Y16F virus stocks were generated as described previously [75]. The sequence of the virus at NS4A was confirmed after each passage by sequencing nested PCR products from generated cDNA using the oligonucleotides indicated in Table 2, as previously described [121]. For HCV infections, cells were incubated in a low volume of serum-free DMEM containing virus at a multiplicity of infection (MOI) of 0.3 for 2-3 hours, after which cDMEM was replenished. To quantify virus, cellular supernatants were analyzed by focus forming assay.

3.4.6 Focus forming assay.

To measure HCV titer, supernatants from infected cells were serially diluted and then used to infect naïve Huh-7.5 cells in triplicate wells of a 48-well plate for 3 hours. At 48 hours post infection, cells were washed with PBS and fixed with 4% methanol-free paraformaldehyde (Sigma) for 30 minutes, and then washed again with PBS. Cells were then permeabilized (0.2% Triton-X-100 (Sigma) in PBS), blocked (10% FBS in PBS), and immunostained with a mouse anti-HCV NS5A antibody (1:500). Infected cells were visualized following incubation with horseradish peroxidase (HRP)-conjugated secondary mouse antibody (1:500; Jackson ImmunoResearch) and VIP Peroxidase Substrate Kit (Vector Laboratories). Foci were counted at 10X magnification, and viral titer was calculated using the following formula: (dilution factor x number of foci x 1000)/volume of infection (in µl), resulting in units of focus forming units / ml (FFU/ml).

3.4.7 Immunoblotting.

Cells were lysed in a modified RIPA buffer (10 mM Tris pH 7.5, 150 mM NaCl, 0.5% sodium deoxycholate, 1% Triton X-100) supplemented with protease inhibitor cocktail (Sigma) and phosphatase inhibitor cocktail (Millipore), and post-nuclear supernatants were harvested by centrifugation. Protein concentration was determined by Bradford assay, and 10 µg quantified protein was resolved by SDS/PAGE, transferred to either PVDF (for NS4A) or nitrocellulose membranes using either the Trans-Blot Turbo System (BioRad) or a wet system (BioRad), and blocked with either 3% bovine serum albumin (Sigma) in PBS with 0.1% Tween (PBS-T) or 10% FBS in PBS-T. Membranes were probed with specific antibodies against proteins of interest, washed 3X with PBS-T, and incubated with species-specific HRP-conjugated antibodies (Jackson ImmunoResearch, 1:5000), washed again 3X with PBS-T, and treated with Clarity enhanced chemiluminescence substrate (BioRad). Membranes were then imaged on X-ray film or by using a LICOR Odyssey FC. Immunoblots imaged using the LICOR Odyssey FC were quantified with ImageStudio software, and raw values of the protein of interest were normalized to those of controls (either Tubulin or GAPDH, as indicated). For immunoblots developed on film, Fiji was used [149]. ImageStudio and Fiji give similar quantification results when compared directly.

3.4.8 Immunoprecipitation.

Quantified protein (between 80-160 µg) was incubated with protein-specific antibodies (R anti-HA (Sigma)) in PBS at 4^{o}C overnight with head over tail rotation. The lysate/antibody mixture was then incubated with Protein A beads for 2 hours. Beads were washed 3X in RIPA buffer for immunoprecipitation and eluted in 2X Laemmli Buffer

(BioRad) supplemented with 5% 2-mercaptoethanol at 50^{o}C for 5 minutes. Proteins were resolved by SDS/PAGE and subjected to immunoblotting as described above.

3.4.9 Immunofluorescence analysis and confocal microscopy.

Huh7 cells in 4-well chamber slides were fixed in 4% formaldehyde, permeabilized with 0.2% Triton-X-100, and immunostained with the following antibodies: mouse anti-HCV NS4A (Genotype 1B, 1:100, Virogen), and rabbit anti-HA (1:100, Sigma). Secondary antibody incubations were done with Alexa Fluor conjugated antibodies (Thermo Fisher) and with Hoescht (Thermo Fisher) for 1 hour. Following antibody incubations, slides were washed with 1X PBS, and mounted with ProLong Gold Antifade mounting medium (Invitrogen). Samples were imaged on a Zeiss 780 Upright Confocal using a 63X/1.25 oil objective and the 405, 488, 561, and 633 laser lines with pinholes set to 1 AU for each channel (Light Microscopy Core).

3.4.10 Antibodies.

Antibodies used for immunoblot and immunofluorescence analysis include: mouse anti-HCV NS4A (Genotype 1B, 1:1000, Virogen), mouse anti-HCV NS5A (Genotype 2A, 1:1000, clone 9e10, gift of Dr. Charles Rice, Rockefeller University), mouse anti-Tubulin (1:5000, Sigma), anti-Flag-HRP (1:2500, Sigma), rabbit anti-Flag (1:1000, Sigma), mouse anti-V5 (1:1000, Sigma), mouse anti-HA (1:1000, Sigma), rabbit anti-GAPDH (1:1000, Cell Signaling Technology), Hoescht (1:500, Thermo Fisher), Alexa Fluor conjugated secondary antibodies (1:500, Life Technologies), and mouse anti-Riplet (1:500, gift from Dr. Sun Hur, Harvard University,[125]).

3.4.11 Statistical Analysis

Student's unpaired *t* test or one-way ANOVA were implemented for statistical analysis of the data using GraphPad Prism software. Graphed values are presented as mean ± SD or SEM (n = 3 or as indicated); *$p \leq 0.05$, **$p \leq 0.01$, and ***$p \leq 0.005$.

Table 2: Oligonucleotides used for RT-qPCR and cloning

Target	Forward Primer (5'-3')	Reverse Primer (5'-3')
GAPDH	AAGGTGAAGGTCGGAGTCAAC	GGGGTCATTGATGGCAACAATA
HPRT1	TGACACTGGCAAAACAATGCA	GGTCCTTTTCACCAGCAAGCT
IFNB1	CTTTGCTATTTTCAGACAAGATTCA	GCCAGGAGGTTCTCAACAAT
IFNL1	CTTCCAAGCCCACCACAACT	GGCCTCCAGGACCTTCAGC
OAS1	TGTCCAAGGTGGTAAAGGGTG	CCGGCGATTTAACTGATCCTG
IFIT1	TCCTTGGGTTCGTCTACAAAT	TTCTCAAAGTCAGCAGCCAGT
IFIT2	CACGCTGTGGCTCATCTGAA	GGCTGGCAAGAATGGAACA
IFIT3	AGTCTAGTCACTTGGGGAAAC	ATAAATCTGAGCATCTGAGAGTC
RSAD2	TGCCACAATGTGGGTGCTTACAC	CTCAAGGGGCAGCACAAAGGAT
MX1	TTCAGCACCTGATGGCCTATC	TGGATGATCAAAGGGATGTGG
IFITM1	ACTAGTAGCCGCCCATAGCC	GCACGTGCACTTTATTGAATG
ISG15	GCGAACTCATCTTTGCCAGTA	CCAGCA TCTTCACCGTCAG
RNF135	GGGTGGCAGTAGAGAAGAGC	CCAGAAGAAAAAGCCTTGCCC
HCV PCR Outer	TACATGTGTTTAGTCGAGGTT	CAAACAGCCACCAAGCAAG
HCV PCR Inner	CAGGACCATCTGGAGTTCTGG	CTTGCTTGGTGGCTGTTTG
RIG-I KO guide 1	TTTCTTGGCTTTATATATCTTGTGGAAA GGACGAAACACCGGGCTAGTGAGGCA CAGCCTGCGGG	GACTAGCCTTATTTTAACTTGCTA TTTCTAGCTCTAAAACCCCGCAG GCTGTGCCTCACTAGCC
RIG-I KO guide 2	TTTCTTGGCTTTATATATCTTGTGGAAA GGACGAAACACCGG GGAGATCTTACCACAAACCTGGG	GACTAGCCTTATTTTAACTTGCTA TTTCTAGCTCTAAAACCCCAGGTT TGTGGTAAGATCTCCC
RIG-I PCR	CCGCTAGTTGCACTTTCGAT	CTTCCCCAGCTTTGAACCTA
MAVS KO guide	CGCTGGAGGTCAGAGGGCTGG	CCAGCCCTCTGACCTCCAGCG

MAVS PCR	GTGGGCTGAGGCCTATAGG	CCCAAATGCCTGACCCACAG
IRF3 KO guide	CCACTGGTGCATATGTTCCC	GGGAACATATGCACCAGTGGC
IRF3 PCR	GGGGATGGACCTTGCAGAGT	CCTGAGCCAGTGCTGACCCT
pEF-Tak-Flag-Riplet	GATGATAAAGCGGCCGCTGCGGGCCTGGGCCT	CTGATCAGCGGGTTTAAACTTACACCTTTACTTGCTTTATTATCAGGTAATTTCC
pEF-NS4A-HA Y16F	AGCTCTGGCCGCGTTTTGCCTGACAACAG	CTGTTGTCAGGCAAAACGCGGCCAGAGCT
pHCV-HP Y16F	CCCGACAGGGAAGTCCTTTTCCGGGAGTTC	GAACTCCCGGAAAAGGACTTCCCTGTCGGG

4. Conclusions

4.1 Summary

The goal of my dissertation research was to define the molecular mechanisms by which the functions of NS3-NS4A in viral replication and immune evasion are regulated. NS3-NS4A plays an important role in viral replication, polyprotein processing, viral assembly, and in immune evasion by cleavage and inactivation of host antiviral proteins, interactions with the viral E1 protein for viral assembly, and by RNA processing through the NS3 helicase domain. The mechanism(s) that coordinates these functions are unknown. We originally hypothesized that membrane localization may dictate NS3-NS4A function, wherein on the ER, NS3-NS4A could function in viral replication, and on the MAM, NS3-NS4A could function in immune evasion. To this point, as NS4A is the membrane targeting co-factor of the protease complex, we focused on the NS4A transmembrane domain and generated a mutant, Y16F, to determine the role of this residue in coordinating NS3-NS4A function.

I began this research by generating an infectious clone of HCV NS3-NS4A WT and Y16F viruses, infected Huh-7.5 and Huh7 cells with these viruses, and measured viral replication. I found that in Huh-7.5 cells, which do not have active RIG-I signaling, both WT and Y16F viruses replicate similarly, suggesting that the Y16F mutation does not prevent overall virus replication. I also validated the replication capacity of the Y16F mutation using an HCV replicon containing either NS3-NS4A WT or NS3-NS4A Y16F. These replicon RNAs were electroporated into Huh-7.5 cells, cells were selected with the antibiotic Geneticin, and cells that survived antibiotic selection and were actively replicating HCV RNA were stained with crystal violet. In these cells, both WT and Y16F replicated similarly, corroborating the idea that the Y16F mutation does not negatively

impact replication capacity. However, in Huh7 cells, which have active RIG-I signaling, Y16F virus replication was reduced compared to WT. Utilizing CRISPR/Cas9 gene editing, I generated Huh7 cell lines in which either RIG-I, MAVS, or IRF3 was deleted. I then infected these cells with either WT or Y16F viruses and measured virus replication. I found that in the Huh7-RIG-I and Huh7-MAVS KO cells, Y16F virus replication was reduced compared to WT, but was restored to WT levels in the Huh7-IRF3 KO cells. Further, HCV NS3-NS4A Y16F was unable to block IRF3 nuclear translocation as well as WT, and this correlated with an inability to block the induction of several ISGs. Taken together, these data suggest that NS4A Y16 is necessary to regulate a pathway that is IRF3-dependent and RIG-I-independent.

I next sought to determine the factor that HCV NS3-NS4A Y16 could be regulating in this new antiviral signaling pathway. To do this, I looked at the known NS3-NS4A host substrates involved in innate immune signaling in Huh7 cells. Using confocal microscopy and immunoprecipitations, I found that NS4A Y16F had reduced interactions with Riplet. Further, I found that Huh-7.5 cells had lower Riplet mRNA and proteins levels compared to Huh7 cells. To determine whether Riplet was the factor regulated by Y16, I complemented Huh-7.5 cells with Riplet and found that in these Riplet-complemented cells, HCV Y16F had reduced replication compared to HCV WT. Additionally, when Riplet lacking the RING domain, the ubiquitin-conjugating domain of RING-containing ligases, the domain essential for ubiquitinating substrates and thus directs the function of Riplet, was complemented into Huh-7.5 cells, both HCV WT and Y16F now replicated similarly.

Taken together, my work has revealed a residue, Y16, in the NS4A transmembrane domain that regulates differential inactivation of MAVS and Riplet, revealing a new branch of innate immune signaling that controls HCV infection.

4.2 Future directions and discussion

4.2.1 What is the non-RIG-I ubiquitinated target of Riplet?

My thesis work has revealed that Riplet may ubiquitinate or interact with another protein that is not RIG-I to induce a signaling cascade to type I IFN that is important for limiting HCV infection. While I have not directly tested if the ubiquitination activity of Riplet is essential for inhibiting HCV infection, my work suggests that ubiquitination of proteins by Riplet, rather than simply protein-protein interactions between Riplet and a signaling protein, is essential for inhibiting HCV. Specifically, I found that the Riplet RING domain is important for regulating HCV Y16F infection (Fig. 13), suggesting that the interaction of Riplet with its E2 ubiquitin ligase and therefore ubiquitination of a downstream substrate, is essential for inhibiting HCV infection. Currently, the only protein identified that is ubiquitinated by Riplet is RIG-I. However, two studies have suggested additional proteins that may interact with Riplet [17, 154]. One study identified a tumor suppressor, which was not directly named, as a potential Riplet-interacting protein, and the authors suggested that this tumor suppressor may be involved in hepatocellular carcinoma resulting from chronic HCV infection [154]. A second study found that Riplet may interact with a protein, Trk-fused gene (TFG), by doing a protein-protein interaction study of Riplet with proteins expressed from a mouse cDNA library

[17]. TFG is an ER-localized protein that functions in tumorigenesis, COPII vesicle transport, NF-κB signaling by interacting with the NF-κB-regulatory proteins TANK and NEMO, and more recently, has been shown to be a negative regulator of RIG-I signaling to IFN by interacting with the E3 ligase TRIM68 [155]. In addition to these ascribed immune signaling roles, TFG may have roles independent of RIG-I-mediated signaling to IFN, as it has been found that Riplet-TFG protein interactions are not necessary for RIG-I-mediated signaling, but rather for Riplet-protein interactions independent of RIG-I [154]. The fact that Riplet interacts with these proteins suggests that Riplet may have roles in tumorigenesis and inflammation, which may also be important for downstream consequences of the initial HCV infection. Along these lines of thinking, the studies presented in Chapters 2 and 3 of this dissertation suggest that Riplet can target some unidentified protein for a non-canonical RIG-I-independent signaling pathway. Thus, it is possible that TFG could be a Riplet-mediated target for Riplet-dependent, RIG-I-independent signaling.

As E3 ubiquitin ligases have a propensity to ubiquitinate multiple proteins, including those functioning in the same signaling axis, it is quite possible that Riplet ubiquitinates other proteins besides those mentioned above. For example, the E3 ubiquitin ligase TRIM25 ubiquitinates both RIG-I and MAVS [18, 117]. Similarly, Riplet may ubiquitinate both RIG-I and some other protein involved in the non-canonical signaling pathway described in Chapters 2 and 3 of this dissertation. In theory, this protein could be another PRR, besides RIG-I, that senses aspects of HCV infection, for example, MDA5 or PKR. However, MDA5 is not a likely candidate in this non-canonical signaling pathway as it does not interact with Riplet, and it is not ubiquitinated by Riplet [17, 124, 125]. However, the other known HCV RNA sensor protein PKR seems like a

good candidate to be a Riplet-interacting protein. The viral dsRNA binding protein PKR is thought to be one of the earliest sensors of HCV infection, even before RIG-I [156]. This interaction of PKR with HCV RNA induces a signaling cascade that leads to induction of antiviral innate immunity [156]. Interestingly, HCV infection leads to the formation of stress granules, cytoplasmic compartments that contain antiviral effector proteins that can limit virus infection, and both PKR and RIG-I have been found in these stress granules [157-159]. In fact, Riplet is also found in these stress granules [17]. Therefore, it is possible that Riplet can interact with these two stress granule-associated proteins RIG-I and PKR given the potential proximity of PKR, RIG-I, and Riplet in the same cytoplasmic compartment.

PKR may not be the Riplet-ubiquitinated target, and the potential Riplet substrate may be a protein that has yet to be identified. Thus, future studies can use immunoprecipitation-mass spectrometry (IP-MS) to identify potential interacting proteins of Riplet. For these experiments, I would want to use the PRY-SPRY domain, as we know it is essential for interactions between the E3 ubiquitin ligase and substrates. RING-containing E3 ubiquitin ligases function through E2 interactions at the RING domain itself and substrate interactions at the PRY-SPRY domain (Fig. 14). Subsequent ubiquitination occurs via the direct transfer of ubiquitin to the substrate. Consequently, there are two interactions that are important for ligase function: (1) the E2 with the RING E3 and (2) the substrate with the RING PRY-SPRY. Deletion of either Riplet domain may help identify the substrate(s) involved in non-canonical antiviral signaling. We have obtained bacterially expressed and purified PRY-SPRY domain of Riplet containing a GST-Tag (gift of Dr. Sun Hur, Harvard University), and future studies could incubate this purified PRY-SPRY domain with lysates of Huh7 cells, perhaps infected with SV to

induced antiviral signaling, followed by immunoprecipitation of GST-PRY-SPRY and mass-spectrometry analysis to identify new Riplet-interacting proteins. Because RIG-I will most likely be the top Riplet-interacting protein identified in the Huh7 cells, I can perform the same GST IP-MS experiment in the Huh7-RIG-I KO cells to identify any top candidate Riplet-interacting proteins that may have been missed in the Huh7 cells. Any candidate proteins that interact with the GST-PRY-SPRY in the absence of RIG-I would be considered potential proteins for further validation. To identify any ubiquitinated targets of Riplet, I can utilize the Flag-Riplet ΔRING construct, which does not signal or impact HCV replication, followed by IP-MS to identify potential Riplet-ubiquitinated substrates. I would expect that if proteins are indeed ubiquitinated by Riplet, these proteins would not be identified in the Flag-Riplet ΔRING conditions but would be identified in conditions in which full-length Flag-Riplet is expressed.

The antiviral innate immune response is tightly regulated to prevent aberrant activation or insufficient activation during virus infections. This signaling program begins within hours of virus sensing, and downstream signaling events and feedback loops are regulated throughout the duration of infection until virus clearance by the induction of ISGs. Therefore, the kinetics of IFN induction and inactivation by viruses is an important determinant of virus infection. NS3-NS4A inactivates two proteins within the RIG-I signaling pathway: MAVS and Riplet. Why NS3-NS4A inactivates two proteins within the same signaling pathway is unclear. One hypothesis could be that these two proteins are inactivated at different time points in infection to either (1) block separate signaling pathways, which my data suggest, or (2) to regulate IFN induction kinetics throughout HCV infection. Inactivation of one protein early during infection and inactivation of another protein at a later time of infection may facilitate HCV replication, which is a

suggested mechanisms of HCV inactivation of PKR [156]. We have not yet examined the kinetics of Riplet inactivation during HCV infection, as our confocal microscopy analysis of Riplet and NS3-NS4A (Fig. 11) was performed only in the context of over-expression. However, examining whether any Riplet localization changes occur during (1) HCV infection and (2) at multiple time points, such as 6-12 hours (during infection), or 12-18 hours (during infection and plasmid over-expression) may delineate the mechanisms for how HCV targets multiple proteins thought to be involved in the IFN induction pathway.

4.2.2 Potential consequences of the phenylalanine mutation

We have shown that mutating the HCV NS4A Y16 residue to phenylalanine disrupts the ability of HCV NS4A to interact with and localize with Riplet, ultimately preventing HCV NS4A from blocking downstream antiviral IFN induction. However, we do not yet know why this mutation in particular disrupts NS4A function. There could be multiple explanations for the phenotypic consequences of the phenylalanine mutation in NS4A, including disrupting potential protein-protein interactions, preventing NS4A phosphorylation, sequestration of NS4A away from substrates, or perhaps a combination of all these mechanisms.

NS4A Y16 may be important for protein-protein interactions. The NS4A transmembrane domain positions the NS3-NS4A protease complex onto membranes for protease function [93]. NMR structural predictions and modeling of the NS4A transmembrane domain onto membranes depict NS4A Y16 as facing towards the phospholipid head groups at the lipid bilayer interface, with the tyrosine hydroxyl group exposed outward and not embedded within the membrane. Thus, it is possible that this

accessible hydroxyl group can mediate protein-protein interactions that are necessary for protease function, such as cleavage of substrates. I have shown that NS4A alone is necessary for NS4A-Riplet interactions, and that NS4A Y16F does not interact with Riplet as well as WT, suggesting that NS4A, and not NS3, is interacting with Riplet and that the hydroxyl group absent in phenylalanine may mediate this interaction.

NS4A Y16 may be phosphorylated, and phosphorylation of NS4A may guide NS3-NS4A function. Preliminary data from our lab has suggested that NS4A is phosphorylated on a tyrosine residue (data not shown). There are 2 tyrosine residues within NS4A: one at position 16 and one at position 45. Mutating tyrosine to phenylalanine generates a non-phosphorylatable residue. One model that may explain the reduced NS4A Y16F binding to Riplet is that phosphorylation of NS4A may play a role in guiding which substrates can be targeted. The accessible hydroxyl group on tyrosine may be phosphorylated by a kinase, and phenylalanine mutation would ablate this phosphorylation. We have not yet validated phosphorylation at Y16, and if this residue is indeed phosphorylated, we do not yet know the identity of the kinase or kinases responsible for its phosphorylation. Future studies using IP-MS can determine the phosphorylated NS4A residue. While we do not yet directly know if NS4A is phosphorylated at position Y16, I have performed an siRNA kinase screen to indirectly identify the kinase(s) that may phosphorylate NS4A (For details, see Appendix B). In this screen, siRNAs targeting all known human kinases were transfected, along with HA-Riplet, into Huh-7.5 stably expressing HCV NS3-NS4A WT. From this initial screen, I have identified 20 kinases, some tyrosine and some serine/threonine kinases, that are candidate NS4A kinases (Table 3). While we hypothesize that NS4A is phosphorylated at Y16, serine/threonine kinases have been shown to function as tyrosine kinases under

certain conditions [160, 161], which is why all human kinases were included in the initial screen. After secondary validation of the 20 candidate kinases, I would next test if these candidate kinases phosphorylate NS4A. If none of the candidate kinases are shown to phosphorylate NS4A, one or more of these kinases may play a role in other aspects of NS4A or NS3 function, Riplet-mediated signaling, or in another aspect of the HCV life cycle, as the kinase screen is an indirect measure of NS4A phosphorylation and instead may indicate that these proteins are important for Riplet localization in an HCV replicon. Interestingly, many of the candidate kinases that I have already identified are members of signaling pathways that are activated during HCV infection, including the MAPK/ERK family, mTOR, and JAK/STAT pathways [162-165]. This suggests that Riplet may function in one of these pathways and/or that NS4A Y16-Riplet interactions may prevent activation of these known anti-HCV signaling pathways, which may lead to viral persistence.

NS4A Y16 may also regulate NS3-NS4A membrane localization, as this tyrosine residue is within the NS4A transmembrane and is positioned near the membrane-bilayer interface [93]. To test membrane localization of NS3-NS4A WT and Y16F, I utilized confocal microscopy of NS4A WT or Y16F-expressing Huh7 cells. I found that there is not differential membrane localization both WT and Y16F localize to the ER (Fig. 14) and mitochondria (**Fig. 15**). However, in cells expressing NS4A Y16F, NS4A staining appears to cluster closer together, and the membranes on which NS4A localizes (mitochondria and ER) are clustered together as well. This suggests that perhaps NS4A Y16F makes NS4A more tightly associated with these known NS3-NS4A membrane localization profiles. This tighter membrane localization may prevent NS4A from binding to accessible substrates, such as those that are cytoplasmic. NS3-NS4A cleaves both

membrane-localized (MAVS, TRIF) and cytoplasmic (DDB1, Riplet) substrates. I have shown that NS3-NS4A Y16F is unable to cleave a cytoplasmic substrate, Riplet, but is able to cleave a membrane-bound substrate, MAVS. Thus, examining whether mutation to phenylalanine impacts the ability of NS3-NS4A to target these other membranes versus cytoplasmic substrates is an interesting avenue of future investigation.

From the data presented in this dissertation, our model of Riplet inactivation by NS4A is that NS4A can inactivate Riplet simply by binding to the PRY-SPRY domain, perhaps sequestering it away from the cytoplasm where it may not be able to ubiquitinate its substrates, which may prevent innate immune activation. Inactivation of host proteins by binding to viral proteins may directly interfere with host proteins by delivering them to the lysosome or proteasome for degradation, as is seen with DENV, or indirectly by preventing intermediate protein-protein interactions. Viruses in the *Flaviviridae* family, such as HCV, Zika virus, and DENV, have similar structural and non-structural proteins, with a viral protease and protease co-factor. The analogous protease complex for DENV consists of the protease NS3 and its co-factor NS2B. DENV infection results in mitochondrial damage, releasing mitochondrial DNA. This induces cGAS-STING signaling that can restrict RNA virus infection by inducing IFN [152]. However, this signaling can be inactivated by the DENV, as DENV inactivates cGAS-STING via NS2B. This inactivation only requires NS2B, not the protease NS3 [152]. NS2B binds to cGAS and cGAS is subsequently degraded by the autophagy machinery. Just as NS2B alters cGas localization, NS3-NS4A alters Riplet localization from its basal cytoplasmic localization to punctate aggregates (Fig. 12). The identity of these punctate aggregates or the fate of Riplet in the presence of NS3-NS4A WT has not been explored. It would be

interesting to determine whether this punctate Riplet is Riplet on its way to the lysosome for degradation, as is seen with cGAS in the presence of NS2B.

4.2.3 Does this Riplet-mediated pathway play a role in limiting other RNA virus infections?

Riplet has antiviral activity against multiple RNA viruses through RIG-I-mediated signaling. The role of Riplet in RIG-I-mediated signaling is becoming more appreciated as recent studies have suggested that Riplet is a major E3 ubiquitin ligase of RIG-I [125, 166]. Riplet ubiquitinates RIG-I via K63-ubiquitin linkages. This ubiquitination is an activating ubiquitination event as it promotes interactions of RIG-I with downstream innate immune adaptor and regulatory proteins. These interactions are crucial as they prime IFN induction [124, 154]. In fact, several viruses can block Riplet function suggest the importance of Riplet in antiviral signaling. For example, the IAV NS1 protein binds to Riplet, and this binding prevents RIG-I ubiquitination and subsequent IFN-β induction and [69]. The inactivation of Riplet by NS1 binding provides further support to our model of NS3-NS4A inactivation of Riplet. Mechanistic insight into viral antagonism of Riplet and Riplet-mediated signaling has only been examined in the context of HCV infection, but further studies on other RNA viruses, such as IAV or VSV, are exciting avenues of research. For example, during infection with other RNA viruses, does Riplet ubiquitinate just RIG-I or can Riplet ubiquitinate other proteins or virus sensors? Viruses in the *Flaviviridae* family encode similar protease complexes; for example, in HCV the protease complex is NS3-NS4A with NS4A being the co-factor, and in DENV, the protease complex is NS2B-NS3, with NS2B being the co-factor. Given the relative functional similarity between these protease complexes and our data showing that HCV NS4A alone interacts with Riplet, it may be possible that DENV NS2B could also interact with

Riplet to block IFN induction. HCV differs from many other RNA viruses in that HCV can establish a persistent infection, while other viruses, such as DENV or IAV, establish an acute infection. Would blocking the non-canonical Riplet-mediated and RIG-I-independent pathway identified in Chapters 2 and 3 of this dissertation be important for establishing this persistent infection, and would more lytic/acute viruses need this secondary Riplet-mediated, RIG-I-independent pathway? The answers to these questions will undoubtedly advance the fields of virology and immunology.

Appendix A

The NS4A Y16F mutation does not alter NS4A membrane localization

I have found that NS3-NS4A Y16F is unable to replicate in Huh7 cells, which have both active RIG-I and Riplet signaling. To determine whether this differential replication was due to the Y16F mutation preventing NS4A membrane localization, I used confocal microscopy with Huh7 cells expressing NS3-NS4A WT or Y16F. NS3-NS4A localizes to the mitochondria and the ER. I transfected Huh7 cells with either NS3-NS4A WT or Y16F with either Tom20 (mitochondrial marker) or calnexin (ER marker). I found that both NS3-NS4A WT and Y16F localize to both the ER (Fig. 14) and mitochondria (Fig. 15), suggesting that altered membrane localization does not account for the inability of NS3-NS4A Y16F to regulate Riplet-mediated signaling.

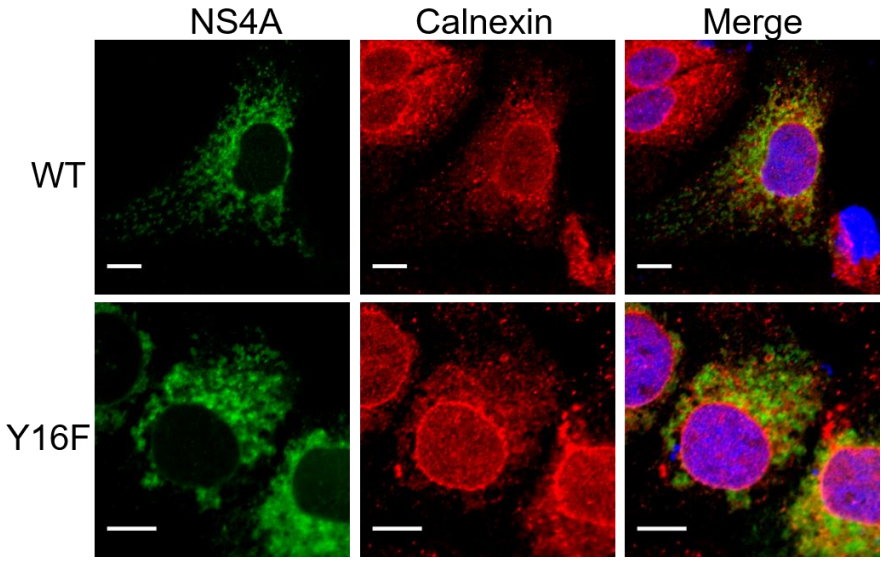

Figure 14: NS4A Y16F localizes to the ER. Confocal micrographs of Huh7 cells expressing either NS3-NS4A WT or Y16F (genotype 1B), that were immunostained with anti-NS4A (green) and anti-calnexin (red), with the nuclei stained with Hoescht (blue). Scale bar: 10 µm

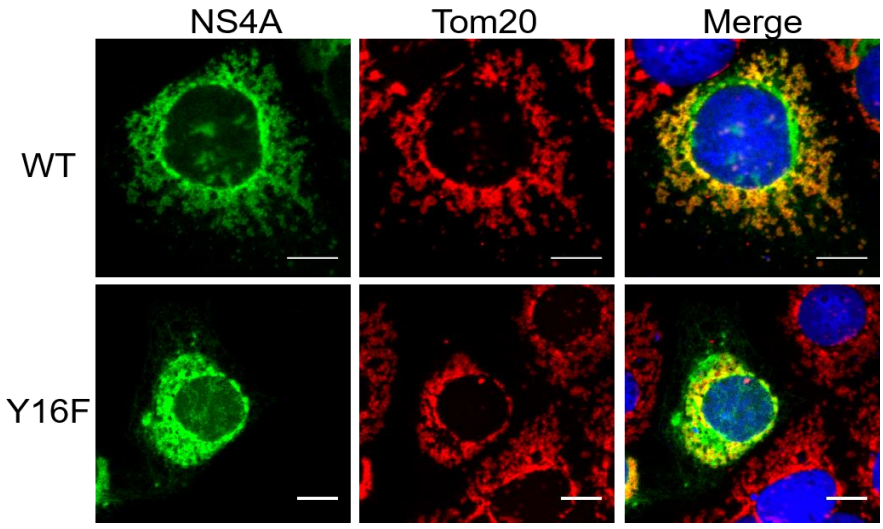

Figure 15: NS4A Y16F localizes to the mitochondria. Confocal micrographs of Huh7 cells expressing either NS3-NS4A WT or Y16F (genotype 1B), that were immunostained with anti-NS4A (green) and anti-Tom20 (red), with the nuclei stained with Hoescht (blue). Scale bar: 10 µm

Appendix B

A kinase screen identifies potential NS4A kinases.

Preliminary data indicate that NS4A is phosphorylated on tyrosine-16 (Y16), likely suggesting that the Y16F mutation generates a non-phosphorylatable residue and that there is a kinase that would be responsible for inducing this phosphorylation on NS4A. As we had difficulty developing a direct way to assess NS4A phosphorylation, we decided to use an indirect measure to assess NS4A phosphorylation to screen for and identify the NS4A kinase**.** Additionally, in cells expressing NS3-NS4A WT and HA-Riplet, Riplet localizes changes from cytoplasmic and diffuse to punctate aggregates, while it remains cytoplasmic and diffuse in cells expressing NS3-NS4A Y16F (Fig. 12). Thus, we developed a kinase screen utilizing the following rationale: If a kinase is indeed the one that phosphorylates NS4A, then when that kinase is depleted from the cell, HA-Riplet should now become cytoplasmic in NS4A-expressing cells. If a kinase is not responsible for phosphorylating NS4A, then HA-Riplet should localize to punctate aggregates in NS4A-expressing cells, as in Fig.12. Our anticipated results of this initial kinase screen are illustrated in Fig. 16, with our phenotype of interest being Result C. In collaboration with the Duke Functional Genomics Core, we reverse-transfected Huh-7.5 HP WT replicon cells (generated from Fig. 5) with siRNAs targeting all known human kinases (in 8 separate 96-well plates, with individual kinases in individual wells, Qiagen Human Whole Genome siRNA Set v1.0) and with HA-Riplet. While we expect that the kinase that phosphorylates NS4A is a tyrosine kinase, we examined all human kinases as serine/threonine kinases may also function as tyrosine kinases under certain conditions [160, 161]. Forty-eight hours post transfection, the cells were fixed and stained for NS4A (Virogen, 1:100, genotype 1B), HA (Sigma, 1:500), and Hoescht (1:500, ThermoFisher).

After staining, individual wells were analyzed using the Zeiss Observer Z1 fluorescent microscope. Cells in which NS4A protein was present and HA-Riplet was cytoplasmic were considered a potential candidate kinase; of the examined kinases, we considered 20 as potential candidate kinases (Table 3). One of these positive candidates is the tyrosine kinase LCK, which in a previous mass spectrometry data set, was shown to weakly interact with NS4A[167]; while an example of a negative candidate is the tyrosine kinase LMTK3, which displayed punctate HA-Riplet staining (Fig. 16).

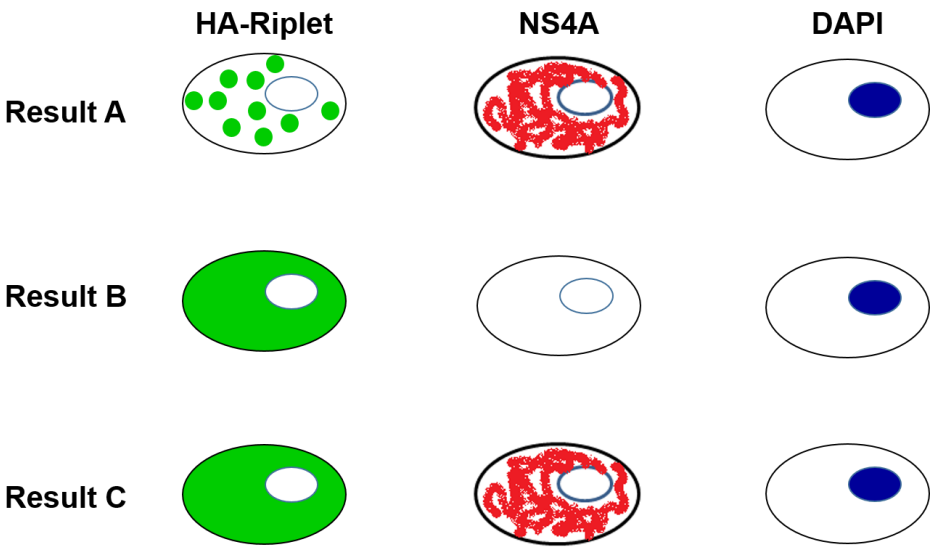

Figure 16: Schematic of the expected results from the initial kinase screen. A candidate will be considered a potential NS4A kinase if the phenotype is that of Result C, where knockdown of the kinase now results in cytoplasmic and diffuse HA-Riplet (green) staining and HCV NS4A (red) is present.

Table 3: NS4A kinases identified in primary kinase screen

Kinase	Ser/Thr or Tyr

LCK	Tyr
CSK	Tyr
BMX	Tyr
CSNK1A1	Ser/Thr
BLK	Tyr
PTK2B	Tyr
JAK2	Tyr
JAK1	Tyr
LTK	Tyr
DDR2	Tyr
RAGE	Tyr
RYK	Tyr
PTK7	Tyr
AURKA	Ser/Thr
TYK2	Tyr
TIE1	Tyr
TNK1	Tyr
MLK4	Ser/Thr
STK31	Tyr
MYLK2	Ser/Thr
SKP	Ser/Thr

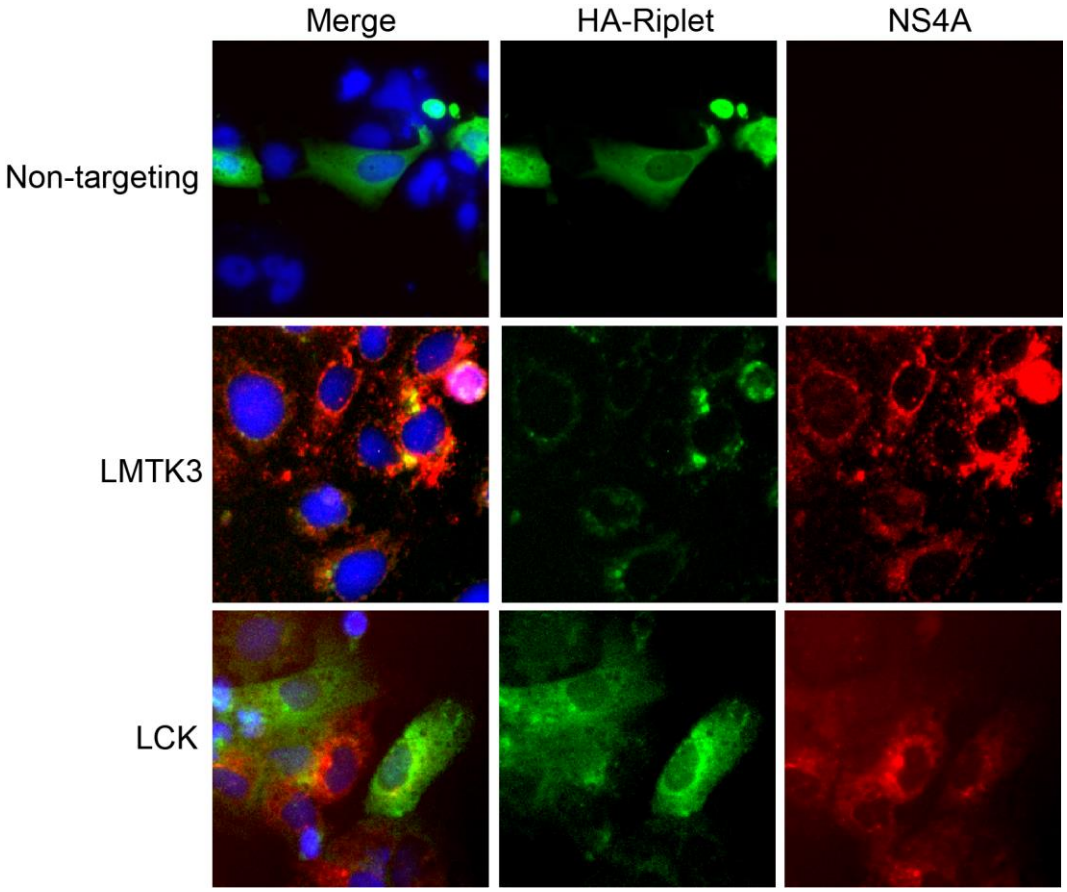

Figure 17: Results of visual screen for NS4A kinases identified LCK as a potential NS4A kinase. Confocal micrographs of Huh-7.5 HP WT replicon (genotype 1B) cells expressing HA-Riplet and either non-targeting siRNA or siRNAs targeting LMTK3 or LCK that were immunostained with anti-HA (green) and anti-NS4A (red), with the nuclei stained with Hoescht (blue). Scale bar: 10 μm**.**

Appendix C

Quantification of immunoblot images used in dissertation

Membranes were imaged on X-ray film or by using a LICOR Odyssey FC. Immunoblots imaged using the LICOR Odyssey FC were quantified with ImageStudio software, and raw values of the protein of interest were normalized to those of controls (either Tubulin or GAPDH, as indicated). For immunoblots developed on film, Fiji was used [149]. ImageStudio and Fiji give similar quantification results when compared directly.

Table 4: Quantification of immunoblots used in Figure 6

RIG-I KO: Fig. 6			
Cell Type		NS5A	Tubulin
Huh7 WT	Replicate 1	14745.77	43021.25
	Replicate 2	0.497	0.891
	Replicate 3	0.365	0.151
Huh7 Y16F	Replicate 1	1072.648	27962.04
	Replicate 2	0.0963	1.02
	Replicate 3	0.224	0.898
Huh-7.5 WT	Replicate 1	160996.4	32602.19
	Replicate 2	33484.29	50209.68
	Replicate 3	12.5	2.94
Huh-7.5 Y16F	Replicate 1	152123.3	30952.02
	Replicate 2	39669.53	48025.35
	Replicate 3	10.7	1.93

RIG-I KO WT	Replicate 1	27071.79	22680.29
	Replicate 2	0.447	0.593
	Replicate 3	0.434	0.125
RIG-I KO Y16F	Replicate 1	929.355	26593.4
	Replicate 2	0.0915	0.308
	Replicate 3	0.0258	0.147

Table 5: Quantification of immunoblots used in Figure 8

IRF3 KO: Fig. 8			
Cell Type		NS5A	GAPDH
Huh7 WT	Replicate 1	0.331	15.3
	Replicate 2	2.15	6.62
	Replicate 3	0.458	3.9
Huh7 Y16F	Replicate 1	0.0214	17.9
	Replicate 2	1.81	10.2
	Replicate 3	0.012	3.85
IRF3 KO WT	Replicate 1	0.0491	21.5
	Replicate 2	1.31	7.62
	Replicate 3	8590.217	17129.24
IRF3 KO Y16F	Replicate 1	0.0533	16.9
	Replicate 2	0.971	8.49
	Replicate 3	10555.3	11990.27

Table 6: Quantification of immunoblots in Figure 10

BX795 inhibitor: Fig. 10			
Cell Type		NS5A	GAPDH
DMSO WT	Replicate 1	1.02	8.2
	Replicate 2	0.463	6.45
	Replicate 3	0.0169	0.0211
DMSO	Replicate 1	0.736	7.7

Y16F	Replicate 2	0.124	11.4
	Replicate 3	0.00397	0.128
BX795 WT	Replicate 1	0.539	7.85
	Replicate 2	0.681	13.4
	Replicate 3	0.0121	0.0265
BX795 Y16F	Replicate 1	1.53	8.31
	Replicate 2	0.831	8.56
	Replicate 3	0.00031	0.0202

Table 7: Quantification of immunoblots used in Figure 11A

Riplet total protein: Fig. 11			
Cell Type		NS5A	Tubulin
Huh7	Replicate 1	0.219	1.05
	Replicate 2	0.419	1.03
	Replicate 3	0.183	0.495
Huh-7.5	Replicate 1	0.0517	1.57
	Replicate 2	0.174	1.34
	Replicate 3	0.0273	0.921

Table 8: Quantification of immunoblots used in Figure 11C

Riplet-V5: Fig. 11			
Cell Type		NS5A	Tubulin
Huh7 WT	Replicate 1	23864	25934.87
	Replicate 2	10.2	12.6
	Replicate 3	23277.04	32028.38
Huh7 Y16F	Replicate 1	8227.388	17790.82
	Replicate 2	4.95	15
	Replicate 3	14774.48	30641.07
Huh-7.5 WT	Replicate 1	8.49	2.57
	Replicate 2	6.14	7.1
	Replicate 3	41744.71	28471.89
Huh-7.5 Y16F	Replicate 1	7.1	3.24
	Replicate 2	9.26	5.39
	Replicate 3	38599.44	27727.17
Huh-7.5 + Riplet-V5	Replicate 1	0.708	4.51
	Replicate 2	0.551	7.93

WT	Replicate 3	31303.89	32906.19
Huh-7.5 + Riplet-V5 Y16F	Replicate 1	0.291	4.44
	Replicate 2	0.12	7.09
	Replicate 3	11498.6	33879.09

Table 9: Quantification of immunoblots used in Figure 12

Riplet-NS4A WT and Y16F IP: Fig. 12			
Cell Type		IP:Flag	IP:HA
WT	Replicate 1	0.0461	4.69
	Replicate 2	0.522	22.5
	Replicate 3	3.61	82.1
Y16F	Replicate 1	0.0186	5.43
	Replicate 2	0.319	50.1
	Replicate 3	1.97	117

Table 10: Quantification of immunoblots used in Figure 13

Flag-Riplet: Fig. 13			
Cell Type		NS5A	GAPDH
Huh-7.5 WT	Replicate 1	24.7	0.939
	Replicate 2	22.4	2.85
	Replicate 3	23.3	1.72
Huh-7.5 Y16F	Replicate 1	23	1.02
	Replicate 2	20	2.69
	Replicate 3	17	1.52
Huh-7.5 + Flag-Riplet WT	Replicate 1	21.5	1.01
	Replicate 2	18.4	3.19
	Replicate 3	8.06	0.921
Huh-7.5 + Flag-Riplet Y16F	Replicate 1	13	1.1
	Replicate 2	15.6	2.41
	Replicate 3	3.62	1.32
Huh-7.5 + Flag-Riplet ΔRING WT	Replicate 1	26.8	0.642
	Replicate 2	19.8	2.87
	Replicate 3	5.44	0.917
Huh-7.5 + Flag-Riplet	Replicate 1	27.7	0.778
	Replicate 2	19.7	3.17

ΔRING Y16F	Replicate 3	4.33	1.2

References

1. Gokhale, N.S., C. Vazquez, and S.M. Horner, *Hepatitis C Virus. Strategies to Evade Antiviral Responses.* Future Virol, 2014. **9**(12): p. 1061-1075.

2. Vazquez, C. and S.M. Horner, *MAVS Coordination of Antiviral Innate Immunity.* J Virol, 2015. **89**(14): p. 6974-7.

3. Goubau, D., S. Deddouche, and C. Reis e Sousa, *Cytosolic sensing of viruses.* Immunity, 2013. **38**(5): p. 855-69.

4. Saito, T., et al., *Regulation of innate antiviral defenses through a shared repressor domain in RIG-I and LGP2.* Proc Natl Acad Sci U S A, 2007. **104**(2): p. 582-7.

5. Satoh, T., et al., *LGP2 is a positive regulator of RIG-I- and MDA5-mediated antiviral responses.* Proc Natl Acad Sci U S A, 2010. **107**(4): p. 1512-7.

6. Rodriguez, K.R., A.M. Bruns, and C.M. Horvath, *MDA5 and LGP2: accomplices and antagonists of antiviral signal transduction.* J Virol, 2014. **88**(15): p. 8194-200.

7. Hornung, V., et al., *5'-Triphosphate RNA is the ligand for RIG-I.* Science, 2006. **314**(5801): p. 994-7.

8. Goubau, D., et al., *Antiviral immunity via RIG-I-mediated recognition of RNA bearing 5'-diphosphates.* Nature, 2014. **514**(7522): p. 372-375.

9. Schnell, G., et al., *Uridine composition of the poly-U/UC tract of HCV RNA defines non-self recognition by RIG-I.* PLoS Pathog, 2012. **8**(8): p. e1002839.

10. Pichlmair, A., et al., *Activation of MDA5 requires higher-order RNA structures generated during virus infection.* J Virol, 2009. **83**(20): p. 10761-9.

11. Triantafilou, K., et al., *Visualisation of direct interaction of MDA5 and the dsRNA replicative intermediate form of positive strand RNA viruses.* J Cell Sci, 2012. **125**(Pt 20): p. 4761-9.

12. Kato, H., et al., *Length-dependent recognition of double-stranded ribonucleic acids by retinoic acid-inducible gene-I and melanoma differentiation-associated gene 5.* J Exp Med, 2008. **205**(7): p. 1601-10.

13. Peisley, A., et al., *Cooperative assembly and dynamic disassembly of MDA5 filaments for viral dsRNA recognition.* Proc Natl Acad Sci U S A, 2011. **108**(52): p. 21010-5.

14. Wu, B., et al., *Structural basis for dsRNA recognition, filament formation, and antiviral signal activation by MDA5.* Cell, 2013. **152**(1-2): p. 276-89.

15. Jiang, F., et al., *Structural basis of RNA recognition and activation by innate immune receptor RIG-I.* Nature, 2011. **479**(7373): p. 423-7.

16. Peisley, A., et al., *Structural basis for ubiquitin-mediated antiviral signal activation by RIG-I.* Nature, 2014. **509**(7498): p. 110-4.

17. Oshiumi, H., et al., *A distinct role of Riplet-mediated K63-Linked polyubiquitination of the RIG-I repressor domain in human antiviral innate immune responses.* PLoS Pathog, 2013. **9**(8): p. e1003533.

18. Gack, M.U., et al., *TRIM25 RING-finger E3 ubiquitin ligase is essential for RIG-I-mediated antiviral activity.* Nature, 2007. **446**(7138): p. 916-920.

19. Berke, I.C. and Y. Modis, *MDA5 cooperatively forms dimers and ATP-sensitive filaments upon binding double-stranded RNA.* Embo j, 2012. **31**(7): p. 1714-26.

20. Wies, E., et al., *Dephosphorylation of the RNA sensors RIG-I and MDA5 by the phosphatase PP1 is essential for innate immune signaling.* Immunity, 2013. **38**(3): p. 437-49.

21. Horner, S.M., *Activation and evasion of antiviral innate immunity by hepatitis C virus.* J Mol Biol, 2014. **426**(6): p. 1198-209.

22. Liu, H.M., et al., *The mitochondrial targeting chaperone 14-3-3epsilon regulates a RIG-I translocon that mediates membrane association and innate antiviral immunity.* Cell Host Microbe, 2012. **11**(5): p. 528-37.

23. Jacobs, J.L. and C.B. Coyne, *Mechanisms of MAVS regulation at the mitochondrial membrane.* J Mol Biol, 2013. **425**(24): p. 5009-19.

24. Baril, M., et al., *MAVS dimer is a crucial signaling component of innate immunity and the target of hepatitis C virus NS3/4A protease.* J Virol, 2009. **83**(3): p. 1299-311.

25. McFadden, M.J., N.S. Gokhale, and S.M. Horner, *Protect this house: cytosolic sensing of viruses.* Curr Opin Virol, 2017. **22**: p. 36-43.

26. Liu, S., et al., *MAVS recruits multiple ubiquitin E3 ligases to activate antiviral signaling cascades.* Elife, 2013. **2**: p. e00785.

27. Fitzgerald, K.A., et al., *IKKepsilon and TBK1 are essential components of the IRF3 signaling pathway.* Nat Immunol, 2003. **4**(5): p. 491-6.

28. Yoneyama, M., W. Suhara, and T. Fujita, *Control of IRF-3 activation by phosphorylation.* J Interferon Cytokine Res, 2002. **22**(1): p. 73-6.

29. Panne, D., et al., *Interferon regulatory factor 3 is regulated by a dual phosphorylation-dependent switch.* J Biol Chem, 2007. **282**(31): p. 22816-22.

30. Mori, M., et al., *Identification of Ser-386 of interferon regulatory factor 3 as critical target for inducible phosphorylation that determines activation.* J Biol Chem, 2004. **279**(11): p. 9698-702.

31. Servant, M.J., N. Grandvaux, and J. Hiscott, *Multiple signaling pathways leading to the activation of interferon regulatory factor 3.* Biochem Pharmacol, 2002. **64**(5-6): p. 985-92.

32. Chen, Z.J., *Ubiquitin signalling in the NF-kappaB pathway.* Nat Cell Biol, 2005. **7**(8): p. 758-65.

33. Orian, A., et al., *SCF(beta)(-TrCP) ubiquitin ligase-mediated processing of NF-kappaB p105 requires phosphorylation of its C-terminus by IkappaB kinase.* Embo j, 2000. **19**(11): p. 2580-91.

34. Oeckinghaus, A. and S. Ghosh, *The NF-kappaB family of transcription factors and its regulation.* Cold Spring Harb Perspect Biol, 2009. **1**(4): p. a000034.

35. Sarasin-Filipowicz, M., et al., *Interferon signaling and treatment outcome in chronic hepatitis C.* Proc Natl Acad Sci U S A, 2008. **105**(19): p. 7034-9.

36. Wieland, S., et al., *Simultaneous detection of hepatitis C virus and interferon stimulated gene expression in infected human liver.* Hepatology, 2014. **59**(6): p. 2121-30.

37. Fusco, D.N., et al., *A genetic screen identifies interferon-alpha effector genes required to suppress hepatitis C virus replication.* Gastroenterology, 2013. **144**(7): p. 1438-49, 1449.e1-9.

38. Metz, P., et al., *Identification of type I and type II interferon-induced effectors controlling hepatitis C virus replication.* Hepatology, 2012. **56**(6): p. 2082-93.

39. Schoggins, J.W., et al., *A diverse range of gene products are effectors of the type I interferon antiviral response.* Nature, 2011. **472**(7344): p. 481-5.

40. Zhao, H., et al., *A functional genomic screen reveals novel host genes that mediate interferon-alpha's effects against hepatitis C virus.* J Hepatol, 2012. **56**(2): p. 326-33.

41. Ishida, Y., et al., *Hepatic IFN-Induced Protein with Tetratricopeptide Repeats Regulation of HCV Infection.* J Interferon Cytokine Res, 2019. **39**(3): p. 133-146.

42. Sen, G.C. and V. Fensterl, *Crystal structure of IFIT2 (ISG54) predicts functional properties of IFITs.* Cell Res, 2012. **22**(10): p. 1407-9.

43. Metz, P., et al., *Interferon-stimulated genes and their role in controlling hepatitis C virus.* J Hepatol, 2013. **59**(6): p. 1331-41.

44. Han, J.Q. and D.J. Barton, *Activation and evasion of the antiviral 2'-5' oligoadenylate synthetase/ribonuclease L pathway by hepatitis C virus mRNA.* RNA, 2002. **8**(4): p. 512-25.

45. Malathi, K., et al., *RNase L releases a small RNA from HCV RNA that refolds into a potent PAMP.* RNA, 2010. **16**(11): p. 2108-19.

46. Taguchi, T., et al., *Hepatitis C virus NS5A protein interacts with 2',5'-oligoadenylate synthetase and inhibits antiviral activity of IFN in an IFN sensitivity-determining region-independent manner.* J Gen Virol, 2004. **85**(Pt 4): p. 959-69.

47. Raychoudhuri, A., et al., *ISG56 and IFITM1 proteins inhibit hepatitis C virus replication.* J Virol, 2011. **85**(24): p. 12881-9.

48. Wilkins, C., et al., *IFITM1 is a tight junction protein that inhibits hepatitis C virus entry.* Hepatology, 2013. **57**(2): p. 461-9.

49. Narayana, S.K., et al., *The Interferon-induced Transmembrane Proteins, IFITM1, IFITM2, and IFITM3 Inhibit Hepatitis C Virus Entry.* J Biol Chem, 2015. **290**(43): p. 25946-59.

50. Yao, L., et al., *Identification of the IFITM3 gene as an inhibitor of hepatitis C viral translation in a stable STAT1 cell line.* J Viral Hepat, 2011. **18**(10): p. e523-9.

51. Amini-Bavil-Olyaee, S., et al., *The antiviral effector IFITM3 disrupts intracellular cholesterol homeostasis to block viral entry.* Cell Host Microbe, 2013. **13**(4): p. 452-64.

52. Gao, L., et al., *Interactions between viral nonstructural proteins and host protein hVAP-33 mediate the formation of hepatitis C virus RNA replication complex on lipid raft.* J Virol, 2004. **78**(7): p. 3480-8.

53. Wang, H., et al., *Oxysterol-binding protein is a phosphatidylinositol 4-kinase effector required for HCV replication membrane integrity and cholesterol trafficking.* Gastroenterology, 2014. **146**(5): p. 1373-85.e1-11.

54. Helbig, K.J., et al., *The antiviral protein viperin inhibits hepatitis C virus replication via interaction with nonstructural protein 5A.* Hepatology, 2011. **54**(5): p. 1506-17.

55. Wang, S., et al., *Viperin inhibits hepatitis C virus replication by interfering with binding of NS5A to host protein hVAP-33.* J Gen Virol, 2012. **93**(Pt 1): p. 83-92.

56. Verhelst, J., P. Hulpiau, and X. Saelens, *Mx proteins: antiviral gatekeepers that restrain the uninvited.* Microbiol Mol Biol Rev, 2013. **77**(4): p. 551-66.

57. Shi, X., et al., *MxA is a positive regulator of type I IFN signaling in HCV infection.* J Med Virol, 2017. **89**(12): p. 2173-2180.

58. Overby, A.K., et al., *Tick-borne encephalitis virus delays interferon induction and hides its double-stranded RNA in intracellular membrane vesicles.* J Virol, 2010. **84**(17): p. 8470-83.

59. Uchida, L., et al., *The dengue virus conceals double-stranded RNA in the intracellular membrane to escape from an interferon response.* Sci Rep, 2014. **4**: p. 7395.

60. Neufeldt, C.J., et al., *The Hepatitis C Virus-Induced Membranous Web and Associated Nuclear Transport Machinery Limit Access of Pattern Recognition Receptors to Viral Replication Sites.* PLoS Pathog, 2016. **12**(2): p. e1005428.

61. Liu, Y., D. Olagnier, and R. Lin, *Host and Viral Modulation of RIG-I-Mediated Antiviral Immunity.* Front Immunol, 2016. **7**: p. 662.

62. Barral, P.M., et al., *MDA-5 is cleaved in poliovirus-infected cells.* J Virol, 2007. **81**(8): p. 3677-84.

63. Li, X.D., et al., *Hepatitis C virus protease NS3/4A cleaves mitochondrial antiviral signaling protein off the mitochondria to evade innate immunity.* Proc Natl Acad Sci U S A, 2005. **102**(49): p. 17717-22.

64. Meylan, E., et al., *Cardif is an adaptor protein in the RIG-I antiviral pathway and is targeted by hepatitis C virus.* Nature, 2005. **437**(7062): p. 1167-72.

65. Loo, Y.M., et al., *Viral and therapeutic control of IFN-beta promoter stimulator 1 during hepatitis C virus infection.* Proc Natl Acad Sci U S A, 2006. **103**(15): p. 6001-6.

66. Bellecave, P., et al., *Cleavage of mitochondrial antiviral signaling protein in the liver of patients with chronic hepatitis C correlates with a reduced activation of the endogenous interferon system.* Hepatology, 2010. **51**(4): p. 1127-36.

67. Li, K., et al., *Immune evasion by hepatitis C virus NS3/4A protease-mediated cleavage of the Toll-like receptor 3 adaptor protein TRIF.* Proc Natl Acad Sci U S A, 2005. **102**(8): p. 2992-7.

68. Davis, M.E., et al., *Antagonism of the phosphatase PP1 by the measles virus V protein is required for innate immune escape of MDA5.* Cell Host Microbe, 2014. **16**(1): p. 19-30.

69. Rajsbaum, R., et al., *Species-specific inhibition of RIG-I ubiquitination and IFN induction by the influenza A virus NS1 protein.* PLoS Pathog, 2012. **8**(11): p. e1003059.

70. Goolsby Hunter, A., et al., *Clinical characteristics, healthcare costs, and resource utilization in hepatitis C vary by genotype.* Curr Med Res Opin, 2017. **33**(5): p. 829-836.

71. Grebely, J., B. Hajarizadeh, and G.J. Dore, *Direct-acting antiviral agents for HCV infection affecting people who inject drugs.* Nat Rev Gastroenterol Hepatol, 2017. **14**(11): p. 641-651.

72. Choo, Q.L., et al., *Isolation of a cDNA clone derived from a blood-borne non-A, non-B viral hepatitis genome.* Science, 1989. **244**(4902): p. 359-62.

73. Feinstone, S.M., et al., *Transfusion-associated hepatitis not due to viral hepatitis type A or B.* N Engl J Med, 1975. **292**(15): p. 767-70.

74. Lohmann, V., et al., *Replication of subgenomic hepatitis C virus RNAs in a hepatoma cell line.* Science, 1999. **285**(5424): p. 110-3.

75. Aligeti, M., A. Roder, and S.M. Horner, *Cooperation between the Hepatitis C Virus p7 and NS5B Proteins Enhances Virion Infectivity.* J Virol, 2015. **89**(22): p. 11523-33.

76. Jiang, J. and G. Luo, *Cell culture-adaptive mutations promote viral protein-protein interactions and morphogenesis of infectious hepatitis C virus.* J Virol, 2012. **86**(17): p. 8987-97.

77. Pokrovskii, M.V., et al., *Novel mutations in a tissue culture-adapted hepatitis C virus strain improve infectious-virus stability and markedly enhance infection kinetics.* J Virol, 2011. **85**(8): p. 3978-85.

78. Kaul, A., et al., *Cell culture adaptation of hepatitis C virus and in vivo viability of an adapted variant.* J Virol, 2007. **81**(23): p. 13168-79.

79. Han, Q., et al., *Compensatory mutations in NS3 and NS5A proteins enhance the virus production capability of hepatitis C reporter virus.* Virus Res, 2009. **145**(1): p. 63-73.

80. Revie, D. and S.Z. Salahuddin, *Human cell types important for hepatitis C virus replication in vivo and in vitro: old assertions and current evidence.* Virol J, 2011. **8**: p. 346.

81. Nakabayashi, H., et al., *Growth of human hepatoma cells lines with differentiated functions in chemically defined medium.* Cancer Res, 1982. **42**(9): p. 3858-63.

82. Blight, K.J., J.A. McKeating, and C.M. Rice, *Highly permissive cell lines for subgenomic and genomic hepatitis C virus RNA replication.* J Virol, 2002. **76**(24): p. 13001-14.

83. Sumpter, R., Jr., et al., *Regulating intracellular antiviral defense and permissiveness to hepatitis C virus RNA replication through a cellular RNA helicase, RIG-I.* J Virol, 2005. **79**(5): p. 2689-99.

84. Kato, T., et al., *Sequence analysis of hepatitis C virus isolated from a fulminant hepatitis patient.* J Med Virol, 2001. **64**(3): p. 334-9.

85. Foy, E., et al., *Control of antiviral defenses through hepatitis C virus disruption of retinoic acid-inducible gene-I signaling.* Proc Natl Acad Sci U S A, 2005. **102**(8): p. 2986-91.

86. Lin, R., et al., *Dissociation of a MAVS/IPS-1/VISA/Cardif-IKKepsilon molecular complex from the mitochondrial outer membrane by hepatitis C virus NS3-4A proteolytic cleavage.* J Virol, 2006. **80**(12): p. 6072-83.

87. Horner, S.M. and M. Gale, Jr., *Regulation of hepatic innate immunity by hepatitis C virus.* Nat Med, 2013. **19**(7): p. 879-88.

88. Kim, J.L., et al., *Crystal structure of the hepatitis C virus NS3 protease domain complexed with a synthetic NS4A cofactor peptide.* Cell, 1996. **87**(2): p. 343-55.

89. Abian, O., et al., *Conformational stability of hepatitis C virus NS3 protease.* Biophys J, 2010. **99**(11): p. 3811-20.

90. Love, R.A., et al., *The crystal structure of hepatitis C virus NS3 proteinase reveals a trypsin-like fold and a structural zinc binding site.* Cell, 1996. **87**(2): p. 331-42.

91. Cicero, D.O., et al., *Structural characterization of the interactions of optimized product inhibitors with the N-terminal proteinase domain of the hepatitis C virus (HCV) NS3 protein by NMR and modelling studies.* J Mol Biol, 1999. **289**(2): p. 385-96.

92. Koch, J.O., et al., *In vitro studies on the activation of the hepatitis C virus NS3 proteinase by the NS4A cofactor.* Virology, 1996. **221**(1): p. 54-66.

93. Brass, V., et al., *Structural determinants for membrane association and dynamic organization of the hepatitis C virus NS3-4A complex.* Proc Natl Acad Sci U S A, 2008. **105**(38): p. 14545-50.

94. Wolk, B., et al., *Subcellular localization, stability, and trans-cleavage competence of the hepatitis C virus NS3-NS4A complex expressed in tetracycline-regulated cell lines.* J Virol, 2000. **74**(5): p. 2293-304.

95. Steinkuhler, C., et al., *Activity of purified hepatitis C virus protease NS3 on peptide substrates.* J Virol, 1996. **70**(10): p. 6694-700.

96. Lin, C., et al., *Hepatitis C virus NS3 serine proteinase: trans-cleavage requirements and processing kinetics.* J Virol, 1994. **68**(12): p. 8147-57.

97. Butkiewicz, N.J., et al., *Enhancement of hepatitis C virus NS3 proteinase activity by association with NS4A-specific synthetic peptides: identification of sequence and critical residues of NS4A for the cofactor activity.* Virology, 1996. **225**(2): p. 328-38.

98. Mottola, G., et al., *Hepatitis C virus nonstructural proteins are localized in a modified endoplasmic reticulum of cells expressing viral subgenomic replicons.* Virology, 2002. **293**(1): p. 31-43.

99. Seth, R.B., et al., *Identification and characterization of MAVS, a mitochondrial antiviral signaling protein that activates NF-kappaB and IRF 3.* Cell, 2005. **122**(5): p. 669-82.

100. Horner, S.M., et al., *Mitochondrial-associated endoplasmic reticulum membranes (MAM) form innate immune synapses and are targeted by hepatitis C virus.* Proc Natl Acad Sci U S A, 2011. **108**(35): p. 14590-5.

101. Martinvalet, D., *The role of the mitochondria and the endoplasmic reticulum contact sites in the development of the immune responses.* Cell Death Dis, 2018. **9**(3): p. 336.

102. Dixit, E., et al., *Peroxisomes are signaling platforms for antiviral innate immunity.* Cell, 2010. **141**(4): p. 668-81.

103. Ferreira, A.R., et al., *Hepatitis C virus NS3-4A inhibits the peroxisomal MAVS-dependent antiviral signalling response.* 2016. **20**(4): p. 750-7.

104. Bender, S., et al., *Activation of Type I and III Interferon Response by Mitochondrial and Peroxisomal MAVS and Inhibition by Hepatitis C Virus.* PLoS Pathog, 2015. **11**(11): p. e1005264.

105. Morikawa, K., et al., *Nonstructural protein 3-4A: the Swiss army knife of hepatitis C virus.* J Viral Hepat, 2011. **18**(5): p. 305-15.

106. Grakoui, A., et al., *Expression and identification of hepatitis C virus polyprotein cleavage products.* J Virol, 1993. **67**(3): p. 1385-95.

107. Schechter, I. and A. Berger, *On the size of the active site in proteases. I. Papain.* Biochem Biophys Res Commun, 1967. **27**(2): p. 157-62.

108. Zhang, R., et al., *Probing the substrate specificity of hepatitis C virus NS3 serine protease by using synthetic peptides.* J Virol, 1997. **71**(8): p. 6208-13.

109. Zhang, Z., et al., *DDX1, DDX21, and DHX36 helicases form a complex with the adaptor molecule TRIF to sense dsRNA in dendritic cells.* Immunity, 2011. **34**(6): p. 866-78.

110. Kang, X., et al., *DDB1 is a cellular substrate of NS3/4A protease and required for hepatitis C virus replication.* Virology, 2013. **435**(2): p. 385-94.

111. Morikawa, K., et al., *Quantitative proteomics identifies the membrane-associated peroxidase GPx8 as a cellular substrate of the hepatitis C virus NS3-4A protease.* Hepatology, 2014. **59**(2): p. 423-33.

112. Brenndorfer, E.D., et al., *Nonstructural 3/4A protease of hepatitis C virus activates epithelial growth factor-induced signal transduction by cleavage of the T-cell protein tyrosine phosphatase.* Hepatology, 2009. **49**(6): p. 1810-20.

113. Swatek, K.N. and D. Komander, *Ubiquitin modifications.* Cell Res, 2016. **26**(4): p. 399-422.

114. Berndsen, C.E. and C. Wolberger, *New insights into ubiquitin E3 ligase mechanism.* Nat Struct Mol Biol, 2014. **21**(4): p. 301-7.

115. Borden, K.L. and P.S. Freemont, *The RING finger domain: a recent example of a sequence-structure family.* Curr Opin Struct Biol, 1996. **6**(3): p. 395-401.

116. Saurin, A.J., et al., *Does this have a familiar RING?* Trends Biochem Sci, 1996. **21**(6): p. 208-14.

117. Castanier, C., et al., *MAVS ubiquitination by the E3 ligase TRIM25 and degradation by the proteasome is involved in type I interferon production after activation of the antiviral RIG-I-like receptors.* BMC Biol, 2012. **10**: p. 44.

118. Okamoto, M., et al., *Regulation of RIG-I Activation by K63-Linked Polyubiquitination.* Front Immunol, 2017. **8**: p. 1942.

119. Vazquez, C., C.Y. Tan, and S.M. Horner, *Hepatitis C virus infection is inhibited by a non-canonical antiviral signaling pathway targeted by NS3-NS4A.* J Virol, 2019.

120. Kohlway, A., et al., *Hepatitis C virus RNA replication and virus particle assembly require specific dimerization of the NS4A protein transmembrane domain.* J Virol, 2014. **88**(1): p. 628-42.

121. Roder, A.E. and C. Vazquez, *The acidic domain of the hepatitis C virus NS4A protein is required for viral assembly and envelopment through interactions with the viral E1 glycoprotein.* 2019. **15**(2): p. e1007163.

122. Moradpour, D., F. Penin, and C.M. Rice, *Replication of hepatitis C virus.* Nat Rev Microbiol, 2007. **5**(6): p. 453-63.

123. Israelow, B., et al., *HepG2 cells mount an effective antiviral interferon-lambda based innate immune response to hepatitis C virus infection.* Hepatology, 2014. **60**(4): p. 1170-9.

124. Oshiumi, H., et al., *Riplet/RNF135, a RING finger protein, ubiquitinates RIG-I to promote interferon-beta induction during the early phase of viral infection.* J Biol Chem, 2009. **284**(2): p. 807-17.

125. Cadena, C., et al., *Ubiquitin-Dependent and -Independent Roles of E3 Ligase RIPLET in Innate Immunity.* Cell, 2019.

126. Wang, N., et al., *Toll-like receptor 3 mediates establishment of an antiviral state against hepatitis C virus in hepatoma cells.* J Virol, 2009. **83**(19): p. 9824-34.

127. Foy, E., et al., *Regulation of interferon regulatory factor-3 by the hepatitis C virus serine protease.* Science, 2003. **300**(5622): p. 1145-8.

128. Kuiken, C., et al., *The Los Alamos hepatitis C sequence database.* Bioinformatics, 2005. **21**(3): p. 379-84.

129. Braun, P. and G. von Heijne, *The aromatic residues Trp and Phe have different effects on the positioning of a transmembrane helix in the microsomal membrane.* Biochemistry, 1999. **38**(30): p. 9778-82.

130. de Planque, M.R., et al., *Interfacial anchor properties of tryptophan residues in transmembrane peptides can dominate over hydrophobic matching effects in peptide-lipid interactions.* Biochemistry, 2003. **42**(18): p. 5341-8.

131. Wimley, W.C. and S.H. White, *Experimentally determined hydrophobicity scale for proteins at membrane interfaces.* Nat Struct Biol, 1996. **3**(10): p. 842-8.

132. Saito, T., et al., *Innate immunity induced by composition-dependent RIG-I recognition of hepatitis C virus RNA.* Nature, 2008. **454**(7203): p. 523-7.

133. Honda, K., A. Takaoka, and T. Taniguchi, *Type I interferon [corrected] gene induction by the interferon regulatory factor family of transcription factors.* Immunity, 2006. **25**(3): p. 349-60.

134. Rustagi, A. and M. Gale, Jr., *Innate antiviral immune signaling, viral evasion and modulation by HIV-1.* J Mol Biol, 2014. **426**(6): p. 1161-77.

135. Clark, K., et al., *Use of the pharmacological inhibitor BX795 to study the regulation and physiological roles of TBK1 and IkappaB kinase epsilon: a distinct upstream kinase mediates Ser-172 phosphorylation and activation.* J Biol Chem, 2009. **284**(21): p. 14136-46.

136. Kato, H., et al., *Differential roles of MDA5 and RIG-I helicases in the recognition of RNA viruses.* Nature, 2006. **441**(7089): p. 101-5.

137. Johnson, C.L., D.M. Owen, and M. Gale, Jr., *Functional and therapeutic analysis of hepatitis C virus NS3.4A protease control of antiviral immune defense.* J Biol Chem, 2007. **282**(14): p. 10792-803.

138. Sumpter, R., Jr., et al., *Viral evolution and interferon resistance of hepatitis C virus RNA replication in a cell culture model.* J Virol, 2004. **78**(21): p. 11591-604.

139. Mali, P., et al., *RNA-guided human genome engineering via Cas9.* Science, 2013. **339**(6121): p. 823-6.

140. Fredericksen, B., et al., *Activation of the interferon-beta promoter during hepatitis C virus RNA replication.* Viral Immunol, 2002. **15**(1): p. 29-40.

141. Yoneyama, M., et al., *The RNA helicase RIG-I has an essential function in double-stranded RNA-induced innate antiviral responses.* Nat Immunol, 2004. **5**(7): p. 730-7.

142. Basler, C.F., et al., *The Ebola virus VP35 protein inhibits activation of interferon regulatory factor 3.* J Virol, 2003. **77**(14): p. 7945-56.

143. Cong, L., et al., *Multiplex genome engineering using CRISPR/Cas systems.* Science, 2013. **339**(6121): p. 819-23.

144. Kennedy, E.M., et al., *Production of functional small interfering RNAs by an amino-terminal deletion mutant of human Dicer.* Proc Natl Acad Sci U S A, 2015. **112**(50): p. E6945-54.

145. Pfisterer, U., et al., *Direct conversion of human fibroblasts to dopaminergic neurons.* Proc Natl Acad Sci U S A, 2011. **108**(25): p. 10343-8.

146. Hiscott, J., *Triggering the innate antiviral response through IRF-3 activation.* J Biol Chem, 2007. **282**(21): p. 15325-9.

147. Shalem, O., et al., *Genome-scale CRISPR-Cas9 knockout screening in human cells.* Science, 2014. **343**(6166): p. 84-87.

148. Heigwer, F., G. Kerr, and M. Boutros, *E-CRISP: fast CRISPR target site identification.* 2014. **11**(2): p. 122-3.

149. Schindelin, J., et al., *Fiji: an open-source platform for biological-image analysis.* Nat Methods, 2012. **9**(7): p. 676-82.

150. Li, K., et al., *Distinct poly(I-C) and virus-activated signaling pathways leading to interferon-beta production in hepatocytes.* J Biol Chem, 2005. **280**(17): p. 16739-47.

151. Gao, D., et al., *REUL is a novel E3 ubiquitin ligase and stimulator of retinoic-acid-inducible gene-I.* PLoS One, 2009. **4**(6): p. e5760.

152. Aguirre, S., et al., *Dengue virus NS2B protein targets cGAS for degradation and prevents mitochondrial DNA sensing during infection.* PLoS Pathog, 2017. **2**: p. 17037.

153. Sharma, S., et al., *Triggering the interferon antiviral response through an IKK-related pathway.* Science, 2003. **300**(5622): p. 1148-51.

154. Oshiumi, H., et al., *The ubiquitin ligase Riplet is essential for RIG-I-dependent innate immune responses to RNA virus infection.* Cell Host Microbe, 2010. **8**(6): p. 496-509.

155. Wynne, C., et al., *TRIM68 negatively regulates IFN-beta production by degrading TRK fused gene, a novel driver of IFN-beta downstream of anti-viral detection systems.* PLoS One, 2014. **9**(7): p. e101503.

156. Arnaud, N., et al., *Hepatitis C virus reveals a novel early control in acute immune response.* PLoS Pathog, 2011. **7**(10): p. e1002289.

157. Onomoto, K., et al., *Critical role of an antiviral stress granule containing RIG-I and PKR in viral detection and innate immunity.* PLoS One, 2012. **7**(8): p. e43031.

158. Pager, C.T., et al., *Modulation of hepatitis C virus RNA abundance and virus release by dispersion of processing bodies and enrichment of stress granules.* Virology, 2013. **435**(2): p. 472-84.

159. Ruggieri, A., et al., *Dynamic oscillation of translation and stress granule formation mark the cellular response to virus infection.* Cell Host Microbe, 2012. **12**(1): p. 71-85.

160. Gibbs, K.a.W., Erica J. and Jaslow, Sarah L. and Bourgeois, Jeffrey S. and Foster, Matthew W. and Guo, Robyn and Brennan, Richard G. and Ko, Dennis C., *The Salmonella Secreted Effector SarA/SteE Mimics Cytokine Receptor Signaling to Activate STAT3.* Cell Host Microbe, 2019.

161. Panagi, I.a.J., Elliott and Zeng, Jingkun and Günster, Regina A. and Stones, Cullum D. and Mak, Hazel and Jin, Enkai and Stapels, Daphne A.C and Subari, Nur Z. and Pham, Trung H. M. and Brewer, Susan M. and Ong, Samantha Y.Q. and Monack, Denise and Helaine, Sophie and Thurston, Teresa, *The Salmonella Effector SteE Converts the Mammalian Serine/Threonine Kinase GSK3 into a Tyrosine Kinase* Cell Host Microbe, 2019.

162. Hayashi, J., et al., *Hepatitis C virus core protein activates the MAPK/ERK cascade synergistically with tumor promoter TPA, but not with epidermal growth factor or transforming growth factor alpha.* Hepatology, 2000. **32**(5): p. 958-61.

163. Pei, R., et al., *Regulation of hepatitis C virus replication and gene expression by the MAPK-ERK pathway.* Virol Sin, 2012. **27**(5): p. 278-85.

164. Peng, L., et al., *Hepatitis C virus NS5A activates the mammalian target of rapamycin (mTOR) pathway, contributing to cell survival by disrupting the interaction between FK506-binding protein 38 (FKBP38) and mTOR.* J Biol Chem, 2010. **285**(27): p. 20870-81.

165. Zhang, L., et al., *IL28B inhibits hepatitis C virus replication through the JAK-STAT pathway.* J Hepatol, 2011. **55**(2): p. 289-98.

166. Hayman, T.J. and A.C. Hsu, *RIPLET, and not TRIM25, is required for endogenous RIG-I-dependent antiviral responses.* Embo j, 2019.

167. Ramage, H.R., et al., *A combined proteomics/genomics approach links hepatitis C virus infection with nonsense-mediated mRNA decay.* Mol Cell, 2015. **57**(2): p. 329-340.

Biography

Christine Vazquez received her Bachelor of Science degree in Molecular and Cellular Biology from Johns Hopkins University in 2011 and her Master of Science degree in Biotechnology/Biodefense from Johns Hopkins University in 2013. While an undergraduate student, Christine worked with Drs. Theodore Bayless and Susan Hutfless at the Johns Hopkins Hospital, where she examined risk factors for inflammatory bowel disease (IBD). Concurrently, Christine worked with Dr. Steven Meltzer at the Johns Hopkins School of Medicine, where she studied the role of microRNAs in progression to IBD-related cancers. For her work with Drs. Bayless and Hutfless, Christine was a contributing author on a publication titled “Family history of inflammatory bowel disease among patients with ulcerative colitis: a systematic review and meta-analysis” published in the *Journal of Crohn’s and Colitis* in 2014. For her work in Dr. Meltzer’s lab, she was a contributing author to two studies published in *Inflammatory Bowel Disease:* “Dynamic changes in the expression of microRNA-31 during inflammatory bowel disease-associated neoplastic transformations” in 2011 and “MicroRNA-224 negatively regulates p21 expression during neoplastic progression in inflammatory bowel disease” in 2013.

In August 2013, Christine began her PhD at Duke University in the department of Molecular Genetics and Microbiology and joined Dr. Stacy Horner’s laboratory in May 2014. While in the Horner lab, Christine investigated the role of a tyrosine residue within the HCV NS4A transmembrane in regulating antiviral innate immunity. Her thesis work was published in *Journal of Virology* in September 2019 and is titled “Hepatitis C virus infection is inhibited by a noncanonical antiviral signaling pathway targeted by NS3-NS4A”. She has contributed to several other publications in the lab, including “The acidic

domain of the hepatitis C virus NS4A protein is required for viral assembly and envelopment through interactions with the viral E1 glycoprotein" published in *Plos Pathogens* in 2019, and "A fluorescent cell-based system for imaging Zika virus infection in real-time" published in *Viruses* in 2018. She has also co-authored a methods paper in *Methods in Molecular Biology* titled "Methods to visualize MAVS subcellular localization" in 2017 and a review article in *Future Virology,* and a first author *Journal of Virology Gem* (mini-review) in 2015 titled "MAVS coordination of antiviral innate immunity" .

Christine has received several awards during graduate school. She was awarded the Duke BioCoRE Scholarship in 2013, a Ford Foundation Predoctoral Fellowship in 2014, the Carl Storm Underrepresented Minority Fellowship to attend a Gordon Research Conference in in 2017, the Burroughs Wellcome Fund Graduate Diversity Enrichment Program Award in 2017, and was a Duke University Infectious Disease Scholar from 2016-2017. Additionally, Christine has been awarded a Best Student Poster Award at departmental symposia. Christine has also won awards to attend national and international conferences.

At Duke, Christine is actively involved in community activities. She is a member of the MGM Women in Science Group, MGM Student Outreach Group, the MGM Diversity and Inclusion Committee, a panelist for the Genetics and Genomics: Epigenetics, Environment, and Ethics course, and the national Skype-A-Scientist program.

Publications to Date:

1 **Vazquez C**, Tan CY, and Horner SM**.** Hepatitis C virus infection is inhibited by a noncanonical antiviral signaling pathway targeted by NS3-NS4A. J. Virol. 2019. Epub ahead of print. doi: 10.1128/JVI.00725-19. PMID: 31534039.

2 Roder AE, **Vazquez C**, Horner SM. The acidic domain of the hepatitis C virus NS4A protein is required for viral assembly and envelopment through interactions with the viral E1 glycoprotein. PLoS Pathog. 2019 Feb 7;15(2):e1007163. doi: 10.1371/journal.ppat.1007163. PMID: 30730994

3 McFadden MJ, Mitchell-Dick A, **Vazquez C**, Roder A, Labagnara K, Silver D, Horner SM. A fluorescent cell-based system for imaging Zika virus infection in real-time. Viruses. 2018 Feb 24;10(2). pii: E95. doi: 10.3390/v10020095. PMID:29495257

4 **Vazquez C**, Beachboard DC, and Horner SM. Methods to Visualize MAVS Subcellular Localization. Methods Mol Biol. 2017;1656:131-142. PMID:28808966

5 Gokhale NS, McIntyre AB, McFadden MJ, Roder AE, Kennedy EM, Gandara JA, Hopcraft SE, Quicke KM, **Vazquez C**, Willer J, Ilkayeva OR, Law BA, Holley CL, Garcia-Blanco MA, Evans MJ, Suthar MS, Bradrick SS, Mason CE, Horner SM. N6-Methyladenosine in Flaviviridae Viral RNA Genomes Regulates Infection. Cell Host Microbe. 2016;20(5):654-65. PMID:27773535

6 **Vazquez C**, Horner SM. MAVS Coordination of Antiviral Innate Immunity. J Virol. 2015;89(14):6974-7. PMID:25948741

7 Gokhale NS, **Vazquez C**, Horner SM. Hepatitis C virus: Strategies to evade antiviral responses. Future Virol. 2014;9(12):1061-75. PMID:25983854

8 Childers RE, Eluri S, **Vazquez C**, Weise RM, Bayless TM, Hutfless, S. Family History of Inflammatory Bowel Disease Among Patients with Ulcerative Colitis: A Systematic Review and Meta-Analysis*.* J Crohns Colitis. 2014 Nov;8(11):1480-97. PMID:24974207

9 Aguirre JD, Clark HM, McIlvin M, **Vazquez C**, Palmere SL, Grab D, Janakiram S, Saito M, and Culotta VC. A Manganese-Rich Environment Supports Superoxide Dismutase Activity in the Lyme Disease Pathogen, Borrelia burgdorferi. Journal of Biological Chemistry. 2013 Mar 22;288(12):8468-78. PMID:23376276

10 Olaru AV, Yamanaka S, **Vazquez C**, Cheng Y, Abraham JM, Mori Y, Bayless TM, Harpaz N, Meltzer SJ. MicroRNA-224 negatively regulates p21 expression during neoplastic progression in inflammatory bowel disease*.* Inflammatory Bowel Disease. 2013 Mar;19(3):471-80. PMID:23399735

11 Olaru AV, Selaru FM, Mori Y, **Vazquez C**, David S, Paun B, Cheng Y, Jin Z, Yang J, Agarwal R, Abraham JM, Dassopoulos T, Harris M, Bayless TM, Kwon J, Harpaz N, Livak F, Meltzer SJ. Dynamic changes in the expression of microRNA-31 during inflammatory bowel disease-associated neoplastic transformations. Inflammatory Bowel Disease 2011 Jan;17(1):221-31. PMID:20848452